Beyond the Standard Model

applications of holography

A THESIS

SUBMITTED TO THE FACULTY OF THE

UNIVERSITY OF MINNESOTA

BY

Yusuf Büyükdağ

IN PARTIAL FULFILLMENT OF THE REQUIREMENTS

FOR THE DEGREE OF

DOCTOR OF PHILOSOPHY

Prof. Tony Gherghetta, Adviser

July, 2020

Acknowledgements

One third of the time that I spent in school was at the University of Minnesota, so I interacted with many physicists who shaped my path voluntarily or involuntarily. Of course friends and family played their role as well to bring me where I am now. Looking back, I am not sure if I would have changed something for a better result, for life is too uncertain to anticipate the consequences. Then let me resist the hindsight bias and start thanking the actors.

I am grateful to Bayram Tekin and İnanç Kanık for introducing higher level physics concepts to me starting in high school. More importantly they helped me build confidence and I realized that I should not give up without trying thanks to them. This was much needed when it was easy to be scared from transitioning into a new field. Bayram Tekin was also the person who told me to apply University of Minnesota since he received his PhD here as well.

In my first year of graduate school, I struggled to find an advisor for summer research. Joseph Kapusta was really kind and accepted me. He introduced me to his post doctoral researcher Clint Young. I appreciate this help a lot and I am happy to have worked with Clint on my first project that ended up as a publication.

I sincerely thank my adviser Tony Gherghetta for all the help and guidance over six years. It felt extremely difficult to demonstrate the talent and the passion expected to even start my research in my second year. Eventually I started applying to other universities to transfer. I was lucky that Tony happened to come back to the University of Minnesota at that time and gave me a chance and space to pursue a research area that aligned with my passions.

I want to thank my collaborators as well. I initially worked with Andrew Miller, another PhD student of Tony, and later I had the chance of interacting with Keith Dienes and Brooks Thomas.

Both in lectures and in the weekly High Energy Theory seminars, I observed a unique way of looking at physics concepts from the trio, Arkady Vainshtein, Mikhail Shifman and Mikhail Voloshin. I especially thank Mikhail Voloshin for his well prepared lectures. I also worked as his teaching assistant and witnessed his very friendly nature. May his memory

and contributions live on in the work of his students and colleagues who were lucky to know him.

At different stages of graduate school, I was lucky to have other physics PhD students and post docs, Hasan Barış Serçe, Daniel Schubring, Alexandros Papageorgiou, Dmitry Chichinadze, Yilikal Ayino, Chris Conklin, Julie Vievering, Gordon Stecklein, Justin Willmert, Pat Meyers, Peter Hansen, Mahendra Dangi, Edwin Ireson, Alex Gilman, Jared Lafer, Ramsey Jones, Yevhen Kurianovych, Minh Nguyen to hang out, play poker, go camping, and do a bunch of other activities. I am happy to have had Caner Ünal and Vladimir Bychkov as roommates. I especially thank Daniel Schubring for struggling together with me to make the weekly journal club work over the years.

I interacted with more social people outside physics department as well. Some of them are from Turkey and I met some of them thanks to my wife. It helped me see different perspectives on a variety of topics related to society. I would especially like to thank Murat Altun who helped me a great deal when I first arrived in United States. He even took his time to teach me how to drive. I failed the driving test twice before finally passing it, but oh well, he tried.

I am glad to be born late enough to benefit from the advanced technology so that I did not have to stay away from my long-time friends, Ekin Yağmur Gönen, Berk Akgün, Irmak Aykın, Mert Atıl, Umur Yılmaz Çevik, Oytun Yapar, Gökhan Uğurlu, Mehmet Can Yavuz, Mert Şahinkoç, Can Küçükgül, Baran Umut Vardar, even though we were physically separated. Thank you guys for making life more fun than it usually tends to be.

I had not appreciated the benefits of volunteering until I did it once and happened to meet my future wife at a volunteer event. It was Alison Link's struggle to figure out how a physicist struggles. I had long periods of frustration with no idea on how to overcome them. She always tried to make other things easier for me so that I had fewer problems to worry about. When the future was extremely vague for me, she was flexible enough to make the fog bearable. I thank her and her parents, Gene Link and Ann Hirsch, for being a second family to me away from home.

No matter what comes out after all the dust settles down, if you do not know that your family will be there by your side, how do you even dare to take the challenge? I have always known in my heart that my parents, Mediha and Saffet Büyükdağ, and my sister Hande Büyükdağ would trust and support me all the time. What a relief that was. Thank you guys for everything that you provided. I cannot wait to go back and enjoy the beach with you guys as a doctor this time – only to be made fun of for not being the medical kind, like Hande.

Anneme, babama ve kardeşime,
Ailem oldukları için şanslı hissettiğim o güzel insanlar.

Abstract

In this thesis, we explore beyond the Standard Model of particle physics by taking advantage of the holography approach. First of all, we consider a supersymmetric model that uses partial compositeness to explain the fermion mass hierarchy and predict the sfermion mass spectrum. Linear mixing between elementary superfields and supersymmetric operators with large anomalous dimensions is responsible for simultaneously generating the fermion and sfermion mass hierarchies. After supersymmetry is broken by the strong dynamics, partial compositeness causes the first- and second-generation sfermions to be split from the much lighter gauginos and third-generation sfermions. The sfermion mass scale is constrained by the observed 125 GeV Higgs boson, leading to stop masses and gauginos around 10–100 TeV and the first two generation sfermion masses around 100–1000 TeV. This gives rise to a splitlike supersymmetric model that explains the fermion mass hierarchy while simultaneously predicting an inverted sfermion mass spectrum consistent with the Large Hadron Collider and flavor constraints. The lightest supersymmetric particle is a gravitino in the keV to TeV range, which can play the role of dark matter.

This brings us to the second topic that we consider, a novel realization of the Dynamical Dark Matter (DDM) framework in which the ensemble of particles collectively constitute dark matter and they are the composite states of a strongly-coupled conformal field theory. Cosmological abundances for these states are then generated through mixing with an additional, elementary state. As a result, the physical fields of the DDM dark sector at low energies are partially composite. We calculate the masses, lifetimes, and abundances of these states — along with the effective equation of state of the entire ensemble. Our results suggest the existence of a potentially rich cosmology associated with partially composite DDM.

Contents

List of Tables

List of Figures

Chapter 1

Introduction

The article published in 1997 [1] by Juan Maldacena is one of the most cited articles in the field of high energy physics. This article conjectures one of the most studied examples of the holographic principle, the anti-de Sitter / conformal field theory (AdS/CFT) correspondence. A number of modifications can be made on the original correspondence and these have been used as an incredible tool to attack a variety of problems. The underlying concept of this famous AdS/CFT correspondence is the so-called holographic principle. In this thesis, we take advantage of the holographic principle to bring new insights and excitement to the major vastly studied concerns of the Standard Model (SM) of particle physics. We particularly focus on supersymmetry and dark matter along with new attempts to approach the holographic principle at the end.

The Higgs boson discovery at the Large Hadron Collider (LHC) [2, 3, 4] has led to new constraints on the parameter space of supersymmetric models. In particular, the explanation of the 125 GeV Higgs boson requires stop (superpartner of the top quark) masses which are large, $\gtrsim$ 1 TeV, causing a significant increase in the tuning of supersymmetric models. In addition, in order to ameliorate the supersymmetric flavor problem without any additional structure, the first- and second-generation sfermions are required to have masses in the 100–1000 TeV range. Satisfying these two requirements leads to a version of split supersymmetry [5, 6], dubbed *minisplit* [7, 8], which explains the 125 GeV Higgs boson while simultaneously maintaining the successful features of supersymmetric models such as gauge coupling unification and a dark matter candidate. Of course, this comes at the price of a meso-tuning, which may be a sign that we live in a multiverse [6], or instead could possibly be explained by a relaxion mechanism [9, 10].

A knowledge of the sfermion mass spectrum has important implications for collider and

flavor experiments seeking to discover supersymmetry (SUSY). In split supersymmetric models, the supersymmetry-breaking scale occurs near the PeV scale, with sfermion masses in the range of 10–1000 TeV. Even though this hierarchy of sfermion masses seems unrelated to the fermion mass hierarchy, it begs the question as to whether these two hierarchies could in fact be explained by the same mechanism. For example, a novel way to account for the fermion mass hierarchy is the idea of partial compositeness [11]. New strong dynamics is responsible for operators with large anomalous dimensions that linearly mix with elementary fermions. Assuming the Higgs boson is elementary, a large Yukawa coupling then arises for mostly elementary fermion mass eigenstates, while composite fermion mass eigenstates have a correspondingly smaller Yukawa coupling. The hierarchy of Yukawa couplings is therefore explained by a set of operators with large, order-one anomalous dimensions.

If one now further assumes that the strong dynamics is responsible for breaking supersymmetry, then an interesting correlation between fermion and sfermion masses results from partial compositeness. Supersymmetric operators that linearly mix with elementary fermions can now communicate supersymmetry breaking to the elementary sector. In this way, composite sfermions obtain large supersymmetry breaking masses, while mostly elementary sfermions obtain hierarchically smaller soft masses. The fermion mass hierarchy is therefore inversely related to the sfermion mass hierarchy: the light (mostly elementary) stop corresponds to the heavy (mostly elementary) top quark, while the heavy (composite) selectron is related to the light (composite) electron. Together with the fact that gauginos and Higgsinos are predominantly elementary—and therefore lighter than the composite sfermions—a "split" supersymmetric spectrum arises where the fermion mass hierarchy is naturally explained. It is the anomalous dimensions of the corresponding supersymmetric operators that simultaneously controls the fermion and sfermion masses. This contrasts with an alternative approach that radiatively generates fermion masses from a sfermion anarchy [12].

Now let us turn to our second topic of focus, which is dark matter. There are many ongoing experiments trying to observe the dark matter particle directly or indirectly. Each of them updates the constraints on its properties one way or another. This current generation of dark matter experiments also guide us in terms of where to look for new physics beyond the Standard Model (BSM). This is the case since SM does not provide an elementary particle as a dark matter candidate. Even if its mass and how it interacts with other particles are not known yet, the majority of dark matter theories proposes a single stable particle. Otherwise, if the dark matter particle decayed into SM particles early, there are many reasons to think

that the successful cosmological predictions of light element abundances provided by Big Bang Nucleosynthesis (BBN) would be ruined.

Dynamical Dark Matter [13, 14] (DDM) provides an alternative framework for dark matter physics in which the notion of dark matter stability is replaced by something more general and powerful: a balancing of decay widths against cosmological abundances across an ensemble of individual dark matter constituents. Within this framework, those dark-sector states with larger decay widths (shorter lifetimes) must have smaller abundances, while those with smaller decay widths (longer lifetimes) can have larger abundances. This balancing allows the ensemble to exhibit a variety of lifetimes that stretch across all cosmological periods, leading to an extremely "dynamic" universe in which quantities such as the total dark matter abundance Ω evolve non-trivially throughout all periods of cosmological history — all while remaining consistent with experimental and observational constraints.

If such a balancing could only be arranged by adjusting the masses and couplings associated with the individual constituent particles of the ensemble by hand, such a dark matter scenario would clearly require an unacceptable degree of fine-tuning. However, it turns out that large collections of particles with the appropriate balancing between decay widths and abundances arise in a number of top-down scenarios for new physics. In such realizations of the DDM framework, the properties of all the constituent particles within the ensemble are completely specified by only a small number of parameters. The masses, lifetimes, abundances, etc. of these particles scale across the ensemble according to a set of scaling relations. Examples of scenarios which yield a DDM-appropriate set of scaling relations include higher-dimensional theories of an axion or axion-like particle propagating in the bulk [15] in which the Kaluza-Klein (KK) resonances collectively constitute the DDM ensemble [14, 16]; theories with additional fields which transform non-trivially under large, spontaneously-broken symmetry groups, in which the ensemble constituents are the physical degrees of freedom within the corresponding symmetry multiplets [17]; and theories with strongly-coupled hidden-sector gauge groups, in which the ensemble constituents are identified with the "hadrons" which emerge in the confining phase of the theory at low energies [18, 19].

This thesis is organized as follows. In Chapter 2, we give a brief historical overview of SM. Some open problems of the model are mentioned, mainly the ones that this thesis focuses on. Additionally, the holographic principle is introduced in detail. In Chapter 3, we show how supersymmetry can be supplemented with the idea of partial compositeness to achieve a reasonable mass spectrum. An extra dimensional dual theory is then used

to execute the numerical computation. In Chapter 4, similarly we propose a Dynamical Dark Matter model that benefits from partial compositeness. Holography once again lets us calculate the consequences of the modifications. In Chapter 5, alternative holographic bases are analyzed. We speculate on how strong dynamics can give rise to light scalar modes.

Chapter 2

Brief history of the Standard Model and the beyond

A century ago, one of the most fundamental concepts for physicists, Quantum Mechanics (QM), was close to taking its final form. Soon it became a tool to be used to describe a number of phenomena even though there were discussions on what it really meant. At that point, the theory of special relativity was a commonly accepted principle and was verified by experimental findings, so someone needed to make sure that Quantum Mechanics was compatible with the constraints of special relativity. Efforts to make these two free of contradictions led to a description of nature with fields whose excitations are considered as particles. The resulting framework was eventually called Quantum Field Theory (QFT) and different versions of it had to be invented to describe different fundamental interactions of the observed particles.

That the first application of QFT was on electrons and photons was probably inevitable since the number of known particles at the time was limited. Even though it started with the purpose of describing the process of the electron's interaction with the photon, eventually the final form of the theory, Quantum electrodynamics (QED), described the interaction of all the electrically charged particles with the photon. QED was used to predict a number of quantities extremely accurately; due to this level of success it was called "the jewel of physics" by Richard Feynman. Despite its success with predictions, the calculations included confusing infinities, which was taken care of by developing renormalization methods. Another outcome of this approach was how fruitful the idea of using internal symmetries on top of the known symmetries of spacetime was. In the case of QED, the underlying symmetry was described by the abelian Lie group, $U(1)$.

How electrons interact with photons was not the only known type of interaction. β-decay was another known mechanism that describes how a certain element decays into a different element. However, the discovery of the exact subatomic interaction called weak interaction had to wait for a few decades. The observation of the proton and neutron was a step towards understanding β-decay, which led Enrico Fermi to come up with a four-fermion interaction. This type of contact force with no range was improved later to a non-contact force with a finite range inspired by the symmetry ideas that worked for the electrodynamics. In this case, however, the symmetry would be described by the non-abelian Lie group, $SU(2)$. That was not the end of the story, since it was soon discovered that the electrodynamics and the weak interaction can be unified. The unified theory had the $U(1) \times SU(2)$ symmetry and was called the electroweak interaction. Some of the elementary particles involved in these interactions were observed a few decades later.

The next type of interaction followed from the discovery of a large number of new particles called hadrons. Initially different ways of classifying these hadrons were proposed. These classification attempts led to the assumption of new elementary particles called quarks that make up the hadrons. Soon it was realized that quarks need to possess an additional quantum number called color. The absence of an observation of a free quark caused disagreements on whether quarks are real particles or mere mathematical tools. The concept of confinement was believed to explain why quarks cannot be broken away from hadrons at low energies and some indirect experimental relations implied that quarks are indeed particles. The high energy limit of the interactions, on the other hand, showed a different behavior where the quarks interacted with each other weakly. This was the discovery of asymptotic freedom. In this regime, how quarks interacted with each other was again explained by recognizing a certain symmetry. It was more complicated than the earlier symmetries and was described by a non-abelian $SU(3)$ Lie group.

How symmetries had central importance has been described in the previous paragraphs for three different interactions. However, the story was slightly different for the weak interaction. Initial attempts to apply the $SU(2)$ symmetry did not really work since the force carriers (gauge bosons) of the theory were observed to be massive. This contradicted the usual expectation for the theories with internal symmetries that had massless gauge bosons like photon. One either had to give up the idea of using a symmetry to describe the weak interaction or had to come up with an answer to what breaks the symmetry. Three different research groups proposed a new type of particle with spin-0, unlike the known matter particles and gauge bosons with spin-1/2 and spin-1 respectively, to solve the puzzle

of symmetry breaking. It took approximately half a century for this new particle called the Higgs boson to be observed but successful predictions of the theory helped it to be widely accepted quickly. The main conclusion of these works was that the $SU(2)$ symmetry responsible for the weak interaction was there only at high energies. Not observing this symmetry at low energies explicitly was therefore explained by the electroweak symmetry breaking (EWSB) mechanism.

After all of this progress, finally the so called Standard Model of particle physics was born. The aforementioned three of four known fundamental forces in the universe and all the known elementary particles are included in this model with huge experimental success. The fourth fundamental force is the gravitational force; however, the theory of general relativity that describes gravity is still a classical theory. There are candidates for quantum gravity but the final word is yet to be said. Despite the incredible success, the SM is not able to explain all the phenomena observed in the universe even if we do not care about quantum gravity. Physicists like myself are glad there are still open questions not answered by the SM, for we would not know what to do in our free time otherwise.

2.1 Shortcomings of the Standard Model, and its antidotes

Usually two types of open problems keep the minds of particle physicists busy. The first one is about the parameters of the SM, e.g. particle masses, mixing angles, etc. Generally one wonders why a certain parameter is small or large, and the SM does not provide an answer for a number of cases. The second problem is about certain observed phenomena which cannot be explained by the SM's particle content or its interactions. These require new particles or modifications of the SM parameters depending on the problem.

2.1.1 How did the electron manage to stay so skinny compared to its cousin the top quark?

The fermions of the SM, f, acquire their masses via their interactions with the Higgs boson, H, described by a term in Lagrangian,

$$\mathcal{L} \supset -y_f f \bar{f} H, \tag{2.1}$$

where y_f is the Yukawa coupling. In particular, different masses are given by different Yukawa interaction strengths times the vacuum expectation value (VEV), $v \approx 174$ GeV, of

	y_f
e	2.8×10^{-6}
u	8.0×10^{-6}
d	1.6×10^{-5}
s	3.3×10^{-4}
μ	5.9×10^{-4}
c	3.7×10^{-3}
τ	1.0×10^{-2}
b	1.7×10^{-2}
t	1.0×10^{0}

Table 2.1: Yukawa couplings for SM fermions at the energy scale, $M_Z \approx 91$GeV.

the Higgs field, $m_f = y_f \langle H \rangle$. The stronger the interaction is, the heavier the particle. Masses of the fermions are known from measurements, and they are quite different for no apparent reason. For example, Yukawa couplings for different fermions can be seen in Table 2.1, where the values are calculated in the minimal subtraction ($\overline{\text{MS}}$) renormalization scheme at the energy scale, $M_Z \approx 91$ GeV [20]. While the lightest fermion (ignoring neutrinos for the moment) is the electron, with a pole mass ~ 0.5 MeV, the heaviest fermion is the top quark with a pole mass ~ 173 GeV. The ratio of the Yukawa coupling for the top quark to the one for the electron again at the energy scale of ~ 91 GeV is $y_t/y_e \sim 3.6 \times 10^5$, which is a large number that makes some particle physicists uncomfortable. This fermion mass hierarchy can be squeezed into small differences between new parameters. Two different approaches that can accomplish this are to consider the SM in an extra dimensional spacetime and to introduce partial compositeness into the world of elementary particles. In Section 2.2 and Chapter 3, we explain these approaches in detail and show how they are equivalent to each other.

2.1.2 What's up with Higgs' mass?

The mass of the Higgs boson is one of the SM parameters. Observation of the Higgs boson at the LHC in 2012 let us measure the mass to be $m_H \sim 125$ GeV. However, theoretically the value of this mass term is very sensitive to Higgs' interactions with other particles [21]. For example, quantum corrections due to its interactions with SM fermions can be calculated by considering the type of Feynman diagrams given in Figure 2.1. Contribution by this diagram would be in the following form,

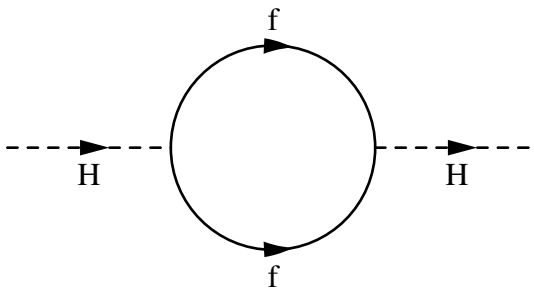

Figure 2.1: Radiative corrections to the mass of the Higgs boson from fermion loops.

$$\Delta m_H^2 = -\frac{|y_f|^2}{8\pi^2}\Lambda_{\rm UV}^2 + ... \tag{2.2}$$

where ellipses imply the corrections that depend on $\Lambda_{\rm UV}$ at most logarithmically. $\Lambda_{\rm UV}$ is considered as the ultraviolet energy cutoff above which new physics (new particles, interactions, etc.) shows up. A naive scale that comes to mind first for this cutoff is the Planck scale, $M_P \sim 10^{18}$ GeV. In this scenario, the quantum corrections to the Higgs mass is much larger than the observed mass. This is really different from the case of the other SM particles. The quantum corrections for them depend only on $\log(M_P/100\ \text{GeV})$, which is much more innocent. However, the issues with the Higgs mass would also indirectly affect the other particles' masses since the elementary particles acquire their masses via the Higgs mechanism. These types of concerns initiated many novel concepts which have become a whole new research field over time. The major research direction on this topic has been to introduce a new symmetry – no less than a *super*symmetry – on top of the existing symmetries of SM. In Chapter 3, we shed light on supersymmetry and how our research contributes to it.

2.1.3 What is it that we do not see? (Spoiler: Dark Matter (DM))

The idea that there is more than what we see with our telescopes dates as far back as the end of the nineteenth century. It was Lord Kelvin who calculated the total mass in the Milky Way galaxy roughly by looking at how the stars move. His conclusion was that this is different

from the estimated total mass of what we see, mainly the stars. Similar considerations of the stellar velocities in the early twentieth century led the astrophysicists of the day to start using the term "dark matter". Dark matter meant the existence of extra matter that is not observed by existing astronomical instruments but that is implied by a number of its effects on visible objects. To name a few, these effects can be seen when one looks into galaxy rotation curves, gravitational lensing, structure formation, etc. Today's observations and calculations indicate that 27% of the universe's energy budget belongs to dark matter.

A good portion of the physics community thinks now that dark matter is composed of elementary particles which are not included in the SM particle content. Whether dark matter particles interact with the known particles other than gravitationally is one of the major questions. Not being visible strongly implies that those other interactions, if they exist, must be tiny. Even if we do not know much about the interactions of dark matter particles, there is a way of classifying them based on their free streaming length. This would be translated as dark matter being "hot", "warm" or "cold", depending on how fast the particles move, where "hot" means the fastest. The widely accepted ΛCDM model of cosmology refers to the "cold" dark matter (CDM). Understanding what dark matter really is is one of the major research efforts of our era and it is becoming ever more popular. Our approach in Chapter 4 combines a few different concepts such as partial compositeness, extra dimensions, and the idea that the dark matter sector is multi-component, which produces interesting predictions and consequences.

2.1.4 And the rest which physicists struggle with

One of the topics that is not yet completely understood is the concept of dark energy. Historically Einstein used the freedom to add a "cosmological" constant to his field equations of general relativity to have a stable universe. However, Hubble's observations later would reveal that the universe is not stable and is actually expanding. The need for the cosmological constant disappears temporarily only to come back eventually to describe the accelerating expansion of the universe. The constant is usually interpreted as the energy density of empty space, so-called dark energy. It makes up 68% of the total energy density, however, the nature of this energy is still mysterious.

Another open research direction is about neutrinos. Initially, β-decay was really puzzling since it looked like energy is not conserved. It took some time to observe neutrinos after their existence was proposed by Pauli to explain the energy conservation in β-decay. For quite a while, they were considered to be massless, so the SM does not have a mass parameter for

neutrinos. The discovery of neutrino oscillations required them to be massive and the SM alone was not enough for a complete description anymore. How neutrinos become massive is still not clear. Whether they are Majorana or Dirac fermions is therefore not known as of today.

The matter-antimatter asymmetry problem is something that gives physicists a headache as well. Even though the SM does not differentiate between matter particles and antimatter particles, the observable universe has mostly matter instead of equal amounts of matter and antimatter. We are glad that we are safe and we do not need to worry about being annihilated by antimatter, but it would be nice to understand why this is the case. These and many more problems are attacked by supplementing the SM with creative new physics ideas all the time.

2.2 Two sides of the same coin

Stephen Hawking and Jacob Bekenstein's complementary work on black hole thermodynamics led to the following famous formula on the entropy of a black hole,

$$S_{\mathrm{BH}} = \frac{k_B A}{4 l_P^2}, \tag{2.3}$$

where k_B is Boltzmann's constant and l_P is the Planck length. The lesson to be learned was that entropy is proportional to the area of the event horizon. This result, combined with the Bekenstein bound on entropy, was the starting point for the holographic principle. Bekenstein came up with an upper bound on the entropy that something with a finite energy can have in a finite region of space. That the black hole entropy saturates this upper bound was the crucial ingredient, which meant that everything you can learn from the volume of a spacetime can be encoded on the boundary of that spacetime.

Gauge/gravity duality is a way of describing the relation between two theories that exist on spacetimes with a different number of dimensions. For example, a theory of gravity in $d + 1$ dimensional spacetime would be dual to a gauge theory without gravity that lives in the d dimensional boundary of it. The two sides include different degrees of freedom and different interactions, however, the duality implies that certain physical observables are calculated to be the same. This remarkable connection lets us understand certain results from two different perspectives with particular advantages. One might prefer the side with gravity due to the ease of calculations, on the other hand, one might choose the side without gravity for a more physical description of the phenomena. All of this results in a dictionary

with entries that translate two sides to each other.

2.2.1 Everyone needs a little bit of string theory, but be careful with excessive doses!

AdS/CFT correspondence is the most famous example of the holographic principle, as we mentioned in Chapter 1. This is a conjecture that originates from supersymmetric string theory in ten-dimensional spacetime. The duality between a theory of gravity and a gauge theory can be summarized as [22],

$$\text{type IIB string theory on } \mathrm{AdS}_5 \times S^5 \Longleftrightarrow \mathcal{N} = 4 \quad SU(N) \text{ 4D gauge theory,} \tag{2.4}$$

where S^5 is the five-dimensional (5D) sphere and $\mathcal{N}$ is the number of supersymmetry generators. The parameters for the theory in AdS_5 space are the curvature scale, k, and the string length, l_s, while the parameters for the gauge theory are the Yang-Mills coupling, g_{YM}, and N. Duality requires the following relation between these parameters,

$$\frac{1}{k^2 l_s^2} = 4\pi g_{\mathrm{YM}}^2 N \,. \tag{2.5}$$

Other than the relation between these parameters, $\mathcal{N} = 4$ supersymmetric gauge theory is symmetric under conformal transformations in four dimensions that matches the isometry group of AdS_5 space. Moreover, the R-symmetry group of the supersymmetric gauge theory is $SU(4) \equiv SO(6)$, which also describes the isometry group of S^5 space. One limit to consider for this duality would be the effective low energy limit of the string theory, $k \ll 1/l_s$, so that we only deal with gravity instead of individual strings. Eq.(2.5) tells us that in this case we are in the strong coupling limit, $g_{\mathrm{YM}}^2 N \gg 1$, of the gauge theory. Therefore, using AdS/CFT correspondence we can map a strongly coupled field theory to a higher dimensional gravity theory where calculations are likely to be more tractable.

2.2.2 Holography for humble people with no strings attached

One of the complicated compactifications of the ten-dimensional string theory gives rise to a five-dimensional geometry called "warped throat". This can be pictured as a slice of an AdS_5 space. Let us consider a warped five-dimensional spacetime (x^μ, y), where $\mu = 0, 1, 2, 3$ are the four-dimensional (4D) coordinates and $-\pi R \leq y \leq \pi R$ is the coordinate of an extra

dimension compactified on a $S^1/\mathbb{Z}_2$ orbifold of radius R. The spacetime metric is anti-de Sitter, given by

$$ds^2 = e^{-2k|y|}\eta_{\mu\nu}\,dx^\mu\,dx^\nu + dy^2 \equiv g_{MN}\,dx^M\,dx^N\,, \tag{2.6}$$

where capital Latin indices $M = (\mu, 5)$ label the 5D coordinates. The 5D spacetime is a slice of AdS_5 geometry, bounded by two 3-branes located at the orbifold fixed points: a UV brane at $y = 0$ and an IR brane at $y = \pi R$.[1]

The cutoff scale of the UV brane is $\Lambda_{\mathrm{UV}} = M_5$, where M_5 is the 5D Planck scale, while the scale of the IR brane is $\Lambda_{\mathrm{IR}} = \Lambda_{\mathrm{UV}}e^{-\pi kR}$. The 4D reduced Planck mass, M_P, is given by [26]

$$M_P^2 = \frac{M_5^3}{k}\left(1 - e^{-2\pi kR}\right) \approx \frac{M_5^3}{k}\,, \tag{2.7}$$

where we are assuming $\pi kR \gg 1$. Note that this expression is consistent with the result Eq.(3.51) derived from partial compositeness.

The natural objects of interest in the five-dimensional theory is the fields, $\Phi(x^\mu, y)$, that live in the bulk. On the contrary, four-dimensional conformal field theory is described by operators, $\mathcal{O}(x)$, with certain scaling dimensions, Δ. These objects can be mapped to each other by duality,

$$\Phi \leftrightarrow \mathcal{O} \quad \text{with} \quad g_5\Phi(x^\mu, y_{\mathrm{UV}}) = \phi_s(x^\mu)\,, \tag{2.8}$$

where ϕ_s is the source field for the operator $\mathcal{O}$, g_5 is an expansion parameter with $\dim[g_5] = -1/2$, and y_{UV} is the location of the UV brane. While for the original AdS/CFT correspondence the boundary of the fifth dimension is at $y_{\mathrm{UV}} \to -\infty$, in our slice of AdS_5 space, $y_{\mathrm{UV}} = 0$. The AdS/CFT correspondence can therefore be expressed as the following relation between the four- and five-dimensional theories,

$$e^{-\left(\mathcal{S}_{\mathrm{holo}}[\phi_s] - \mathcal{S}_{\mathrm{holo}}[\phi_s=0]\right)} = \left\langle e^{-\int d^4p\ \frac{1}{\Lambda_{\mathrm{UV}}^{\Delta-3}}\phi_s\mathcal{O}} \right\rangle, \tag{2.9}$$

where $\mathcal{S}_{\mathrm{holo}}$ is the on-shell action after the bulk equations of motion are solved. One can learn a great deal of information from this relation, for example calculating the n-point functions of the operators, $\langle\mathcal{O}...\mathcal{O}\rangle$, of a strongly coupled gauge theory becomes an easier task to accomplish. A thorough analysis of the duality is given in Chapter 5.

[1] We do not specify a particular mechanism to stabilize the extra dimension. In a supersymmetric theory, one possibility is supersymmetrization of the Goldberger-Wise mechanism [23, 24, 25].

Chapter 3

Supersymmetry, what is so super about this symmetry?

The trouble with the radiative corrections from fermion loops to Higgs mass is mentioned in Section 2.1.2. The insight behind supersymmetry can be seen by looking at the radiative corrections from scalar loops this time as shown in Figure 3.1. Contribution by this diagram would be in the following form [21],

$$\Delta m_H^2 = \frac{y_S}{16\pi^2}\Lambda_{\rm UV}^2 + \ldots \tag{3.1}$$

where y_S is the coupling for the interaction between the scalars, S, and the Higgs described by a Lagrangian term, $-y_S|H|^2|S|^2$, and ellipses imply the corrections that depend on $\Lambda_{\rm UV}$ at most logarithmically. The key here is the sign difference between these two quadratic divergences, Eq.(2.2) and Eq.(3.1), for large $\Lambda_{\rm UV}$ considering that the sign of y_S is restricted to be positive to bound the scalar potential from below. If one comes up with a symmetry that relates every fermion to two of such scalars with $y_S = |y_f|^2$, these two radiative contributions cancel each other. What else can compete with such a precise cancellation? Only the cancellation that also holds for all higher loops of radiative corrections. This is simply what supersymmetry offers us.

Similar to how the momentum operator is the generator of the translational symmetry of the spacetime, the spinor operator, Q, is the generator of the supersymmetry that transforms bosons and fermions into each other in the following way,

$$Q|\text{fermion}\rangle = |\text{boson}\rangle \quad \text{and} \quad Q|\text{boson}\rangle = |\text{fermion}\rangle\,. \tag{3.2}$$

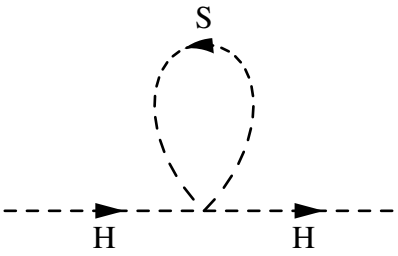

Figure 3.1: Radiative corrections to the mass of the Higgs boson from scalar loops.

These are called superpartners. The superpartner of a SM fermion is called "sfermion", which follows the general rule of naming convention for specific sfermions like the superpartner of electron, "selectron". On the other hand, bosons of SM have superpartners under the name of "bosino", again following the convention for specific bosinos like the superpartner of Higgs, "Higgsino". Then the irreducible representations of the supersymmetry algebra include even numbers of fermions and bosons, which are called supermultiplets. For the simplest case of only one supersymmetry generator, $\mathcal{N} = 1$, these supermultiplets contain only one fermion and one boson. For example, a supermultiplet that consists of a spin-1/2 Weyl fermion and a spin-0 complex scalar is called a chiral supermultiplet. A supermultiplet with a spin-1/2 Weyl fermion and a spin-1 real vector is called a vector supermultiplet. If the vector boson is a massless gauge field of SM, its superpartner is called "gaugino". Another type of supermultiplet would be the gravity supermultiplet (if gravity is included in the theory), which has a spin-2 graviton and its superpartner spin-3/2 "gravitino".

We discussed in Chapter 2 that two of the three symmetry groups of SM, $U(1) \times SU(2)$, describe the electroweak interactions above the energy scale of roughly a few hundred GeV. Gauge couplings g' and g represent the strengths of the interactions described by the symmetry groups $U(1)$ and $SU(2)$ respectively. If one solves SM renormalization group equations, it can be seen that these two couplings take the same value around the energy scale of 10^{13} GeV [21]. This is nice, since it means that two different symmetry groups had the same coupling before the universe cooled down to lower energies. Only one parameter instead of two is more economical and simpler. However, the gauge coupling (interaction strength) of the third symmetry group, $SU(3)$, does not meet the other two to give an even simpler explanation. Our hero, supersymmetry, helps here as well. The Minimal Supersymmetric Standard Model (MSSM) is the simplest supersymmetric extension of the SM with only one generator, $\mathcal{N} = 1$, which has the right particle content to make the magic happen. It modifies the differential equations that determine how the gauge couplings evolve

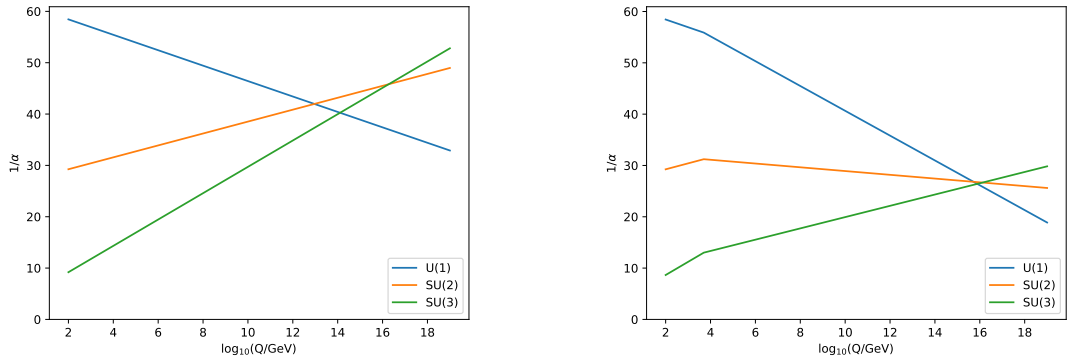

Figure 3.2: Two-loop renormalization group evolution of the inverse gauge couplings $1/\alpha_a$ in the SM (on the left) and the MSSM (on the right), where $\alpha_a = g_a^2/(4\pi)$ and Q is the renormalization scale. In the MSSM case, the sparticle masses are treated as a common threshold at 5 TeV [21].

with the energy scale so that all three meet at a higher energy scale (grand unified theory scale $\sim 10^{16}$ GeV) to be a single gauge coupling fundamentally. This effect can be seen in Figure 3.2. This so-called gauge coupling unification is another benefit of supersymmetry.

In Chapter 2, we mentioned that there is a tremendous effort to understand what the dark matter particle is. One of the candidates was the idea of Weakly Interacting Massive Particles (WIMPs) that were produced thermally in the early universe. If these particles interact with the SM particles via electroweak force on top of the gravitational interaction, their mass is required to be around 100 GeV for the correct DM abundance. This matched the initial expectation for the mass of new particles in the simplest supersymmetric extensions of the SM very well so that this was called a "WIMP miracle". The absence of the observation of such particles forced physicists to make the models more complicated, however, supersymmetry still supplies a new particle as a dark matter candidate. Since in the supersymmetric models with a certain parity called "R-parity" (where SM particles and their superpartners have opposite parities) the lightest supersymmetric particle (LSP) is absolutely stable, such an electrically neutral stable LSP is an attractive candidate for a cold dark matter. Three possible types of such particles are the lightest sneutrino, the gravitino and the lightest neutralino (superpartners of the electrically neutral gauge bosons of the electroweak interaction and neutral Higgsino). Direct searches mostly ruled out the sneutrino option in simpler models of supersymmetry. The remaining two have their advantages and disadvantages in model building. Gravitino as a dark matter particle might need to be considered more and more often in the absence of observation, since its interaction with SM particles is much weaker

compared to a neutralino dark matter.

The supersymmetry generator, Q, commutes with the generators of gauge transformations in the SM, so particles in a supermultiplet have the same SM quantum numbers, e.g. electric charge, color charge, etc. Moreover, it commutes with the squared mass operator, $-P^2$, which means that the superpartners have the same mass. However, this implication rings the alarm bells since we have not observed selectron with mass ~ 0.5 MeV even with our very sophisticated particle accelerators (or any other superpartner that has the same mass with its SM partner). This implies that the supersymmetry must be broken at a higher energy scale and it is not observed at the lower energies. Details of the mechanism that breaks supersymmetry are not known, while the consequences dictate the superpartners to be heavy enough to avoid detection so far. For example, one of the recent results from the LHC shows that, for simplified supersymmetric models, the lower bound for the stop mass is around 1.25 TeV, for a Bino with a mass below 200 GeV [27]. Moreover, long-lived gluino masses are bounded from below by ~ 2 TeV [28]. Qualitatively these limits will place an effective lower bound on the soft mass scale of our model. Certain assumptions about the supersymmetry breaking mechanism such as that a new strongly coupled QCD-like gauge theory is responsible for it have phenomenological benefits. Combined with the idea of partial compositeness for SM particles, this assumption about the nature of the supersymmetry breaking mechanism would be handy to explain the inverted hierarchy of the superpartner mass spectrum. This can be contrasted with the electroweak symmetry breaking mechanism where an elementary particle, Higgs, is responsible. Therefore, the same framework would explain the ordinary fermion mass hierarchy as well.

3.1 Higgs confirmed his attendance but SUSY is a maybe

A four-dimensional description of partial compositeness for the fermion mass hierarchy was previously considered in [22, 29]. In this chapter, we generalize this description to the supersymmetric case, using results from [30]. Assuming that electroweak symmetry is broken in the elementary sector (with an elementary Higgs), we consider the linear mixing of elementary superfields with supersymmetric operators in the 4D gauge theory. This mixing is responsible not only for the fermion mass hierarchy but also for the transmission of the (dynamical) supersymmetry breaking in the composite sector to the elementary sector. This leads to relations that determine the fermion and sfermion mass hierarchy in terms of the anomalous dimensions of supersymmetric operators. These types of theories are similar to

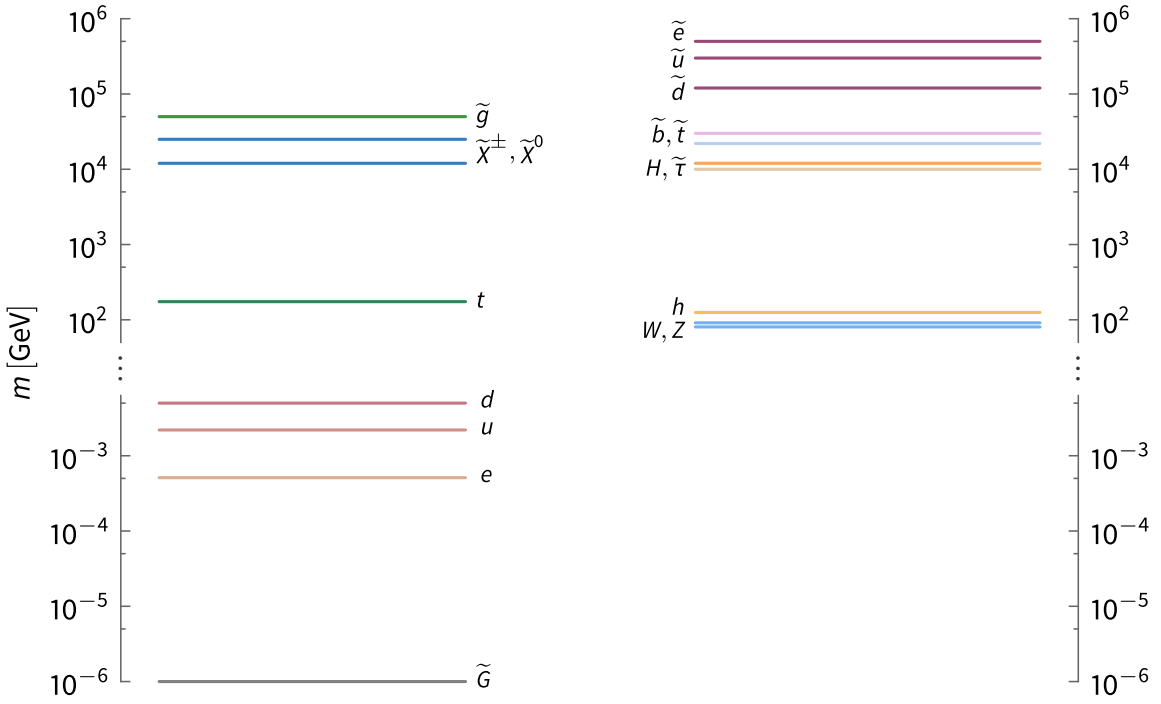

Figure 3.3: Schematic diagram depicting a possible particle spectrum of the partially composite supersymmetric model. The left (right) column depicts the fermions (bosons). The sfermion mass hierarchy is inversely related to the fermion mass hierarchy and the LSP is the gravitino.

single-sector models of supersymmetry breaking, which were originally proposed in [31, 32] and further studied in [33, 34, 35, 36, 37]. A shortened version of this work summarizing the main results can be found in [38].

The nonperturbative nature of the strong dynamics only allows the sfermion mass spectrum to be qualitatively determined. To obtain a more detailed sfermion spectrum that is consistent with a 125 GeV Higgs boson, we use the anti-de Sitter/conformal field theory correspondence to model the strong dynamics associated with partial compositeness in a slice of five-dimensional anti-de Sitter space [26]. The supersymmetric Higgs sector is localized on the UV brane, while supersymmetry breaking is confined to the IR brane. The supersymmetric matter fields are bulk fields with the top quark (light fermions) localized near the UV (IR) brane. In the dual, five-dimensional gravity description, the overlap of fermion profiles [39] with the UV-localized Higgs field mimics the partial compositeness and explains the fermion mass hierarchy [40]. The Standard Model Yukawa couplings are used to constrain the bulk fermion profiles, which then determine the soft masses at the IR

scale. Both the Higgs-sector soft masses and the soft trilinear scalar couplings arise at loop order, due to radiative corrections from the bulk that transmit the breaking of supersymmetry. Renormalization group evolution is then used to run the soft masses down to the electroweak scale and obtain the 125 GeV Higgs boson mass.

Using this procedure, we analyze two benchmark scenarios: one for the case that the gaugino masses arise from a singlet spurion and the other in nonsinglet spurion case. We find that the observed Higgs boson mass naturally accommodates sparticle spectra that hierarchically suppress the masses of the stops and the other third-generation sfermions below the mass scale of the first- and second-generation sfermions. In particular, if the masses of the first- and second-generation sfermions are restricted to be above 100 TeV to additionally suppress flavor-changing neutral currents that arise in supersymmetric models, the stop masses lie in the range of 20–100 TeV, while the masses of the lightest stau and neutralino may be as low as 10 TeV. Previous attempts to explain the sfermion mass hierarchy in a slice of AdS_5, before the Higgs boson mass was known, were considered in [33, 34]. The results presented in this chapter were the first predictions for the sfermion mass spectrum from partial compositeness that are compatible with a 125 GeV Higgs boson. Additionally, we included for the first time the full one-loop radiative corrections to the bulk scalar soft masses squared, the Higgs-sector soft terms, and the soft trilinear scalar couplings. For stops and other UV-localized sfermions, these corrections provide the dominant soft mass contributions, and accordingly have important phenomenological consequences. For the Higgs sector, they control the breaking of electroweak symmetry.

A schematic diagram of a possible mass spectrum in the partially composite supersymmetric model is depicted in Figure 3.3. It assumes an elementary Higgs sector interacting with a mostly elementary top quark sector (UV localized). The first- and second-generation fermions are composites (IR localized) of a strongly coupled sector that is also responsible for dynamically breaking supersymmetry. The strong dynamics therefore leads to a sfermion mass spectrum that is inversely related to the fermion mass spectrum. Furthermore, the graviton supermultiplet is elementary, and, since it couples gravitationally, the gravitino receives a small supersymmetry-breaking contribution, becoming the lightest supersymmetric particle with a mass $\gtrsim 1$ keV. This differs from other split-supersymmetry models where the gravitino is usually the heaviest superpartner. Finally, even though the first two generations of matter are composite, gauge coupling unification still occurs at approximately 10^{16} GeV, as in the usual supersymmetric Standard Model (assuming any underlying strong dynamics is SU(5) symmetric). It should also be noted that the elementary matter is present at the

grand unified theory (GUT) scale with order-one Yukawa couplings. This helps one avoid the tension that occurs from Yukawa coupling unification in the usual grand unification scenarios, where the lighter first two fermion generations are elementary (i.e. do not mix with a composite sector), and consequently have tiny Yukawa couplings at the GUT scale.

The rest of this chapter is summarized as follows: in Section 3.2, we review the idea of partial compositeness in the context of the fermion mass hierarchy. This is then generalized to a supersymmetric model when supersymmetry is assumed to be broken by the strong dynamics. This gives rise to a sfermion mass hierarchy that inverts the fermion mass ordering. We then construct the gravitational dual of this model in a slice of AdS_5 in Section 3.3. In Section 3.4, we summarize the constraints arising on the parameter space from various phenomenological and theoretical requirements. We select two representative benchmark scenarios and perform a full numerical analysis. We conclude by presenting the resulting spectra.

3.2 Looks like electron's sibling selectron ate all the food

3.2.1 The fermion mass hierarchy

We begin by briefly reviewing how partial compositeness explains the fermion mass hierarchy [22, 29]. Consider two sectors, an elementary sector with a Weyl fermion ψ and a composite sector with a (charge-conjugate) fermion operator $\mathcal{O}^c_\psi$. The scaling dimension of the fermion operator is written as $3/2 + \delta$, where δ denotes the deviation from the canonical scaling dimension. The Lagrangian at the UV scale, $\Lambda_{\rm UV}$, is taken to have the form

$$\mathcal{L}_\psi = i\psi^\dagger \bar{\sigma}^\mu \partial_\mu \psi - \frac{1}{\Lambda_{\rm UV}^{\delta-1}} \left(\psi \mathcal{O}^c_\psi + \text{h.c.} \right) , \tag{3.3}$$

where the Minkowski metric $\eta_{\mu\nu} = \text{diag}(-,+,+,+)$ and an order-one UV coefficient has been assumed in the second term. The mixing term in Eq.(3.3) means that after confinement at an IR scale, $\Lambda_{\rm IR}$, the mass eigenstates are an admixture of elementary and composite states. This is analogous to γ-ρ mixing in QCD. To obtain analytic estimates of this mixing, the strong dynamics is assumed to be described by a large-N gauge theory, where N is the number of colors. In the large-N limit, the two-point function for a composite operator, $\mathcal{O}$ can be written as $\langle \mathcal{O}(p)\, \mathcal{O}(-p) \rangle = \sum_n a_n^2/(p^2 + \widetilde{m}_n^2)$ to leading order in $1/N$, where $a_n = \langle 0|\mathcal{O}|n\rangle \propto \sqrt{N}/(4\pi)$ is the matrix element for $\mathcal{O}$ to create the $n^{\rm th}$ state from the vacuum

and $\widetilde{m}_n$ is the mass of that state [41].

Applying these results to fermions, we consider a simple three-state system containing an elementary Weyl fermion ψ, together with a lowest-lying composite Dirac fermion $(\widetilde{\psi}_1, \widetilde{\psi}_1^c)$, with mass, $\widetilde{m}_{\psi 1} = g_{\psi 1}\Lambda_{\rm IR}$, where $g_{\psi 1}$ is an order-one coupling. Note that having a composite Dirac fermion follows from assuming that the strong dynamics does not break any Standard Model gauge symmetries. The Lagrangian at the scale $\Lambda_{\rm IR}$ is given by

$$\mathcal{L}_\psi = i\psi^\dagger \bar{\sigma}^\mu \partial_\mu \psi + i\widetilde{\psi}_1^\dagger \bar{\sigma}^\mu \partial_\mu \widetilde{\psi}_1 + i\widetilde{\psi}_1^{\dagger c} \bar{\sigma}^\mu \partial_\mu \widetilde{\psi}_1^c - \varepsilon_\psi \Lambda_{\rm IR} \left(\psi \widetilde{\psi}_1^c + \text{h.c.}\right) - \widetilde{m}_{\psi 1} \left(\widetilde{\psi}_1 \widetilde{\psi}_1^c + \text{h.c.}\right). \tag{3.4}$$

The dimensionless coupling ε_ψ is defined at the IR scale to be

$$\varepsilon_\psi \equiv \widetilde{\varepsilon}_\psi(\Lambda_{\rm IR})\, \frac{\sqrt{N}}{4\pi} = \frac{1}{\sqrt{Z_\psi}} \left(\frac{\Lambda_{\rm IR}}{\Lambda_{\rm UV}}\right)^{\delta-1} \frac{\sqrt{N}}{4\pi} \approx \frac{1}{\sqrt{\zeta_\psi}} \sqrt{\frac{\delta - 1}{\left(\frac{\Lambda_{\rm IR}}{\Lambda_{\rm UV}}\right)^{2(1-\delta)} - 1}}, \tag{3.5}$$

where the running parameter $\widetilde{\varepsilon}_\psi(\mu)$ satisfies

$$\mu \frac{d\widetilde{\varepsilon}_\psi}{d\mu} = (\delta - 1)\widetilde{\varepsilon}_\psi + \zeta_\psi \frac{N}{16\pi^2}\, \widetilde{\varepsilon}_\psi^3, \tag{3.6}$$

and ζ_ψ is an order-one constant due to the (unknown) strong dynamics [29], and the coefficient Z_ψ is the wavefunction renormalization of the elementary fermion. In the final expression we have taken the large-N approximation of Z_ψ.

The diagonalization of the Lagrangian, Eq.(3.4), generates fermionic admixtures of the elementary and composite states [42]. In particular, the massless fermion eigenstate is given by

$$|\psi_0\rangle \approx \mathcal{N}_\psi \left\{|\psi\rangle - \frac{\varepsilon_\psi}{g_{\psi 1}} |\widetilde{\psi}_1\rangle\right\} \approx \mathcal{N}_\psi \left\{|\psi\rangle - \frac{1}{g_{\psi 1}\sqrt{\zeta_\psi}} \sqrt{\frac{\delta - 1}{\left(\frac{\Lambda_{\rm IR}}{\Lambda_{\rm UV}}\right)^{2(1-\delta)} - 1}}\, |\widetilde{\psi}_1\rangle\right\}, \tag{3.7}$$

where $\mathcal{N}_\psi$ is a normalization constant. This expression shows that for $\delta \geq 1$ the mass eigenstate is mostly elementary, while for $0 \leq \delta < 1$ the state has a sizeable composite admixture. These admixtures play a crucial role in determining mass hierarchies.

At the UV scale, the chiral elementary fermions $\psi_{L,R}$ are coupled to the elementary Higgs field H via the Yukawa interaction $\lambda \psi_L \psi_R H$, where λ is an order-one proto-Yukawa coupling and the Higgs field is assumed to develop a vacuum expectation value $\langle H \rangle = v/\sqrt{2}$. Diagonalizing the fermion Lagrangian at the IR scale with the Higgs contribution gives the

fermion mass expression

$$\hat{m}_{\psi 0} \approx \frac{\lambda}{\sqrt{Z_L Z_R}} \frac{v}{\sqrt{2}} \mathcal{N}_\psi^2 \approx \begin{cases} \dfrac{\lambda}{\zeta_\psi}(\delta - 1)\dfrac{16\pi^2}{N}\dfrac{v}{\sqrt{2}} & \delta \geq 1 \\ \dfrac{\lambda}{\zeta_\psi}(1 - \delta)\dfrac{16\pi^2}{N}\dfrac{v}{\sqrt{2}}\left(\dfrac{\Lambda_{\rm IR}}{\Lambda_{\rm UV}}\right)^{2(1-\delta)} & 0 \leq \delta < 1\,, \end{cases} \tag{3.8}$$

where for simplicity we have assumed that $\delta \equiv \delta_L = \delta_R$, $g_{\psi 1} \equiv g_{\psi_L 1} = g_{\psi_R 1}$, $\varepsilon_\psi \equiv \varepsilon_{\psi_L} = \varepsilon_{\psi_R}$, and we explicitly included the normalization factor from Eq.(3.7). The wavefunction coefficients $Z_{L,R}$ are approximated as in Eq.(3.5), and for $0 \leq \delta < 1$ we have assumed $\varepsilon_\psi \lesssim g_{\psi 1}$. Notice that when $\delta \geq 1$ there is no power-law suppression in the Yukawa coupling since the mass eigenstates are mostly elementary and have order-one couplings to the elementary Higgs field. This, for instance, would explain the Yukawa coupling of the top quark. This contrasts with the case $0 \leq \delta < 1$, where the mass eigenstates have a sizeable composite admixture with a power-law suppressed Yukawa interaction (due to the fact that the proto-Yukawa coupling λ in the elementary sector is divided by the large wavefunction renormalization factor, $\sqrt{Z_L Z_R}$, at the IR scale). These states describe the remaining light fermions in the Standard Model, where for each flavor i there is a corresponding operator with anomalous dimension δ_i. Therefore, the hierarchical Yukawa couplings result from order-one anomalous dimensions of operators. In the supersymmetric generalization, these anomalous dimensions also determine the magnitude of the corresponding sfermion masses.

3.2.2 Supersymmetric partial compositeness

3.2.2.1 Chiral supermultiplet

Next, we consider the supersymmetric generalization of partial compositeness. Consider the elementary chiral superfield $\Phi = \phi + \sqrt{2}\theta\psi + \theta\theta F$, where ϕ is a complex scalar field, ψ is a Weyl fermion, and F is an auxiliary field. In addition, we introduce a supersymmetric chiral operator $\mathcal{O} = \mathcal{O}_\phi + \sqrt{2}\theta\mathcal{O}_\psi + \theta\theta\mathcal{O}_F$. The scaling dimension of the scalar operator is $\dim[\mathcal{O}_\phi] = 1 + \delta_\mathcal{O}$, the scaling dimension of the fermion operator is $\dim[\mathcal{O}_\psi] = \frac{3}{2} + \delta_\mathcal{O}$, and the scaling dimension of the auxiliary operator is $\dim[\mathcal{O}_F] = 2 + \delta_\mathcal{O}$, where $\delta_\mathcal{O} \geq 0$ [30].

The supersymmetric Lagrangian contains separate elementary and composite sectors, together with linear mixing terms of the form $[\Phi\mathcal{O}^c]_F$ for each chiral superfield. The

superfield Lagrangian at the scale $\Lambda_{\rm UV}$ is given by

$$\mathcal{L}_\Phi = [\Phi^\dagger \Phi]_D + \frac{1}{\Lambda_{\rm UV}^{\delta-1}} ([\Phi \mathcal{O}^c]_F + \text{h.c.}) \,, \tag{3.9}$$

where $\mathcal{O}^c$ is the charge-conjugate composite operator with anomalous dimension δ and we have assumed an order-one UV coefficient.[1] The composite sector is assumed to confine at the infrared scale $\Lambda_{\rm IR}$, and thus, for the large-N strong dynamics, the two-point function $\langle \mathcal{O}\mathcal{O} \rangle$ is again assumed to be a sum over one-particle states. The Lagrangian at the IR scale can be written as

$$\mathcal{L}_\Phi = [\Phi^\dagger \Phi]_D + [\widetilde{\Phi}_1^{c\dagger} \widetilde{\Phi}_1^c]_D + [\widetilde{\Phi}_1^\dagger \widetilde{\Phi}_1]_D + \varepsilon_\Phi \Lambda_{\rm IR} ([\Phi \widetilde{\Phi}_1^c]_F + \text{h.c.}) + \widetilde{m}_{\Phi 1} ([\widetilde{\Phi}_1 \widetilde{\Phi}_1^c]_F + \text{h.c.}) \,, \tag{3.10}$$

where $\widetilde{\Phi}_1$ ($\widetilde{\Phi}_1^c$) is the lowest-lying composite chiral superfield corresponding to $\mathcal{O}$ ($\mathcal{O}^c$) and $\widetilde{m}_{\Phi 1} = g_{\Phi 1} \Lambda_{\rm IR}$ is the lowest-lying resonance mass, with $g_{\Phi 1}$ an order-one coupling. Note that we have neglected heavier resonances and higher-order terms in Eq.(3.10). The Lagrangian contains mixing terms between the elementary superfield Φ and the lowest-lying composite superfield $\widetilde{\Phi}_1^c$. The dimensionless constant ε_Φ is defined at the IR scale to be

$$\varepsilon_\Phi \equiv \widetilde{\varepsilon}_\Phi(\Lambda_{\rm IR}) \frac{\sqrt{N}}{4\pi} = \frac{1}{\sqrt{Z_\Phi}} \left(\frac{\Lambda_{\rm IR}}{\Lambda_{\rm UV}} \right)^{\delta-1} \frac{\sqrt{N}}{4\pi} \approx \begin{cases} \dfrac{\sqrt{\delta-1}}{\sqrt{\zeta_\Phi}} \left(\dfrac{\Lambda_{\rm IR}}{\Lambda_{\rm UV}} \right)^{\delta-1} & \delta > 1 \\ \dfrac{\sqrt{1-\delta}}{\sqrt{\zeta_\Phi}} & 0 \le \delta < 1 \,, \end{cases} \tag{3.11}$$

where $\widetilde{\varepsilon}_\Phi$ satisfies

$$\mu \frac{d\widetilde{\varepsilon}_\Phi}{d\mu} = (\delta - 1)\widetilde{\varepsilon}_\Phi + \zeta_\Phi \frac{N}{16\pi^2} \widetilde{\varepsilon}_\Phi^3 \,, \tag{3.12}$$

with ζ_Φ an order-one constant. Note that the supersymmetric nonrenormalization theorem guarantees that ε_Φ only depends on the wavefunction renormalization, unlike the nonsupersymmetric case, where the vertex renormalization piece in Eq.(3.5) was neglected. Just as for the fermions in Section 3.2.1, the mixing terms in the Lagrangian Eq.(3.10) cause the scalar mass eigenstates to be admixtures of elementary and composite states.

[1] A kinetic mixing between the elementary and composite sectors of the form $\Lambda_{\rm UV}^{-\delta_\mathcal{O}} [\Phi^\dagger \mathcal{O} + \text{h.c.}]_D$ has been omitted in our minimal setup.

Complex scalar: At the IR scale, the supersymmetric Lagrangian Eq.(3.10) for the chiral supermultiplet has the component form

$$\begin{aligned}\mathcal{L}_{\text{scalar}} = &-\partial_\mu\phi^\dagger\partial^\mu\phi + F^\dagger F + \varepsilon_\Phi\Lambda_{\text{IR}}\left(\phi\widetilde{F}_1^c + F\widetilde{\phi}_1^c + \text{h.c.}\right) - \partial_\mu\widetilde{\phi}_1^{c\dagger}\partial^\mu\widetilde{\phi}_1^c \\ &+ \widetilde{F}_1^{c\dagger}\widetilde{F}_1^c - \partial_\mu\widetilde{\phi}_1^\dagger\partial^\mu\widetilde{\phi}_1 + \widetilde{F}_1^\dagger\widetilde{F}_1 + \widetilde{m}_{\Phi 1}\left(\widetilde{\phi}_1\widetilde{F}_1^c + \widetilde{F}_1\widetilde{\phi}_1^c + \text{h.c.}\right) .\end{aligned} \tag{3.13}$$

Eliminating the auxiliary fields gives rise to the Lagrangian

$$\begin{aligned}\mathcal{L}_{\text{scalar}} = &-\partial_\mu\phi^\dagger\partial^\mu\phi - \varepsilon_\Phi^2\Lambda_{\text{IR}}^2\phi^\dagger\phi - \varepsilon_\Phi g_{\Phi 1}\Lambda_{\text{IR}}^2\left(\phi^\dagger\widetilde{\phi}_1 + \text{h.c.}\right) - \partial_\mu\widetilde{\phi}_1^\dagger\partial^\mu\widetilde{\phi}_1 \\ &- \widetilde{m}_{\Phi 1}^2\widetilde{\phi}_1^\dagger\widetilde{\phi}_1 - \partial_\mu\widetilde{\phi}_1^{c\dagger}\partial^\mu\widetilde{\phi}_1^c - \left(g_{\Phi 1}^2 + \varepsilon_\Phi^2\right)\Lambda_{\text{IR}}^2\widetilde{\phi}_1^{c\dagger}\widetilde{\phi}_1^c ,\end{aligned} \tag{3.14}$$

where in the basis $(\phi, \widetilde{\phi}_1, \widetilde{\phi}_1^c)$, the mass matrix is given by

$$\mathcal{M}_\phi^2 = \begin{pmatrix} \varepsilon_\Phi^2 & \varepsilon_\Phi g_{\Phi 1} & 0 \\ \varepsilon_\Phi g_{\Phi 1} & g_{\Phi 1}^2 & 0 \\ 0 & 0 & \varepsilon_\Phi^2 + g_{\Phi 1}^2 \end{pmatrix}\Lambda_{\text{IR}}^2 . \tag{3.15}$$

Note that there is a mass mixing between the elementary state ϕ and the composite state, $\widetilde{\phi}_1$. Nevertheless, when this matrix is diagonalized, there is a massless eigenstate which can be written as:

$$|\phi_0\rangle \approx \mathcal{N}_\Phi\left\{|\phi\rangle - \frac{\varepsilon_\Phi}{g_{\Phi 1}}|\widetilde{\phi}_1\rangle\right\} , \tag{3.16}$$

where $\mathcal{N}_\Phi$ is a normalization constant, while the massive eigenstates are given by

$$\begin{aligned}|\phi_1\rangle &\approx \mathcal{N}_\Phi\left\{\frac{\varepsilon_\Phi}{g_{\Phi 1}}|\phi\rangle + |\widetilde{\phi}_1\rangle\right\} \\ |\phi_2\rangle &\approx |\widetilde{\phi}_1^c\rangle .\end{aligned} \tag{3.17}$$

Thus, we see that the massless eigenstate is an admixture of the elementary and composite states and that the massive eigenstate is a complex scalar with squared mass $(\varepsilon_\Phi^2 + g_{\Phi 1}^2)\Lambda_{\text{IR}}^2$. Note that the eigenstates are expressed in the mass-mixing basis, unlike the kinetic-mixing basis used in [42]. While both bases are equivalent at the level of mass eigenstates, supersymmetry breaking in the mass-mixing basis is shown in Section 3.3.3 to give consistent results with the 5D gravity model.

Fermion: Similarly, the fermion part of the supersymmetric Lagrangian Eq.(3.10) at the IR scale is given by:

$$\mathcal{L}_{\text{fermion}} = i\psi^\dagger\bar{\sigma}^\mu\partial_\mu\psi + i\widetilde{\psi}_1^\dagger\bar{\sigma}^\mu\partial_\mu\widetilde{\psi}_1 + i\widetilde{\psi}_1^{c\dagger}\bar{\sigma}^\mu\partial_\mu\widetilde{\psi}_1^c - \varepsilon_\Phi\Lambda_{\text{IR}}\left(\psi\widetilde{\psi}_1^c + \text{h.c.}\right) - \widetilde{m}_{\Phi 1}\left(\widetilde{\psi}_1\widetilde{\psi}_1^c + \text{h.c.}\right) . \tag{3.18}$$

In the basis $(\psi, \widetilde{\psi}_1^c, \widetilde{\psi}_1)$, this leads to the following fermion mass matrix:

$$\mathcal{M}_\psi = \frac{1}{2}\begin{pmatrix} 0 & \varepsilon_\Phi & 0 \\ \varepsilon_\Phi & 0 & g_{\Phi 1} \\ 0 & g_{\Phi 1} & 0 \end{pmatrix}\Lambda_{\text{IR}} . \tag{3.19}$$

The mass eigenstates correspond to a massless Weyl fermion and a massive Dirac state with mass $\sqrt{\varepsilon_\Phi^2 + g_{\Phi 1}^2}\Lambda_{\text{IR}}$. The massless eigenstate is given by

$$|\psi_0\rangle \approx \mathcal{N}_\Phi\left\{|\psi\rangle - \frac{\varepsilon_\Phi}{g_{\Phi 1}}|\widetilde{\psi}_1\rangle\right\} , \tag{3.20}$$

while the massive eigenstates are

$$|\psi_{1,2}\rangle \approx \frac{\mathcal{N}_\Phi}{\sqrt{2}}\left\{\frac{\varepsilon_\Phi}{g_{\Phi 1}}|\psi\rangle + |\widetilde{\psi}_1\rangle \pm \sqrt{1 + \frac{\varepsilon_\Phi^2}{g_{\Phi 1}^2}}\,|\widetilde{\psi}_1^c\rangle\right\} . \tag{3.21}$$

Thus, partial compositeness leads to a massless complex scalar and Weyl fermion which combine into a chiral supermultiplet. Using the results Eq.(3.16) and Eq.(3.11), the massless scalar eigenstate ϕ_0 is given by

$$|\phi_0\rangle \approx \mathcal{N}_\Phi\left\{|\phi\rangle - \frac{1}{g_{\Phi 1}\sqrt{\zeta_\Phi}}\sqrt{\frac{\delta - 1}{\left(\frac{\Lambda_{\text{IR}}}{\Lambda_{\text{UV}}}\right)^{2(1-\delta)} - 1}}\,|\widetilde{\phi}_1\rangle\right\} . \tag{3.22}$$

Similarly to the fermion case Eq.(3.7), the massless scalar eigenstates are mostly elementary for $\delta > 1$, whereas for $0 \leq \delta < 1$ they are an admixture of elementary and composite states. In fact, supersymmetry guarantees that the admixtures for both the fermion and scalar field in the chiral multiplet are the same.

3.2.2.2 Vector supermultiplet

Next, we consider the supersymmetric generalization of partial compositeness for gauge fields. For simplicity, we consider the case of an Abelian U(1) gauge field, and assume our discussion can be generalized to non-Abelian gauge fields. In the nonsupersymmetric case, the source field A_μ mixes with the conserved U(1) current J_μ and induces a kinetic mixing of the form $F^{\mu\nu}\widetilde{F}_{\mu\nu 1}$ [42, 43], where $\widetilde{F}_{\mu\nu 1}$ is the field strength of the lowest-lying composite field, $\widetilde{A}_{\mu 1}$. To supersymmetrize this coupling we introduce the vector superfield, $V = \theta^\dagger\bar{\sigma}^\mu\theta A_\mu + \theta^\dagger\theta^\dagger\theta\lambda + \theta\theta\theta^\dagger\lambda^\dagger + \frac{1}{2}\theta\theta\theta^\dagger\theta^\dagger D$, with field strength superfield $W_\alpha = \lambda_\alpha + \theta_\alpha D + \frac{i}{2}(\sigma^\mu\bar{\sigma}^\nu\theta)_\alpha F_{\mu\nu} + i\theta\theta(\sigma^\mu\partial_\mu\lambda^\dagger)_\alpha$. The conserved current J_μ can be embedded into a linear supermultiplet $\mathcal{J}$, which satisfies the condition $D^2\mathcal{J} = D^{\dagger 2}\mathcal{J} = 0$ and guarantees current conservation [44].

The supersymmetric Lagrangian at the UV scale is given by

$$\mathcal{L}_V = \left(\frac{1}{4}[W^\alpha W_\alpha]_F + \text{h.c.}\right) + 2\widetilde{\varepsilon}_V[V\mathcal{J}]_D\,, \tag{3.23}$$

where $\widetilde{\varepsilon}_V$ is the mixing parameter. Since $[V\mathcal{J}]_D$ can be transformed into a kinetic term such as $[W^\alpha\widetilde{W}_\alpha]_F$ + h.c., where $\widetilde{W}$ is the field-strength superfield operator associated with a composite vector superfield operator $\widetilde{V}$, we omit such a term in the Lagrangian.

After confinement, the IR Lagrangian for the source V, together with the lowest-lying composite vector $\widetilde{V}_1$, field-strength superfield $\widetilde{W}_1^\alpha$, and chiral adjoint superfield $\widetilde{\Phi}_{V1}$, can be written as

$$\mathcal{L}_V = \left(\frac{1}{4}[W^\alpha W_\alpha]_F + \frac{1}{4}[\widetilde{W}_1^\alpha\widetilde{W}_{1\alpha}]_F + \text{h.c.}\right) + \Lambda_{\text{IR}}^2\left[\left(\varepsilon_V V + g_{V1}\widetilde{V}_1 + \frac{\widetilde{\Phi}_{V1} + \widetilde{\Phi}_{V1}^\dagger}{\sqrt{2}\Lambda_{\text{IR}}}\right)^2\right]_D\,, \tag{3.24}$$

where g_{V1} is the composite vector coupling, and the dimensionless constant, $\varepsilon_V \equiv \widetilde{\varepsilon}_V(\Lambda_{\text{IR}})\sqrt{N}/(4\pi)$ parametrizes the mixing at the IR scale. The running parameter $\widetilde{\varepsilon}_V(\mu)$ satisfies

$$\mu\frac{d\widetilde{\varepsilon}_V}{d\mu} = \zeta_V\frac{N}{16\pi^2}\widetilde{\varepsilon}_V^3\,, \tag{3.25}$$

with ζ_V an order-one constant that comes from the (unknown) strong dynamics. This immediately leads to the solution

$$\widetilde{\varepsilon}_V(\Lambda_{\text{IR}}) = \frac{1}{\sqrt{\frac{1}{\widetilde{\varepsilon}_V^2} + \frac{\zeta_V N}{8\pi^2}\log(\frac{\Lambda_{\text{UV}}}{\Lambda_{\text{IR}}})}} \approx \frac{1}{\sqrt{2\zeta_V\log(\frac{\Lambda_{\text{UV}}}{\Lambda_{\text{IR}}})}}\frac{4\pi}{\sqrt{N}}\,, \tag{3.26}$$

where we have taken the large-N limit in the last term.

The component fields of the vector supermultiplet can be identified by noting that the IR Lagrangian Eq.(3.24) is invariant under the supergauge transformations

$$\begin{aligned} V &\to V + i\left(\Omega^\dagger - \Omega\right) \\ \widetilde{V}_1 + \frac{\widetilde{\Phi}_{V1} + \widetilde{\Phi}^\dagger_{V1}}{\sqrt{2} g_{V1} \Lambda_{\rm IR}} &\to \widetilde{V}_1 + \frac{\widetilde{\Phi}_{V1} + \widetilde{\Phi}^\dagger_{V1}}{\sqrt{2} g_{V1} \Lambda_{\rm IR}} - i \frac{\varepsilon_V}{g_{V1}} \left(\Omega^\dagger - \Omega\right), \end{aligned} \tag{3.27}$$

where Ω is a chiral superfield gauge-transformation parameter. Choosing the Wess-Zumino gauge for V, the superfields then take the form

$$\begin{aligned} V &= \theta^\dagger \bar{\sigma}^\mu \theta A_\mu + \theta^\dagger \theta^\dagger \theta \lambda + \theta\theta\theta^\dagger \lambda^\dagger + \frac{1}{2}\theta\theta\theta^\dagger\theta^\dagger D \\ \widetilde{V}_1 &= \theta^\dagger \sigma^\mu \theta \bar{A}_{\mu 1} + \theta^\dagger \theta^\dagger \theta \widetilde{\lambda}_1 + \theta\theta\theta^\dagger \widetilde{\lambda}^\dagger_1 + \frac{1}{2}\theta\theta\theta^\dagger\theta^\dagger \widetilde{D}_1 \\ \widetilde{\Phi}_{V1} &= \widetilde{\phi}_{V1} + \sqrt{2}\theta\widetilde{\chi}_1 + \theta\theta\widetilde{F}_{V1} + i\theta^\dagger\bar{\sigma}^\mu\theta\partial_\mu\widetilde{\phi}_{V1} - \frac{i}{\sqrt{2}}\theta\theta\theta^\dagger\bar{\sigma}^\mu\partial_\mu\widetilde{\chi}_1 + \frac{1}{4}\theta\theta\theta^\dagger\theta^\dagger\Box\widetilde{\phi}_{V1}, \end{aligned} \tag{3.28}$$

where $\Box = \partial_\mu\partial^\mu$. Here, $\bar{A}_{\mu 1}$, $\widetilde{\phi}_{V1}$, $\widetilde{\lambda}_1$, and $\widetilde{\chi}_1$ are dynamical (composite) fields, while $\widetilde{F}_{V1}$ and $\widetilde{D}_1$ are auxiliary (composite) fields. Now, the Lagrangian Eq.(3.24) can be diagonalized to obtain the mass eigenstates.

Gauge field: Using Eq.(3.24) and Eq.(3.2.2.2), the gauge field component Lagrangian becomes

$$\mathcal{L}_{\rm gauge} = -\frac{1}{4}F^{\mu\nu}F_{\mu\nu} - \frac{1}{4}\bar{F}_1^{\mu\nu}\bar{F}_{\mu\nu 1} - \frac{1}{2}\Lambda^2_{\rm IR}\left(\varepsilon_V A_\mu + g_{V1}\bar{A}_{\mu 1} + \partial_\mu\widetilde{\varphi}_1\right)^2, \tag{3.29}$$

which is invariant under the gauge transformations

$$\begin{aligned} A_\mu &\to A_\mu + \partial_\mu\zeta \\ \widetilde{A}_{\mu 1} \equiv \bar{A}_{\mu 1} + \frac{\partial_\mu\widetilde{\varphi}_1}{g_{V1}} &\to \widetilde{A}_{\mu 1} - \frac{\varepsilon_V}{g_{V1}}\partial_\mu\zeta, \end{aligned} \tag{3.30}$$

where ζ is a gauge parameter and $\widetilde{\varphi}_1 \equiv i(\widetilde{\phi}_{V1} - \widetilde{\phi}^*_{V1})/(2\Lambda_{\rm IR})$. Note that in the limit of no mixing between the elementary and composite sectors ($\varepsilon_V = 0$), the lowest-lying massive

composite state, $\widetilde{A}_{\mu 1}$, has a mass $\widetilde{m}_{V1} = g_{V1}\Lambda_{\rm IR}$. The appearance of a mass term for A_μ is similar to what happens for vector-meson dominance in QCD [45].

The mass eigenstates are obtained by diagonalizing the squared mass term in Eq.(3.29), where in the basis $(A_\mu, \widetilde{A}_{\mu 1})$, the mass matrix is given by

$$\mathcal{M}_A^2 = \begin{pmatrix} \varepsilon_V^2 & \varepsilon_V g_{V1} \\ \varepsilon_V g_{V1} & g_{V1}^2 \end{pmatrix} \Lambda_{\rm IR}^2 \,. \tag{3.31}$$

This gives rise to one massless and one massive eigenstate. For canonical kinetic terms, the massless gauge boson eigenstate becomes

$$|A_{\mu 0}\rangle \approx \mathcal{N}_V \left\{ |A_\mu\rangle - \frac{\varepsilon_V}{g_{V1}} |\widetilde{A}_{\mu 1}\rangle \right\} , \tag{3.32}$$

while the massive gauge boson eigenstate is given by

$$|A_{\mu 1}\rangle \approx \mathcal{N}_V \left\{ \frac{\varepsilon_V}{g_{V1}} |A_\mu\rangle + |\widetilde{A}_{\mu 1}\rangle \right\} , \tag{3.33}$$

where $\mathcal{N}_V$ is a normalization constant. The eigenstates are expressed in the mass-mixing basis instead of the kinetic-mixing basis used in [42], since supersymmetry is assumed to be broken in this basis. The massless eigenmode Eq.(3.32) now transforms under a gauge transformation as $A_{\mu 0} \to A_{\mu 0} + (1 + \varepsilon_V^2/g_{V1}^2)\partial_\mu \zeta$, while, as expected, $A_{\mu 1}$ no longer transforms. The massive eigenstate $A_{\mu 1}$ obtains a mass

$$m_{V1}^2 = (\varepsilon_V^2 + g_{V1}^2)\Lambda_{\rm IR}^2 \approx \left[g_s^2(\Lambda_{\rm IR}) + g_{V1}^2 \right] \Lambda_{\rm IR}^2 \,, \tag{3.34}$$

where in the second expression, we have used $g_s(\Lambda_{\rm IR}) \approx (\widetilde{\varepsilon}_V/\sqrt{Z_V})(\sqrt{N}/4\pi) = \varepsilon_V$, which follows from the large-N corrections to the elementary-field gauge coupling g_s. The diagonal gauge-field Lagrangian for the two-state system is then given by

$$\mathcal{L}_{\rm gauge} = -\frac{1}{4} F_0^{\mu\nu} F_{0\mu\nu} - \frac{1}{4} F_1^{\mu\nu} F_{\mu\nu 1} - \frac{1}{2} m_{V1}^2 A_{\mu 1}^2 \,, \tag{3.35}$$

where the gauge coupling of the massless mode is obtained from

$$g_s(\Lambda_{\rm IR}) \psi^\dagger \bar{\sigma}^\mu A_\mu \psi - g_{V1} \widetilde{\psi}_1^\dagger \bar{\sigma}^\mu \widetilde{A}_{\mu 1} \widetilde{\psi}_1 + g_{V1} \widetilde{\psi}_1^{c\dagger} \bar{\sigma}^\mu \widetilde{A}_{\mu 1} \widetilde{\psi}_1^c = g \psi_0^\dagger \bar{\sigma}^\mu A_{\mu 0} \psi_0 + \cdots \tag{3.36}$$

Using Eq.(3.20) and Eq.(3.32), this leads to the expression

$$\frac{1}{g^2} = \left[\mathcal{N}_\Phi^2 \mathcal{N}_V \left(g_s(\Lambda_{\rm IR}) + g_{V1}\frac{\varepsilon_\Phi^2}{g_\Phi^2}\frac{\varepsilon_V}{g_{V1}}\right)\right]^{-2} \approx \frac{1}{g_s^2(\Lambda_{\rm IR})} + \frac{1}{g_{V1}^2}\,. \tag{3.37}$$

Finally, note that by eliminating D and $\widetilde{D}_1$ in the scalar field part of the Lagrangian, one can check that the real part of the composite scalar field $\widetilde{\phi}_{V1}$ also obtains a mass, identical to that of the gauge field $A_{\mu 1}$.

Gaugino: The gaugino part of the vector supermultiplet Lagrangian Eq.(3.24) is given by

$$\mathcal{L}_{\rm gaugino} = i\lambda^\dagger\bar{\sigma}^\mu\partial_\mu\lambda + i\widetilde{\lambda}_1^\dagger\bar{\sigma}^\mu\partial_\mu\widetilde{\lambda}_1 + i\widetilde{\chi}_1^\dagger\bar{\sigma}^\mu\partial_\mu\widetilde{\chi}_1 - \Lambda_{\rm IR}\left(\varepsilon_V\lambda\widetilde{\chi}_1 + g_{V1}\widetilde{\lambda}_1\widetilde{\chi}_1 + \text{h.c.}\right)\,. \tag{3.38}$$

In the limit $\varepsilon_V = 0$, the massive composite state is a Dirac fermion with mass $\widetilde{m}_{V1} = g_{V1}\Lambda_{\rm IR}$. Using the basis $(\lambda, \widetilde{\chi}_1, \widetilde{\lambda}_1)$ and the orthogonal matrix

$$O_{1/2} = \frac{1}{\sqrt{\varepsilon_V^2 + g_{V1}^2}}\begin{pmatrix} g_{V1} & 0 & -\varepsilon_V \\ \frac{\varepsilon_V}{\sqrt{2}} & -\sqrt{\frac{\varepsilon_V^2+g_{V1}^2}{2}} & \frac{g_{V1}}{\sqrt{2}} \\ \frac{\varepsilon_V}{\sqrt{2}} & \sqrt{\frac{\varepsilon_V^2+g_{V1}^2}{2}} & \frac{g_{V1}}{\sqrt{2}} \end{pmatrix}, \tag{3.39}$$

the mass terms in Eq.(3.38) can be diagonalized via

$$O_{1/2}\begin{pmatrix} 0 & \frac{\varepsilon_V}{2} & 0 \\ \frac{\varepsilon_V}{2} & 0 & \frac{g_{V1}}{2} \\ 0 & \frac{g_{V1}}{2} & 0 \end{pmatrix} O_{1/2}^T = \begin{pmatrix} 0 & 0 & 0 \\ 0 & -\frac{\sqrt{\varepsilon_V^2+g_{V1}^2}}{2} & 0 \\ 0 & 0 & \frac{\sqrt{\varepsilon_V^2+g_{V1}^2}}{2} \end{pmatrix}, \tag{3.40}$$

which gives rise to a massless Weyl fermion and a massive Dirac fermion. The massless gaugino eigenstate is given by

$$|\lambda_0\rangle \approx \mathcal{N}_V\left\{|\lambda\rangle - \frac{\varepsilon_V}{g_{V1}}|\widetilde{\lambda}_1\rangle\right\}\,. \tag{3.41}$$

Thus, the massless gaugino is an admixture of the elementary gaugino λ and the composite gaugino $\widetilde{\lambda}_1$. The massive Dirac fermion state has the decomposition

$$|\lambda_{1,2}\rangle \approx \frac{\mathcal{N}_V}{\sqrt{2}} \left\{ \frac{\varepsilon_V}{g_{V1}} |\lambda\rangle + |\widetilde{\lambda}_1\rangle \pm \sqrt{1 + \frac{\varepsilon_V^2}{g_{V1}^2}} |\widetilde{\chi}_1\rangle \right\}$$
$$\approx \frac{\mathcal{N}_V}{\sqrt{2}} \left\{ \frac{1}{g_{V1}\sqrt{2\zeta_V \log(\frac{\Lambda_{\rm UV}}{\Lambda_{\rm IR}})}} |\lambda\rangle + |\widetilde{\lambda}_1\rangle \pm |\widetilde{\chi}_1\rangle \right\}, \tag{3.42}$$

assuming $\varepsilon_V \ll 1$ and dropping terms of $O(\varepsilon_V^2)$ and higher in the second expression, with mass eigenvalues

$$m_{V1,2} \approx \pm\sqrt{g_s^2\,(\Lambda_{\rm IR}) + g_{V1}^2}\,\Lambda_{\rm IR}\,. \tag{3.43}$$

This mass agrees with that obtained for the gauge field $A_{\mu 1}$ and scalar field ϕ_{V1}, as expected by supersymmetry.

Using Eq.(3.32), the massless gauge boson eigenstate is found to be

$$|A_{\mu 0}\rangle \approx \mathcal{N}_V \left\{ |A_\mu\rangle - \frac{1}{g_{V1}\sqrt{2\zeta_V \log(\frac{\Lambda_{\rm UV}}{\Lambda_{\rm IR}})}} |\widetilde{A}_{\mu 1}\rangle \right\}. \tag{3.44}$$

Assuming a large hierarchy ($\Lambda_{\rm UV} \gg \Lambda_{\rm IR}$) and order-one values for the couplings, this expression shows that the massless eigenstate is mostly elementary, but with a sizeable composite admixture. The corresponding gauge coupling for this massless state is given in Eq.(3.37). Similarly the massless gaugino eigenstate becomes

$$|\lambda_0\rangle \approx \mathcal{N}_V \left\{ |\lambda\rangle - \frac{1}{g_{V1}\sqrt{2\zeta_V \log(\frac{\Lambda_{\rm UV}}{\Lambda_{\rm IR}})}} |\widetilde{\lambda}_1\rangle \right\}, \tag{3.45}$$

where we have used Eq.(3.41). By supersymmetry, the overall normalization constant, $\mathcal{N}_V$, and composite admixture are the same as in Eq.(3.44).

3.2.2.3 Gravity supermultiplet

Next, we consider the supersymmetric generalization of partial compositeness for gravity fields. In the nonsupersymmetric case the graviton $h_{\mu\nu}$ mixes with the conserved energy-

momentum tensor $T_{\mu\nu}$, inducing a kinetic mixing between the graviton and massive spin-2 resonances [42] (which is completely analogous to graviton-f_2 mixing in QCD). In the supersymmetric extension, the graviton $h_{\mu\nu}$ and gravitino ψ_μ can be embedded into the real supergravity field,

$$H_\mu = -\frac{1}{\sqrt{2}}(\theta^\dagger \bar{\sigma}^\nu \theta) h_{\mu\nu} - i\theta\theta\theta^\dagger \lambda_\mu^\dagger + i\theta^\dagger\theta^\dagger\theta\lambda_\mu + \cdots, \tag{3.46}$$

where we have assumed the gauge $\psi_\mu/2 \equiv \lambda_\mu + \sigma_\mu\bar{\sigma}^\rho\lambda_\rho/3$ and only written the graviton and gravitino parts. The conserved energy-momentum tensor $T_{\mu\nu}$ can be embedded into the supercurrent Θ_μ, which satisfies the condition $-i\bar{\sigma}^\mu D\Theta_\mu = D^\dagger X$, where X is an antichiral superfield, and guarantees current conservation: $\partial_\mu T^{\mu\nu} = 0$ [44]. The supersymmetric Lagrangian at the UV scale is given by

$$\mathcal{L}_H = \frac{4}{3}[H_\mu E^\mu]_D + \frac{2\widetilde{\varepsilon}_H}{\Lambda_{\rm UV}}[H_\mu \Theta^\mu]_D, \tag{3.47}$$

where $\widetilde{\varepsilon}_H$ is the mixing parameter and E^μ is the Einstein superfield [46]. In an analogous fashion to the gauge boson case, the IR Lagrangian after confinement can be written as

$$\mathcal{L}_H = \frac{4}{3}[H_\mu E^\mu]_D + \frac{4}{3}[\widetilde{H}_{\mu 1}\widetilde{E}_1^\mu]_D + 2\Lambda_{\rm IR}^2\left[\left(\varepsilon_H H^\mu + g_{H1}\widetilde{H}_1^\mu\right)^2\right]_D, \tag{3.48}$$

where $\varepsilon_H = \widetilde{\varepsilon}_H(\Lambda_{\rm IR})\sqrt{N}/(4\pi)$ and $\widetilde{H}_{\mu 1}$ is a composite real superfield with corresponding Einstein superfield $\widetilde{E}_1^\mu$. The running parameter $\widetilde{\varepsilon}_H(\mu) \equiv (\widetilde{\varepsilon}_H/\sqrt{Z_H})(\mu/\Lambda_{\rm UV})$ satisfies

$$\mu\frac{d\widetilde{\varepsilon}_H}{d\mu} = \widetilde{\varepsilon}_H + \zeta_H\frac{N}{16\pi^2}\widetilde{\varepsilon}_H^3, \tag{3.49}$$

with ζ_H an order-one constant that arises from the (unknown) strong dynamics. The solution is then given by

$$\widetilde{\varepsilon}_H(\Lambda_{\rm IR}) = \frac{\Lambda_{\rm IR}}{\Lambda_{\rm UV}}\frac{1}{\sqrt{\frac{1}{\widetilde{\varepsilon}_H^2} + \frac{\zeta_H N}{16\pi^2}\left(1 - \left(\frac{\Lambda_{\rm IR}}{\Lambda_{\rm UV}}\right)^2\right)}} \approx \frac{1}{\sqrt{\zeta_H}}\frac{\Lambda_{\rm IR}}{\Lambda_{\rm UV}}\frac{4\pi}{\sqrt{N}}, \tag{3.50}$$

where in the last term, we have taken the large-N limit. Since the graviton couples to the energy-momentum tensor with strength $1/M_P$ (where $M_P = 2.4 \times 10^{18}$ GeV is the reduced Planck mass), we obtain the matching condition $1/M_P \equiv \varepsilon_H/\Lambda_{\rm IR}$ at the IR scale, which

leads to the relation

$$M_P \approx \sqrt{\zeta_H}\,\Lambda_{\rm UV}\sqrt{1-\left(\frac{\Lambda_{\rm IR}}{\Lambda_{\rm UV}}\right)^2} \approx \sqrt{\zeta_H}\,\Lambda_{\rm UV}\,. \tag{3.51}$$

To identify the component fields of the gravity supermultiplet, we note that the IR Lagrangian Eq.(3.48) is invariant under the supergauge transformations

$$\begin{aligned} H_\mu &\to H_\mu + \Delta_\mu \\ \widetilde{H}_{\mu 1} &\to \widetilde{H}_{\mu 1} - \frac{\varepsilon_H}{g_{H1}}\Delta_\mu\,, \end{aligned} \tag{3.52}$$

where Δ_μ is a real superfield gauge-transformation parameter. Choosing an analog of the Wess-Zumino gauge for H_μ, the superfields take the form

$$\begin{aligned} H_\mu &= -\frac{1}{\sqrt{2}}\theta^\dagger\bar\sigma^\nu\theta\, h_{\mu\nu} - i\theta\theta\theta^\dagger\lambda^\dagger_\mu + i\theta^\dagger\theta^\dagger\theta\lambda_\mu + \frac{1}{2}\theta\theta\theta^\dagger\theta^\dagger D_\mu + \cdots \\ \widetilde{H}_{\mu 1} &= \widetilde{C}_{\mu 1} - i\theta\widetilde{\omega}_{\mu 1} + i\theta^\dagger\widetilde{\omega}^\dagger_{\mu 1} - \theta^\dagger\bar\sigma^\nu\theta\,\widetilde{V}_{\mu\nu 1} - i\theta\theta\theta^\dagger\left(\widetilde{\lambda}^\dagger_{\mu 1} - \frac{i}{2}\bar\sigma^\nu\partial_\nu\widetilde{\omega}_{\mu 1}\right) \\ &\quad + i\theta^\dagger\theta^\dagger\theta\left(\widetilde{\lambda}_{\mu 1} - \frac{i}{2}\sigma^\nu\partial_\nu\widetilde{\omega}^\dagger_{\mu 1}\right) + \frac{1}{2}\theta\theta\theta^\dagger\theta^\dagger\left(\widetilde{D}_{\mu 1} + \frac{1}{2}\Box\widetilde{C}_{\mu 1}\right) + \cdots\,, \end{aligned} \tag{3.53}$$

where we have neglected terms with auxiliary fields. The gravity component fields are then defined to be

$$\begin{aligned} \widetilde{h}_{\mu\nu 1} &\equiv \frac{\widetilde{V}_{\mu\nu 1} + \widetilde{V}_{\nu\mu 1}}{\sqrt{2}} \\ \widetilde{C}_{\mu 1} &\equiv \frac{1}{\sqrt{3}\Lambda_{\rm IR}}\frac{1}{g_{H1}}\widetilde{h}_{\mu 1} \\ \frac{1}{2}\widetilde{\psi}_{\mu 1} &\equiv \widetilde{\lambda}_{\mu 1} + \frac{1}{3}\sigma_\mu\bar\sigma^\rho\widetilde{\lambda}_{\rho 1} \\ \widetilde{b}^\sigma_1 &\equiv \widetilde{D}^\sigma_1 + \frac{1}{2}\epsilon^{\nu\mu\kappa\sigma}\partial_\kappa\widetilde{V}_{\nu\mu 1} \\ \widetilde{\omega}_{\mu 1} &\equiv \frac{1}{\Lambda_{\rm IR}}\frac{1}{2g_{H1}}\widetilde{\chi}_{\mu 1}\,. \end{aligned} \tag{3.54}$$

Note that $\widetilde{h}_{\mu\nu 1}$, $\widetilde{\psi}_{\mu 1}$, $\widetilde{\chi}_{\mu 1}$, and $\widetilde{h}_{\mu 1}$ are dynamical (composite) fields, while $\widetilde{b}_{\mu 1}$ is an auxiliary (composite) field.

Graviton: Using Eq.(3.48) the graviton field component Lagrangian becomes

$$\mathcal{L}_{\text{graviton}} = \frac{1}{\sqrt{2}} h_{\mu\nu} E^{\mu\nu} + \frac{1}{\sqrt{2}} \widetilde{h}_{\mu\nu 1} \widetilde{E}_1^{\mu\nu} - \frac{1}{2} \Lambda_{\text{IR}}^2 \left(\varepsilon_H h_{\mu\nu} + g_{H1} \widetilde{h}_{\mu\nu 1} \right)^2 , \tag{3.55}$$

where $E_{\mu\nu} \equiv (\partial_\mu \partial_\nu h^\lambda_\lambda + \Box h_{\mu\nu} - \partial_\mu \partial^\lambda h_{\lambda\nu} - \partial_\nu \partial^\lambda h_{\lambda\mu} - \eta_{\mu\nu} \Box h^\lambda_\lambda + \eta_{\mu\nu} \partial^\lambda \partial^\rho h_{\lambda\rho})/\sqrt{2}$. The Lagrangian is invariant under the gauge transformation

$$\begin{aligned} h_{\mu\nu} &\to h_{\mu\nu} - \frac{1}{2} \left(\partial_\mu \zeta_\nu + \partial_\nu \zeta_\mu \right) \\ \widetilde{h}_{\mu\nu 1} &\to \widetilde{h}_{\mu\nu 1} + \frac{1}{2} \frac{\varepsilon_H}{g_{H1}} \left(\partial_\mu \zeta_\nu + \partial_\nu \zeta_\mu \right) , \end{aligned} \tag{3.56}$$

where ζ_μ is a gauge parameter. Note that in the limit of no mixing between the elementary and composite sectors ($\varepsilon_H = 0$), the lowest-lying massive composite state, $\widetilde{h}_{\mu\nu 1}$, has a mass $\widetilde{m}_{H1} = g_{H1} \Lambda_{\text{IR}}$. The mass eigenstates are obtained by diagonalizing the mass term in Eq.(3.55). The massless graviton eigenstate is then

$$|h_{\mu\nu 0}\rangle \approx \mathcal{N}_H \left\{ |h_{\mu\nu}\rangle - \frac{\varepsilon_H}{g_{H1}} |\widetilde{h}_{\mu\nu 1}\rangle \right\} , \tag{3.57}$$

and the massive graviton eigenstate is given by

$$|h_{\mu\nu 1}\rangle \approx \mathcal{N}_H \left\{ \frac{\varepsilon_H}{g_{H1}} |h_{\mu\nu}\rangle + |\widetilde{h}_{\mu\nu 1}\rangle \right\} , \tag{3.58}$$

where $\mathcal{N}_H$ is a normalization constant. The massless eigenmode $h_{\mu\nu 0}$ now transforms under a gauge transformation as $h_{\mu\nu 0} \to h_{\mu\nu 0} - (1 + \varepsilon_H^2/g_{H1}^2)(\partial_\mu \zeta_\nu + \partial_\nu \zeta_\mu)/2$, while, as expected, $h_{\mu\nu 1}$ no longer transforms. The massive eigenstate $h_{\mu\nu 1}$ obtains a squared mass, $m_{H1}^2 \approx (\varepsilon_H^2 + g_{H1}^2) \Lambda_{\text{IR}}^2$. The diagonal gravity Lagrangian for the two-state system is then given by

$$\mathcal{L}_{\text{graviton}} = \frac{1}{\sqrt{2}} h_0^{\mu\nu} E_{\mu\nu 0} + \frac{1}{\sqrt{2}} h_1^{\mu\nu} E_{\mu\nu 1} - \frac{1}{2} m_{H1}^2 h_{\mu\nu 1}^2 . \tag{3.59}$$

By eliminating b_μ and $\widetilde{b}_{\mu 1}$ in the vector-field part of the Lagrangian, one can check that the composite vector field $\widetilde{h}_{\mu 1}$ also obtains a mass identical to that of the graviton field $\widetilde{h}_{\mu\nu 1}$. For simplicity, we have not included the scalar components, but they obtain a similar mass by supersymmetry.

Gravitino: The gravitino part of the gravity supermultiplet Lagrangian Eq.(3.48) at the IR scale is given by

$$\begin{aligned}\mathcal{L}_{\text{gravitino}} = &-\frac{1}{2}\epsilon^{\mu\nu\rho\kappa}\psi_\mu\sigma_\nu\partial_\rho\psi^\dagger_\kappa - \frac{1}{2}\epsilon^{\mu\nu\rho\kappa}\widetilde{\psi}_{\mu1}\sigma_\nu\partial_\rho\widetilde{\psi}^\dagger_{\kappa1} - \frac{1}{2}\epsilon^{\mu\nu\rho\kappa}\widetilde{\chi}_{\mu1}\sigma_\nu\partial_\rho\widetilde{\chi}^\dagger_{\kappa1} \\ &- \frac{1}{4}\Lambda_{\text{IR}}\left(\varepsilon_H\psi_\mu\left[\sigma^\mu,\bar{\sigma}^\nu\right]\widetilde{\chi}_{\nu1} + g_{H1}\widetilde{\psi}_{\mu1}\left[\sigma^\mu,\bar{\sigma}^\nu\right]\widetilde{\chi}_{\nu1} + \text{h.c.}\right),\end{aligned} \tag{3.60}$$

where $\widetilde{\psi}_{\mu1}$ and $\widetilde{\chi}_{\mu1}$ are both contained in the tensor supermultiplet $\widetilde{H}_{\mu1}$. In the limit $\varepsilon_H = 0$ the massive composite state is a Dirac fermion with mass $\widetilde{m}_{H1}$. Using the basis $(\psi_\mu, \widetilde{\chi}_{\mu1}, \widetilde{\psi}_{\mu1})$, the mass term in Eq.(3.60) can be diagonalized via the transformation

$$O_{3/2}\begin{pmatrix} 0 & \frac{\varepsilon_H}{2} & 0 \\ \frac{\varepsilon_H}{2} & 0 & \frac{g_{H1}}{2} \\ 0 & \frac{g_{H1}}{2} & 0 \end{pmatrix} O^T_{3/2} = \begin{pmatrix} 0 & 0 & 0 \\ 0 & -\frac{\sqrt{\varepsilon_H^2+g_{H1}^2}}{2} & 0 \\ 0 & 0 & \frac{\sqrt{\varepsilon_H^2+g_{H1}^2}}{2} \end{pmatrix}, \tag{3.61}$$

with the orthogonal matrix

$$O_{3/2} = \frac{1}{\sqrt{\varepsilon_H^2+g_{H1}^2}}\begin{pmatrix} g_{H1} & 0 & -\varepsilon_H \\ \frac{\varepsilon_H}{\sqrt{2}} & -\sqrt{\frac{\varepsilon_H^2+g_{H1}^2}{2}} & \frac{g_{H1}}{\sqrt{2}} \\ \frac{\varepsilon_H}{\sqrt{2}} & \sqrt{\frac{\varepsilon_H^2+g_{H1}^2}{2}} & \frac{g_{H1}}{\sqrt{2}} \end{pmatrix}, \tag{3.62}$$

which gives rise to a massless Weyl fermion and a massive Dirac fermion. The massless gravitino eigenstate then becomes

$$|\psi_{\mu0}\rangle \approx \mathcal{N}_H\left\{|\psi_\mu\rangle - \frac{\varepsilon_H}{g_{H1}}|\widetilde{\psi}_{\mu1}\rangle\right\}. \tag{3.63}$$

Thus, the massless gravitino is an admixture of the elementary gravitino ψ_μ and the composite gravitino $\widetilde{\psi}_{\mu1}$. The massive Dirac fermion state is given by

$$\begin{aligned}|\psi_{\mu1,2}\rangle &\approx \frac{\mathcal{N}_H}{\sqrt{2}}\left\{\frac{\varepsilon_H}{g_{H1}}|\psi_\mu\rangle + |\widetilde{\psi}_{\mu1}\rangle \pm \sqrt{1+\frac{\varepsilon_H^2}{g_{H1}^2}}|\widetilde{\chi}_{\mu1}\rangle\right\} \\ &\approx \frac{\mathcal{N}_H}{\sqrt{2}}\left\{\frac{1}{g_{H1}\sqrt{\zeta_H}}\frac{\Lambda_{\text{IR}}}{\Lambda_{\text{UV}}}|\psi_\mu\rangle + |\widetilde{\psi}_{\mu1}\rangle \pm |\widetilde{\chi}_{\mu1}\rangle\right\},\end{aligned} \tag{3.64}$$

where $\varepsilon_H \ll 1$ and terms of $O(\varepsilon_H^2)$ and higher have been dropped in the second expression. The mass eigenvalues are

$$m_{H1,2} = \pm\sqrt{\varepsilon_H^2 + g_{H1}^2}\Lambda_{\rm IR}\,, \tag{3.65}$$

which agrees with that obtained for the graviton field $\widetilde{h}_{\mu\nu 1}$ and the vector field $\widetilde{h}_{\mu 1}$, as expected by supersymmetry. Using Eq.(3.57), the massless graviton eigenstate is found to be

$$|h_{\mu\nu 0}\rangle \approx \mathcal{N}_H \left\{ |h_{\mu\nu}\rangle - \frac{1}{g_{H1}\sqrt{\zeta_H}} \frac{\Lambda_{\rm IR}}{\Lambda_{\rm UV}} |\widetilde{h}_{\mu\nu 1}\rangle \right\} . \tag{3.66}$$

Assuming $\Lambda_{\rm IR} \ll \Lambda_{\rm UV}$, this shows that the massless eigenstate is mostly elementary with a tiny composite admixture. The gravitino part of the Lagrangian Eq.(3.48) is a special case ($\delta = 2$) of the fermion Lagrangian Eq.(3.4). After diagonalizing the mass terms, the massless gravitino eigenstate becomes

$$|\psi_{\mu 0}\rangle \approx \mathcal{N}_H \left\{ |\psi_{\mu}\rangle - \frac{1}{g_{H1}\sqrt{\zeta_H}} \frac{\Lambda_{\rm IR}}{\Lambda_{\rm UV}} |\widetilde{\psi}_{\mu 1}\rangle \right\} , \tag{3.67}$$

where we have used Eq.(3.63). By supersymmetry, the composite admixture is the same as in Eq.(3.66), and thus the gravitino is again mostly elementary.

3.2.3 Supersymmetry breaking

Supersymmetry is assumed to be broken in the composite sector by the strong dynamics and will be parameterized by a composite spurion, chiral superfield, $\mathcal{X} = \theta\theta\mathcal{F}$, where the vacuum expectation value $\langle \mathcal{F} \rangle \equiv F_{\mathcal{X}} \neq 0$. In the large-$N$ limit, we have $F_{\mathcal{X}} \propto (\sqrt{N}/4\pi)\Lambda_{\rm IR}^2$ [47].

3.2.3.1 Sfermion masses

Supersymmetry-breaking scalar masses are only generated for the composite sector fields, since there is no direct coupling of the supersymmetry-breaking spurion to the elementary fields. For instance, the massive chiral superfield $\widetilde{\Phi}_1$ directly couples to the supersymmetry breaking in the composite sector via the following D-term:

$$\xi_4 \frac{g_{\Phi 1}^2}{\Lambda_{\rm IR}^2} [\mathcal{X}^\dagger \mathcal{X} \widetilde{\Phi}_1^\dagger \widetilde{\Phi}_1]_D = \xi_4 g_{\Phi 1}^2 \frac{|F_{\mathcal{X}}|^2}{\Lambda_{\rm IR}^2} \widetilde{\phi}_1^\dagger \widetilde{\phi}_1\,, \tag{3.68}$$

where ξ_4 is a dimensionless parameter, which for a large-N gauge theory is proportional to $16\pi^2/N$ [41]. This D-term interaction gives a supersymmetry-breaking mass to the composite scalar field $\widetilde{\phi}_1$. Given the scalar admixture Eq.(3.22), the corresponding sfermion squared mass becomes:

$$\hat{m}^2_{\phi 0} \approx \mathcal{N}^2_\Phi \varepsilon^2_\Phi \xi_4 \frac{|F_\mathcal{X}|^2}{\Lambda^2_{\rm IR}} \approx \begin{cases} \dfrac{\xi_4}{\zeta_\Phi}(\delta-1)\left(\dfrac{\Lambda_{\rm IR}}{\Lambda_{\rm UV}}\right)^{2(\delta-1)} \dfrac{|F_\mathcal{X}|^2}{\Lambda^2_{\rm IR}} & \delta \geq 1 \\ \dfrac{\xi_4}{\zeta_\Phi}(1-\delta)\dfrac{|F_\mathcal{X}|^2}{\Lambda^2_{\rm IR}} & 0 \leq \delta < 1\,, \end{cases} \tag{3.69}$$

where we have assumed $\varepsilon_\Phi \lesssim g_{\Phi 1}$. Note that the sfermion mass is power-law suppressed for $\delta > 1$. This is because the mass eigenstate is mostly elementary and therefore can only obtain a supersymmetry-breaking mass via mixing with the composite sector. This contrasts with the case $0 \leq \delta < 1$, where the mass eigenstate has a sizeable composite admixture and therefore directly feels the supersymmetry breaking from the composite sector without any power-law suppression. In this way, a sfermion mass hierarchy can be explained by anomalous dimensions of supersymmetric operators.

Note, however, that as δ is increased beyond one, the scalar squared mass becomes increasingly small, since the scalar is becoming more elementary [using Eq.(3.22)]. Eventually, radiative corrections are sufficiently large that they provide the dominant contribution to the sfermion squared mass. For instance, the sfermion-fermion-gaugino interaction with a massive gaugino leads to the one-loop contribution

$$\delta \hat{m}^2_{\phi 0} \approx \frac{g_i^2}{16\pi^2} \hat{m}^2_{\lambda_i 0}\,, \tag{3.70}$$

where g_i ($i = 1, 2, 3$) are the Standard Model $\mathrm{U}(1)_Y \times \mathrm{SU}(2)_L \times \mathrm{SU}(3)$ gauge couplings, respectively. Note that this radiative correction is assumed to be finite. Therefore, there is a maximum value of the anomalous dimension δ^*, beyond which the gaugino-mediated contribution Eq.(3.70) dominates.

3.2.3.2 Gaugino masses

The spurion superfield $\mathcal{X}$ can also be used to generate gaugino masses. Since the massless gaugino Eq.(3.45) contains a $\widetilde{\lambda}_1$ admixture, supersymmetry breaking in the composite sector

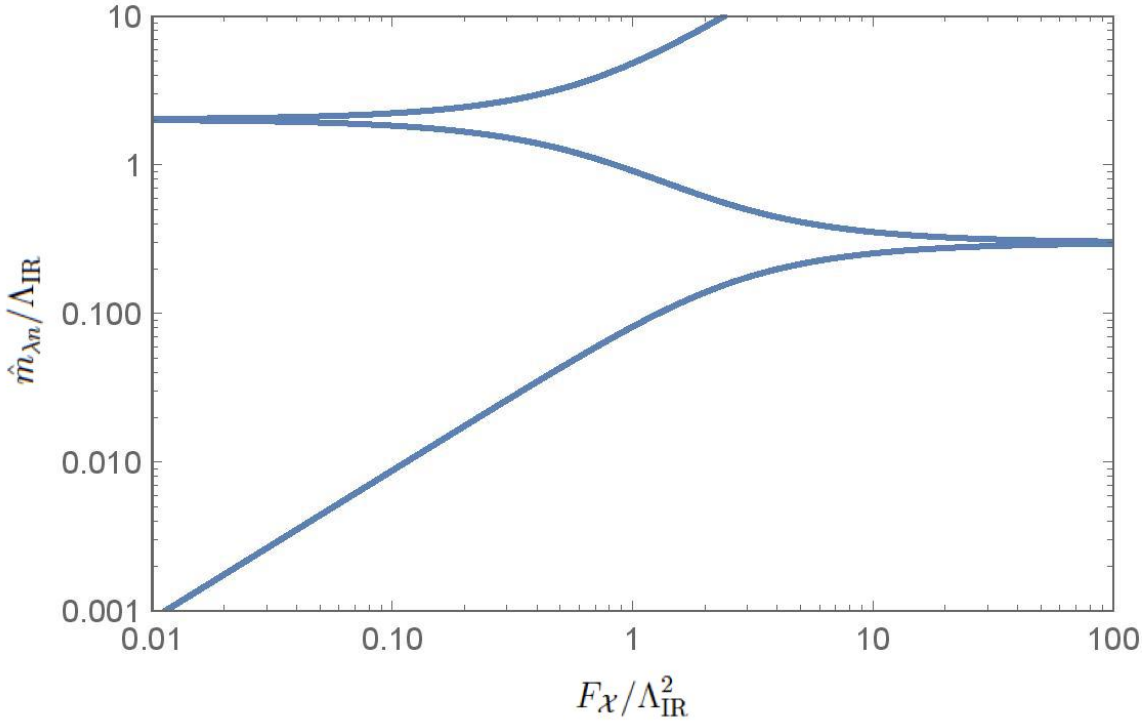

Figure 3.4: Gaugino mass eigenvalues for $g_{V1} = 2$, $\varepsilon_V = 0.3$, and $\xi_3 = 1$ as a function of the supersymmetry-breaking order parameter $F_{\mathcal{X}}$.

is transmitted by the following interactions:

$$\frac{\xi_3}{2}\frac{g_{V1}^2}{\Lambda_{\rm IR}}\left([\mathcal{X}\widetilde{W}_1^\alpha \widetilde{W}_{1\alpha}]_F + \text{h.c.}\right), \tag{3.71}$$

where ξ_3 is proportional to $4\pi/\sqrt{N}$ for a large-N gauge theory. The supersymmetry-breaking interaction Eq.(3.71), adds the Majorana mass term $\xi_3 g_{V1}^2 (F_{\mathcal{X}}/2\Lambda_{\rm IR})\widetilde{\lambda}_1\widetilde{\lambda}_1$ + h.c. to the gaugino mass terms in Eq.(3.38). Note that there is no $\widetilde{\chi}_1$ mass term because the interaction $[\mathcal{X}\widetilde{V}_1^2]_D$ is not gauge invariant. Diagonalization of the mass matrix then leads to a gaugino mass

$$\hat{m}_{\lambda 0} = \mathcal{N}_V^2 \varepsilon_V^2 \xi_3 \frac{F_{\mathcal{X}}}{\Lambda_{\rm IR}} \approx g^2 \xi_3 \frac{F_{\mathcal{X}}}{\Lambda_{\rm IR}}, \tag{3.72}$$

where we have used the gauge coupling relation Eq.(3.37) and $\varepsilon_V \approx g_s(\Lambda_{\rm IR})$. The result Eq.(3.72) is consistent with simply using Eq.(3.45) and the fact that the massless mode only has a $\widetilde{\lambda}_1$ admixture. Notice that the gaugino mass is suppressed by a $\log(\Lambda_{\rm UV}/\Lambda_{\rm IR})$ factor due to the fact that the elementary gaugino mixes with the composite sector via a marginal coupling. This causes the gauginos to be generically lighter than the heavy composite

sfermions with $0 \leq \delta < 1$, leading to a "split" spectrum.

As we discussed, when δ is greater than the critical value δ^*, the gaugino mass radiative correction Eq.(3.70) gives the dominant contribution to the scalar masses. The critical value δ^* occurs when $\delta \hat{m}^2_{\phi 0} \approx \hat{m}^2_{\phi 0}$, and using Eq.(3.72) it takes the value

$$\delta^* \approx 1 + \frac{\log\left[\frac{4\pi}{g_i}\log(\frac{\Lambda_{\rm UV}}{\Lambda_{\rm IR}})\right]}{\log(\frac{\Lambda_{\rm UV}}{\Lambda_{\rm IR}})}, \tag{3.73}$$

where we have included only the dominant gauge-coupling contribution. Thus, for $\delta > \delta^*$, the gaugino is heavier than the corresponding sfermion mass by a factor of $\sqrt{\alpha_i/(4\pi)}$. Note that when $\sqrt{F_\chi} \gg \Lambda_{\rm IR}$, the lightest gaugino becomes a Dirac fermion with a mass

$$\hat{m}_{\lambda 0} \approx \varepsilon_V \Lambda_{\rm IR} \approx \frac{\Lambda_{\rm IR}}{\sqrt{2\zeta_V \log(\frac{\Lambda_{\rm UV}}{\Lambda_{\rm IR}})}}. \tag{3.74}$$

This value parametrically matches the gaugino mass that is found in a 5D supersymmetric Standard Model where supersymmetry breaking arises from "twisted" boundary conditions [33]. The Dirac limit can also be seen in Figure 3.4, which shows the elementary state λ marrying the composite Weyl fermion $\widetilde{\chi}_1$ as $\sqrt{F_\chi}$ becomes larger, giving rise to a Dirac mass,$\sim g_s(\Lambda_{\rm IR})\,\Lambda_{\rm IR}$, that is smaller than the mass Eq.(3.43) that applies when $\sqrt{F_\chi} \ll \Lambda_{\rm IR}$.

3.2.3.3 Gravitino masses

The supersymmetry breaking from the composite sector gives rise to a positive vacuum energy. This contribution can be cancelled by introducing a constant superpotential W, which induces a mass term for the elementary gravitino

$$-\frac{1}{4}\frac{W}{M_P^2}\,\psi_\rho\left[\sigma^\mu, \bar{\sigma}^\rho\right]\psi_\mu + \text{h.c.} \tag{3.75}$$

At the IR scale, this term becomes

$$-\frac{1}{4Z_H}\frac{W}{M_P^2}\,\psi_\rho\left[\sigma^\mu, \bar{\sigma}^\rho\right]\psi_\mu + \text{h.c.} \approx -\frac{1}{4\zeta_H \widetilde{\varepsilon}_H^2}\frac{4\pi}{\sqrt{N}}\frac{F_\chi}{\sqrt{3}M_P}\,\psi_\rho\left[\sigma^\mu, \bar{\sigma}^\rho\right]\psi_\mu + \text{h.c.}, \tag{3.76}$$

where Z_H is defined from $\widetilde{\varepsilon}_H(\Lambda_{\rm IR})$ in Section 3.2.2.3 and in the second equation, we have tuned $|F_\chi|^2 N/(16\pi^2) \approx 3|W|^2/M_P^2$ so that the cosmological constant vanishes. Note that this means the elementary sector is supersymmetric AdS_4, with Minkowski space obtained

after the “uplift" from the supersymmetry-breaking composite sector. Diagonalization of the mass matrix [given in Eq.(3.61)] with the inclusion of Eq.(3.76) then leads to a gravitino mass

$$\hat{m}_{\psi_\mu 0} \approx \xi_3 \frac{F_\chi}{\sqrt{3} M_P}, \tag{3.77}$$

where $F_\chi \ll \Lambda_{\rm IR} M_P$, $\mathcal{N}_H \approx 1$, and $\xi_3 = 1/(\zeta_H \widetilde{\varepsilon}_H^2)(4\pi/\sqrt{N})$. The result Eq.(3.77) is consistent with simply using Eq.(3.67) and the fact that the massless mode is mostly elementary. Since $\Lambda_{\rm IR} \ll M_P$, the gravitino is generically much lighter than the heavy composite sfermions with $0 \leq \delta < 1$. There is also a heavy Dirac gravitino mostly comprised of $\widetilde{\psi}_{\mu 1}$ and $\widetilde{\chi}_{\mu 1}$ with mass $\sim\sqrt{\varepsilon_H^2 + g_{H1}^2}\Lambda_{\rm IR}$.

In the opposite limit $F_\chi \gg \Lambda_{\rm IR} M_P$, one gravitino Weyl state decouples, and the elementary state ψ_μ marries the composite state $\widetilde{\psi}_{\mu 1}$ [33] such that the lightest gravitino then becomes a Dirac fermion with a mass $\hat{m}_{\psi_\mu 0} \approx g_{H1}\Lambda_{\rm IR}$. This is similar to what occurs for the gaugino, except that since the mixing is very small, the Dirac limit is reached much more slowly for the gravitino.

3.2.3.4 Higgs soft mass

There is no direct coupling of the supersymmetry-breaking spurion to the elementary fields, and therefore the Higgs soft mass can only be generated radiatively, via loops of fields with a composite admixture. In particular, gaugino and sfermion loops can transmit the supersymmetry-breaking effects to the elementary sector.

The first type of sfermion contributions are due to Yukawa interactions. These lead to the Higgs soft squared mass

$$\begin{aligned}
(\Delta \hat{m}_H^2)_y &\approx \frac{y_\delta^2(\Lambda_{\rm IR})}{16\pi^2}\, \hat{m}_{\phi 0}^2 \log\Big(\frac{\Lambda_{\rm IR}}{\rm TeV}\Big) \\
&\approx \frac{\lambda^2}{16\pi^2} \frac{\mathcal{N}_\Phi^2}{Z_\Phi^2}\, \hat{m}_{\phi 0}^2 \log\Big(\frac{\Lambda_{\rm IR}}{\rm TeV}\Big) \\
&\approx \frac{16\pi^2 \lambda^2}{N^2} \frac{\mathcal{N}_\Phi^4}{\zeta_\Phi^3} \left(\frac{\delta - 1}{1 - \left(\frac{\Lambda_{\rm IR}}{\Lambda_{\rm UV}}\right)^{2(\delta-1)}}\right)^3 \left(\frac{\Lambda_{\rm IR}}{\Lambda_{\rm UV}}\right)^{2(\delta-1)} \xi_4 \frac{|F_\chi|^2}{\Lambda_{\rm IR}^2} \log\Big(\frac{\Lambda_{\rm IR}}{\rm TeV}\Big),
\end{aligned} \tag{3.78}$$

where $y_\delta(\Lambda_{\rm IR}) \equiv \hat{m}_{\psi 0}/\langle H \rangle$ is the Yukawa coupling from Section 3.2.1 with $\delta = \delta_L = \delta_R$ chosen for simplicity, λ is the proto-Yukawa coupling, $\mathcal{N}_\Phi$ is a normalization constant given in Eq.(3.16), and Z_Φ is defined in Eq.(3.11).

The second type of sfermion corrections are due to D-term gauge interactions and the mixing term $V - \widetilde{\Phi}_{V1}$. Since the scalar and the auxiliary field component of $\widetilde{\Phi}_{V1}$ mediates the supersymmetry breaking, the easiest way to estimate the D-term contribution is to approximately solve for $\widetilde{\Phi}_{V1}$ in order to determine how the elementary D-term is coupled to the composite sfermions. This procedure generates the following correction:

$$\begin{aligned}(\Delta\hat{m}_H^2)_D &\approx Y(H)\,Y(\phi)\,\frac{g_1(\Lambda_{\rm IR})}{8\pi^2}\varepsilon_V\left(\log\Big(\frac{\Lambda_{\rm IR}}{\rm TeV}\Big)+\frac{\mathcal{N}_\Phi^2}{2\varepsilon_\Phi^2\left(1+\frac{m_{\Phi1}^2}{\Lambda_{\rm IR}^2}\right)}\right)\hat{m}_{\phi0}^2\\ &\approx Y(H)\,Y(\phi)\,\frac{g_1(\Lambda_{\rm IR})}{8\pi^2}\varepsilon_V\mathcal{N}_\Phi^2\left(\frac{\log(\frac{\Lambda_{\rm IR}}{\rm TeV})}{\zeta_\Phi}\frac{\delta-1}{(\frac{\Lambda_{\rm IR}}{\Lambda_{\rm UV}})^{2(1-\delta)}-1}+\frac{\mathcal{N}_\Phi^2}{2\left(1+\frac{m_{\Phi1}^2}{\Lambda_{\rm IR}^2}\right)}\right)\xi_4\frac{|F_\mathcal{X}|^2}{\Lambda_{\rm IR}^2},\end{aligned} \tag{3.79}$$

where g_1 is the $\mathrm{U}(1)_Y$ gauge coupling, Y denotes the hypercharge, and $m_{\Phi1}^2 = (\varepsilon_\Phi^2 + g_{\Phi1}^2)\Lambda_{\rm IR}^2$. Finally, the corrections that involve gauginos arise from gauge interactions. The dominant contribution is given by

$$(\Delta\hat{m}_H^2)_g \approx 4C(R_H)\,\mathcal{N}_V^2\,\frac{g_2^2(\Lambda_{\rm IR})}{8\pi^2}\hat{m}_{\lambda0}^2\log\Big(\frac{\Lambda_{\rm IR}}{\rm TeV}\Big), \tag{3.80}$$

where g_2 is the SU(2) gauge coupling and $C(R)$ is the quadratic Casimir of the representation R. In Figure 3.5, we plot the approximate expressions Eq.(3.78), Eq.(3.79), and Eq.(3.80) for a single sfermion (with $Y(\phi) = 1$) and gaugino, assuming $\sqrt{\xi_4/\zeta_\Phi}\,F_\mathcal{X} = \xi_3 F_\mathcal{X} = (4.75\times10^{10}\ \mathrm{GeV})^2$, $\Lambda_{\rm IR} = 2\times10^{16}$ GeV, $\Lambda_{\rm IR}/\Lambda_{\rm UV} \approx 0.026$, $g_{\Phi_L1}g_{\Phi_R1}(16\pi^2/N)\lambda \approx 1$, $g_{V1}^2 \approx g_5^2 k$, and $\zeta_{\Phi_i,V} \approx 1/g_{\Phi_i,V1}^2$, where $i = L, R$. Furthermore, for later comparison with the 5D calculation, we use values for $m_{\Phi1}^2$ and m_{V1}^2 corresponding to the 5D Kaluza-Klein masses. Only the maximal contribution arising from the Yukawa interaction (corresponding to $\delta_L = \delta$ and $\delta_R = 1$) is shown in the figure. All contributions are qualitatively similar to the precise 5D results that are given in Section 3.3.3.

3.2.4 Higgsino mass

Since the Higgs supermultiplet is elementary, there is no direct coupling to the supersymmetry-breaking spurion in the composite sector, and therefore the generation of a μ-term via a Giudice-Masiero mechanism [48] is forbidden. Instead, to generate a sizeable μ-term, we

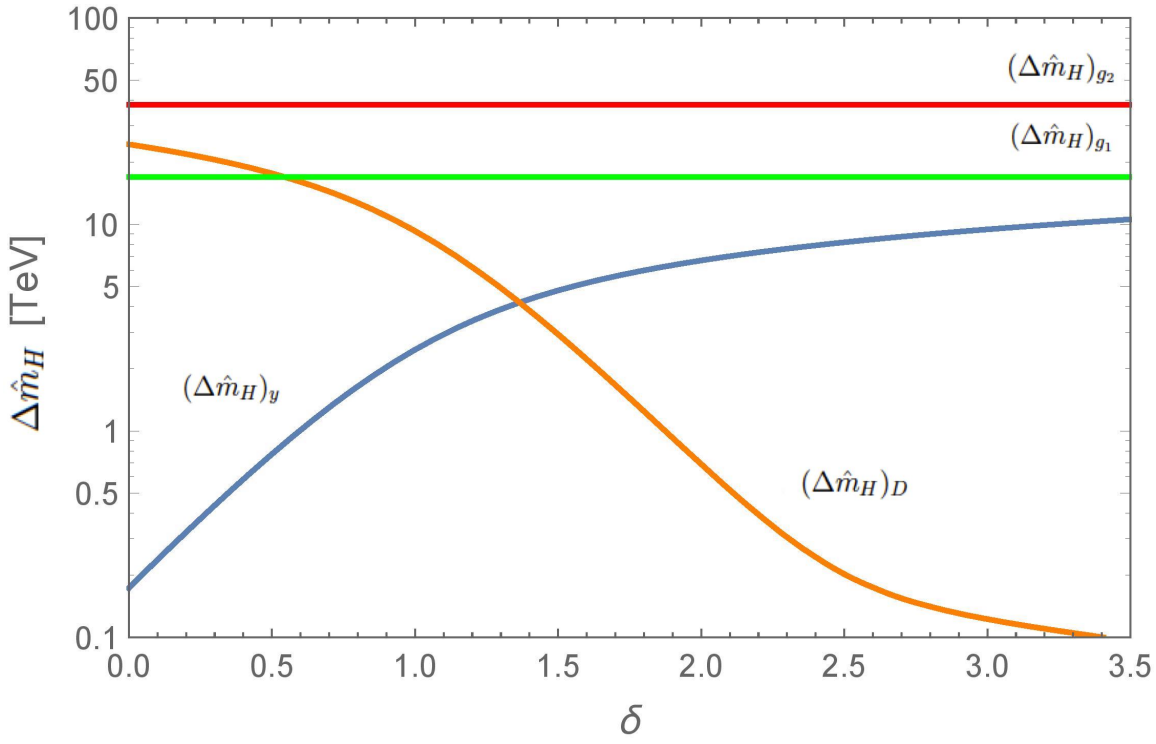

Figure 3.5: One-loop corrections to the Higgs mass parameter that arise from gauge, Yukawa, and D-term interactions due to a single sfermion or gaugino as a function of the anomalous dimension δ.

consider the Kim-Nilles mechanism [49] and introduce an elementary Standard Model singlet S, together with a global U(1) Peccei-Quinn symmetry, where H_u, H_d, S have the charges $+1, +1, -1$, respectively.[2] This global symmetry then allows the following nonrenormalizable superpotential term:

$$W_{KN} = \frac{\kappa_\mu}{2M_P} S^2 H_u H_d \,, \tag{3.81}$$

where κ_μ is a dimensionless coupling. Assuming that the Peccei-Quinn symmetry is spontaneously broken by a nonzero vacuum expectation value $\langle S \rangle \sim f$, an effective μ-term of size

$$\mu \approx \frac{\kappa_\mu f^2}{2M_P} \tag{3.82}$$

is then generated. Since the global symmetry is anomalous (and assuming all other sources of breaking are small), the pseudo Nambu-Goldstone boson associated with the spontaneous symmetry breaking can be identified with the axion. This axion is of the

[2]To allow for Yukawa interactions with the Higgs fields, the fermions $Q, L, \bar{u}, \bar{d}, \bar{e}$ must have charges $-1, -1, 0, 0, 0$ respectively.

invisible DFSZ type, and is consistent with the present astrophysical constraints provided that 10^9 GeV $\lesssim f \lesssim 10^{12}$ GeV. For this range of f, the μ-term Eq.(3.82) can easily accommodate values in the range 0.1 TeV $\lesssim \mu \lesssim$ 100 TeV. Thus, using the Kim-Nilles mechanism, we can solve the strong-CP problem and generate the required values of the μ term.

3.2.5 The sfermion mass hierarchy

In a supersymmetric model, partial compositeness relates the fermion and sfermion mass hierarchies. To explicitly see this relation we consider a numerical example involving the electron and the top quark. In order to explain the fermion mass hierarchy, the top quark must be mostly elementary with $\delta_t > 1$ (i.e., irrelevant mixing), while the electron must have a sizeable composite admixture with $0 < \delta_e < 1$ (i.e., relevant mixing). Using the fermion mass expressions Eq.(3.8), the ratio of the Yukawa couplings at the IR scale is then given by

$$\frac{y_e}{y_t} \approx \frac{1-\delta_e}{\delta_t - 1}\left(\frac{\Lambda_{\rm IR}}{\Lambda_{\rm UV}}\right)^{2(1-\delta_e)} . \tag{3.83}$$

The ratio of the electron to the top-quark Yukawa coupling is determined in terms of $\delta_{e,t}$, and for a sufficiently large hierarchy between $\Lambda_{\rm IR}$ and $\Lambda_{\rm UV}$, depends sensitively on the anomalous dimension δ_e. It is plotted in Figure 3.6 for various values of $\Lambda_{\rm IR}/\Lambda_{\rm UV}$, assuming that the Yukawa coupling ratio is approximately $y_e/y_t \approx 10^{-5}$ over most IR scales. Note that Eq.(3.83) is a simplified expression for δ values not very close to one, but exact expressions are used in the figure.

Using the sfermion mass expressions Eq.(3.69) and Eq.(3.70), we similarly obtain the ratio of the selectron squared mass to the stop squared mass at the IR scale:

$$\frac{\hat{m}^2_{\tilde{e}}}{\hat{m}^2_{\tilde{t}}} = \begin{cases} \dfrac{1-\delta_e}{\delta_t - 1}\left(\dfrac{\Lambda_{\rm IR}}{\Lambda_{\rm UV}}\right)^{2(1-\delta_t)} & \delta_t < \delta_t^* \\ \dfrac{4\pi}{\alpha_3}(1-\delta_e)\log^2\left(\dfrac{\Lambda_{\rm UV}}{\Lambda_{\rm IR}}\right) & \delta_t \geq \delta_t^* . \end{cases} \tag{3.84}$$

Note that this expression is separately valid for left- and right-handed scalar masses and only the gluino contribution is included in Eq.(3.70) for the gaugino-mediated contribution to the stop squared mass. Interestingly, the two expressions Eq.(3.83) and Eq.(3.84) differ only in the exponents for $\delta_t < \delta_t^*$, while for $\delta_t \geq \delta_t^*$ the ratio no longer depends on δ_t. As shown in Figure 3.6, the allowed region is $0 \lesssim \delta_e \lesssim 0.9$ and $1 \lesssim \delta_t \lesssim 1.8$, depending on

the value of $\Lambda_{\rm IR}/\Lambda_{\rm UV}$. The largest value of the ratio $\hat{m}_{\tilde{e}}/\hat{m}_{\tilde{t}}$ is approximately 140 (390) for $\Lambda_{\rm IR}/\Lambda_{\rm UV} \approx 10^{-3}$ (10^{-16}). Note that the Yukawa coupling ratio contours in Figure 3.6, end at δ_t^* because the sfermion mass ratio becomes approximately constant as seen in Eq.(3.84).

Although these are naïve tree-level results obtained at the IR scale, they clearly reveal an inverted mass hierarchy for the sparticle spectrum where $\hat{m}_{\tilde{e}}/\hat{m}_{\tilde{t}} \sim$ 10–350. To obtain a physical mass spectrum, this range is further restricted due to renormalization group (RG) effects. We next include these effects, as well as a number of phenomenological constraints, such as the 125 GeV Higgs boson. Since the strong dynamics is nonperturbative, the AdS/CFT correspondence is used to calculate the mass spectrum in a slice of five-dimensional AdS.

3.3 The extra dimension comes to the rescue

3.3.1 Supersymmetry in a slice of AdS

In order for the classical metric solution to be valid, the AdS curvature must be small enough compared to the 5D Planck scale so that higher-order curvature terms in the 5D gravitational action can be neglected. This requires $k/M_5 \lesssim 2$ [50], but, in the following, we have taken k to be generically smaller, choosing $k/M_5 = 0.1$. Besides gravity, we introduce the matter and gauge field content of the Minimal Supersymmetric Standard Model in the bulk. Since only Dirac fermions are allowed by the 5D Lorentz algebra, the bulk supersymmetry has eight supercharges, corresponding to $\mathcal{N} = 2$ supersymmetry from the 4D perspective. All fields that propagate in the AdS bulk are thus in $\mathcal{N} = 2$ representations of supersymmetry, but the orbifold compactification breaks this to an $\mathcal{N} = 1$ supersymmetry at the massless level, preserving four supercharges [40, 33]. The massless modes which form this 4D MSSM are the zero-mode solutions in the Kaluza-Klein decompositions of the 5D fields.

The quadratic part of the 5D bulk action of a hypermultiplet containing complex scalar fields ϕ and ϕ^c and Dirac fermion Ψ living in a slice of AdS_5 is given by [40]

$$S_5 = \int d^5x\,\sqrt{-g}\left[-|\partial_M\phi|^2 - m_\phi^2|\phi|^2 - |\partial_M\phi^c|^2 - m_{\phi^c}^2|\phi^c|^2 + i\bar{\Psi}\Gamma^M D_M\Psi - i m_\Psi\bar{\Psi}\Psi\right], \quad (3.85)$$

where $g = \det(g_{MN})$ is the determinant of the AdS metric Eq.(2.6) and the curved space covariant derivative $D_M = \partial_M + \omega_M$ includes the spin connection ω_M. The bulk masses are

given by

$$\begin{aligned} m_\Psi &= c\sigma' \\ m^2_{\phi,\phi^c} &= ak^2 + b\sigma'', \end{aligned} \tag{3.86}$$

where $\sigma = k|y|$ and a, b, c are dimensionless parameters. Performing a KK decomposition,

$$\begin{aligned} \phi(x^\mu, y) &= \sum_{n=0}^{\infty} \phi_n(x^\mu)\zeta'_{\phi n}(y) \\ \psi_{L,R}(x^\mu, y) &= \sum_{n=0}^{\infty} \psi_{L,Rn}(x^\mu)\zeta'_{\psi_{L,R}n}(y), \end{aligned} \tag{3.87}$$

where $\psi_{L,R}(x^\mu, y)$ are the left and right handed projections of $\Psi(x^\mu, y)$, the zero-mode profiles (with respect to a flat metric) are [39, 40]

$$\zeta_{\psi_{L,R}0}(y) = e^{-\frac{3}{2}k|y|}\zeta'_{\psi_{L,R}0}(y) = \sqrt{\frac{(\frac{1}{2} \mp c)k}{e^{2(\frac{1}{2}\mp c)\pi kR} - 1}} e^{(\frac{1}{2}\mp c)k|y|} \tag{3.88}$$

$$\zeta_{\phi 0}(y) = e^{-k|y|}\zeta'_{\phi 0}(y) = \sqrt{\frac{(b-1)k}{e^{2(b-1)\pi kR} - 1}} e^{(b-1)k|y|}, \tag{3.89}$$

where the upper (lower) sign is used for the L (R) component and $a = b(b-4)$ must be satisfied for a massless scalar mode. This is automatic for a hypermultiplet, where supersymmetry requires that $b = 3/2 \mp c$, such that $\zeta_{\psi_{L,R}0}(y) = \zeta_{\phi_{L,R}0}(y) \propto e^{(\frac{1}{2}\mp c)k|y|}$ as expected for the zero-mode fermions and scalar fields in a hypermultiplet.

In a vector supermultiplet, the profile for the zero mode of the gauge boson is

$$\zeta_{A0}(y) = \zeta'_{A0}(y) = \frac{1}{\sqrt{2\pi R}}\,, \tag{3.90}$$

while that for the gaugino corresponds to $\zeta_{\psi_L 0}(y)$ in Eq.(3.88) with $c = 1/2$, and therefore matches Eq.(3.90). Similarly for the graviton supermultiplet the zero-mode graviton profile is given by Eq.(3.89) with $b = 0$, and for the gravitino the profile is $\zeta_{\psi_L 0}(y)$ in Eq.(3.88) with $c = 3/2$, which again matches by supersymmetry.

When supersymmetry is broken, the sfermion and gaugino zero modes acquire soft masses $\hat{m}_{\phi 0}$ and $\hat{m}_{\lambda 0}$. The boundary mass terms on the IR brane induce a backreaction on the KK profiles of these fields. In this case, the zero-mode profiles are determined in the

same manner as the profiles of massive KK states:

$$\hat{\zeta}_{\phi 0}(y) = \hat{N}_\phi\, e^{k|y|}\Big[\, J_{2-b}\Big(\frac{\hat{m}_{\phi 0}}{k}e^{k|y|}\Big) - \frac{J_{1-b}(\frac{\hat{m}_{\phi 0}}{k})}{Y_{1-b}(\frac{\hat{m}_{\phi 0}}{k})}Y_{2-b}\Big(\frac{\hat{m}_{\phi 0}}{k}e^{k|y|}\Big)\,\Big]$$

$$\hat{\zeta}_{\lambda 0}(y) = \hat{N}_\lambda\, e^{k|y|}\Big[\, J_{1}\Big(\frac{\hat{m}_{\lambda 0}}{k}e^{k|y|}\Big) - \frac{J_{0}(\frac{\hat{m}_{\lambda 0}}{k})}{Y_{0}(\frac{\hat{m}_{\lambda 0}}{k})}Y_{1}\Big(\frac{\hat{m}_{\lambda 0}}{k}e^{k|y|}\Big)\,\Big], \tag{3.91}$$

where $\hat{N}_{\phi,\lambda}$ are determined by the normalization conditions [51]

$$\begin{aligned}
&\int_{-\pi R}^{\pi R} dy\, \Big(\hat{\zeta}_{\phi 0}(y)\Big)^2 = 1 \\
&\int_{-\pi R}^{\pi R} dy\, \Big(\hat{\zeta}_{\lambda 0}(y)\Big)^2 = 1 + g^2(2\pi k R)\frac{1}{2}\frac{F}{\Lambda_{\rm IR}\hat{m}_{\lambda 0}}\frac{1}{k}\Big(\hat{\zeta}_{\lambda 0}(\pi R)\Big)^2 \,.
\end{aligned} \tag{3.92}$$

Again due to the broken supersymmetry, the super-Higgs effect gives rise to the gravitino coupling on the UV brane, and the gravitino acquires a mass $\hat{m}_{\psi_\mu 0}$. This boundary mass term induces a backreaction on the gravitino KK profiles, such that the zero-mode profile is given

$$\hat{\zeta}_{\psi_\mu 0}(y) = \hat{N}_{3/2}\, e^{k|y|}\Big[\, J_{2}\Big(\frac{\hat{m}_{\psi_\mu 0}}{k}e^{k|y|}\Big) - \frac{J_{1}(\frac{\hat{m}_{\psi_\mu 0}}{k})}{Y_{1}(\frac{\hat{m}_{\psi_\mu 0}}{k})}Y_{2}\Big(\frac{\hat{m}_{\psi_\mu 0}}{k}e^{k|y|}\Big)\,\Big], \tag{3.93}$$

where

$$\int_{-\pi R}^{\pi R} dy\, \Big(\hat{\zeta}_{\psi_\mu 0}(y)\Big)^2 = 1 + \frac{1}{2}\frac{F}{\sqrt{3}M_P\hat{m}_{\psi_\mu 0}}\frac{1}{k}\Big(\hat{\zeta}_{\psi_\mu 0}(0)\Big)^2 \,, \tag{3.94}$$

determines the normalization $\hat{N}_{3/2}$.

As we discussed before, in a bulk hypermultiplet, the fermion and scalar zero-mode profiles depend on the bulk fermion mass parameter c. By the AdS/CFT correspondence, the scaling dimension of fermionic operators in the 4D dual theory is $\dim[\mathcal{O}_\psi] = 3/2 + |c \pm 1/2|$, and for scalar operators it is $\dim[\mathcal{O}_\phi] = 1 + |c \pm 1/2|$, where the upper (lower) sign is used for left-handed (right-handed) fields. Thus, there is direct relation $\delta_i = |c_i \pm 1/2|$ between the anomalous dimensions δ_i in the 4D dual theory (introduced in Section 3.2.2) and the bulk fermion mass parameters c_i. Furthermore, for a bulk vector supermultiplet, the zero-mode profiles of the gauge field and gaugino field are flat, such that the bulk mass parameter of the Majorana fermion gaugino is $c = 1/2$. Similarly, the gravity supermultiplet contains a graviton with the UV-localized zero mode ($\propto e^{-ky}$) and a spin-3/2 Rarita-Schwinger fermion

(the gravitino), whose bulk mass parameter is fixed to be $c = 3/2$.

The warped geometry naturally generates a separation of scales that can be used to explain the hierarchy between the scale of supersymmetry breaking and the Planck scale. The IR brane is therefore identified with the scale where supersymmetry is broken; the bulk and UV brane remain supersymmetric. The Higgs fields are localized on the UV brane, while the rest of the MSSM fields propagate in the bulk and couple to the Higgs fields with brane-localized Yukawa couplings. As discussed in Section 3.3.2, the degree of overlap between a particular bulk fermion zero-mode profile and a UV-localized Higgs field determines its effective 4D Yukawa coupling and thus the size of the corresponding fermion mass. In this setup, third-generation fermions are therefore UV localized, whereas the lighter first- and second-generation fermions are more IR localized.

Since the localization of the fermion in each chiral supermultiplet determines the corresponding scalar localization, this 5D fermion geography has distinctive consequences in the SUSY sector: the third-generation sfermions are generally UV localized and the first- and second-generation sfermions are IR localized. Due to the properties of localization, the effective coupling strength of each superfield on the IR brane is inversely related to its coupling strength on the UV brane. Therefore, when supersymmetry is broken on the IR brane, as discussed in Section 3.3.3, the localization of the sfermions induced by the fermion mass spectrum results in an inverted scalar soft mass spectrum: light fermions have heavy superpartners, while heavy fermions have light superpartners. We next construct the details of this distinctive supersymmetric particle spectrum.

3.3.2 The fermion mass hierarchy

Consider first the generation of the fermion mass hierarchy [40, 52]. In our 5D spacetime, the SM fermion mass hierarchy is determined from the overlap of the bulk SM fermion zero modes with the UV-localized Higgs fields. The Yukawa interactions take the form

$$\begin{aligned} S_5 &= \int d^5x\, \sqrt{-g}\, Y^{(5)}_{ij} \Big[\bar{\psi}_{iL}(x^\mu, y)\, \psi_{jR}(x^\mu, y) + \text{h.c.} \Big] H(x^\mu)\, \delta(y) \\ &\equiv \int d^4x \left[y_{ij}\, \bar{\psi}_{iL0}(x^\mu)\, \psi_{jR0}(x^\mu)\, H(x^\mu) + h.c + \cdots \right], \end{aligned} \tag{3.95}$$

where the $Y^{(5)}_{ij}$ (with flavor indices $i, j = 1, 2, 3$) are dimensionful (inverse mass) 5D Yukawa couplings, $\psi_{L(R)}$ is a Dirac spinor that contains an $\mathrm{SU}(2)_L$ doublet (singlet) of the MSSM

as its zero mode, and H is the appropriate Higgs field. Using the 5D fermion zero-mode[3] profiles Eq.(3.88), the effective 4D SM Yukawa couplings y_{ij} are then given by [40]

$$y_{ij} = Y^{(5)}_{ij}\,\zeta_{\psi_{iL}0}(0)\,\zeta_{\psi_{jR}0}(0) = Y^{(5)}_{ij}\,k\sqrt{\frac{\frac{1}{2}-c_{iL}}{e^{2(\frac{1}{2}-c_{iL})\pi kR}-1}}\sqrt{\frac{\frac{1}{2}+c_{jR}}{e^{2(\frac{1}{2}+c_{jR})\pi kR}-1}}\,. \tag{3.96}$$

By assuming that the dimensionless 5D couplings $Y^{(5)}_{ij}k$ are of order one, and since $\pi kR \gg 1$, the hierarchy in the 4D Yukawa couplings y_{ij} is generated by the order one bulk mass parameters c_i of the fermions. Recall that in the 4D dual theory, this is equivalent to choosing the anomalous dimensions δ_i.

After electroweak symmetry breaking, the neutral components of each MSSM Higgs doublet acquire VEVs, $v_u = \langle H^0_u\rangle$ and $v_d = \langle H^0_d\rangle$, which are related by $\tan\beta \equiv v_u/v_d$, and the fermions obtain masses

$$\begin{aligned}(\hat{m}_e)_{ij} &= (y_e)_{ij}\,v\cos\beta\\ (\hat{m}_d)_{ij} &= (y_d)_{ij}\,v\cos\beta\\ (\hat{m}_u)_{ij} &= (y_u)_{ij}\,v\sin\beta\,,\end{aligned} \tag{3.97}$$

where $(\hat{m}_{u,d,e})_{ij}$ and $(y_{u,d,e})_{ij}$ are the SM fermion mass and Yukawa coupling matrices, respectively, and $v^2 \equiv v_u^2 + v_d^2 \approx (174\,\text{GeV})^2$ is the SM Higgs VEV. In the mass basis, these matrices are diagonal. Neglecting quark mixing (see [51, 53] for a fuller treatment) the interaction basis coincides with the mass basis, resulting (given values for $\tan\beta$ and Λ_{IR}) in a system with 24 free parameters $(Y^{(5)}_{e,d,u})_{ii}$ and c_{L_i,e_i,Q_i,d_i,u_i} and nine constraint equations following from Eq.(3.97). If we take a universal value for the 5D Yukawa couplings such that $(Y^{(5)}_{e,d,u})_{ii} = Y^{(5)}k$, there remains one parameter degree of freedom within each generation of leptons and within each generation of quarks, which we choose as the doublet c parameters c_{L_i,Q_i}, without loss of generality.

The relations Eq.(3.97) hold for the running masses. Ultimately, we are interested in the bulk mass parameters at the IR-brane scale, where they determine the soft masses received by the sfermions when supersymmetry is broken. Therefore, before we perform the 4D-5D Yukawa matching, we first evolve the 4D Yukawa couplings to the IR-brane scale. In Figure 3.7, we give an example of the resulting matching, showing the allowed range of localizations (c parameters) of the SM leptons and quarks when the 5D Yukawa

[3]Use of the zero-mode approximation for the profiles, where the backreaction of the boundary Higgs-generated fermion mass is neglected, is a valid approximation provided $v^2/\Lambda^2_{\text{UV}} \ll 1$.

coupling takes the universal value $Y^{(5)}k = 1$ and $\Lambda_{\rm IR} = 2 \times 10^{16}$ GeV. Generally, we see that the largeness of the third-generation Yukawa couplings requires the third-generation fermions for both leptons and quarks to be UV-localized (white region), while the smaller Yukawa couplings of the first and second generations lead to IR localization (darker gray region). Although it is always possible to make one of the chiral fermions in each generation UV-localized, only for the third generation can this be done without making at least one of the other chiral fermions IR localized.

We note in passing that in the quark sector, since both singlet fields in a given generation must be separately matched to the same doublet field according to Eq.(3.96), the asymmetry between the 4D couplings y_{u_i} and y_{d_i} precludes the solution $c_{Q_i} = -c_{d_i} = -c_{u_i}$ unless $y_{u_i}/y_{d_i} = Y^{(5)}_{u_i}/Y^{(5)}_{d_i}$. In this case, the 4D Yukawa coupling hierarchies are simply moved into the 5D couplings. This behavior is an indication of the universality of the warped extra dimension: while it can explain the magnitude of the Yukawa coupling hierarchies, since it is flavor-blind, the underlying flavor structure remains as an order-one feature. In practice, we take $Y^{(5)}k$ to have a universal value and absorb the flavor structure completely into the quark c parameters. A similar situation does not arise in the lepton sector as we do not include Yukawa couplings for the neutrinos. Neutrinos can be naturally incorporated in a warped extra dimension to generate the required neutrino masses [39, 54, 55, 56, 57].

3.3.3 Supersymmetry breaking

Supersymmetry is assumed to be broken on the IR brane and is parameterized by the introduction of a spurion superfield $X = \theta\theta F_X$ that couples to the sfermions and the gauginos. The sfermions and gauginos acquire tree-level soft masses with a characteristic scale $F/\Lambda_{\rm IR}$, where $F = F_X e^{-2\pi kR}$, modulated by their overlap with the IR brane. A gravitino mass of order F/M_P is generated by the super-Higgs effect. The Higgs fields receive no tree-level soft masses, as they are confined to the UV brane and do not couple directly to the supersymmetry-breaking spurion. We do not include any mechanism to generate tree-level trilinear soft scalar couplings, although, like the Higgs-sector soft terms, they arise radiatively.

Contributions to the soft masses also generically arise from anomaly mediation. Since the gravitino mass is Planck-scale suppressed (as opposed to the other soft masses, which are suppressed by the IR-brane scale), the anomaly-mediated contribution typically is subdominant to the effects (both at tree level and loop level) of the supersymmetry-breaking sector on the IR brane. An additional source of supersymmetry breaking arises due to the

stabilization of the radion of the extra dimension, which generically requires a nonzero F-term for the radion superfield (equivalently, the introduction of a constant superpotential on the IR brane). The scale of the radion-mediated contribution to the soft masses depends on the details of the stabilization model. We are interested in the regime where such effects are subdominant to the effects of the supersymmetry-breaking sector on the IR brane. In the model of [25], this can be accomplished if the Goldberger-Wise bulk hypermultiplet is sufficiently UV localized.

3.3.3.1 Gravitino mass

When supersymmetry is spontaneously broken on the IR boundary, the effective 4D cosmological constant receives a positive contribution from the VEV of F_X. In the 5D warped geometry, this contribution can be canceled by the addition of a constant superpotential W on the UV brane [58, 59, 60, 61, 62, 63, 25], which introduces a boundary mass term for the gravitino:

$$S_5 = \int d^5x \sqrt{-g} \left[\frac{1}{4} \frac{W}{M_5^3} \psi_\mu \left[\sigma^\mu, \bar{\sigma}^\nu \right] \psi_\nu + \text{h.c.} \right] \delta(y) \,. \tag{3.98}$$

The cosmological constant vanishes when

$$|F|^2 \approx 3 \frac{|W|^2}{M_P^2} , \tag{3.99}$$

such that the lightest gravitino obtains a Majorana mass:

$$\hat{m}_{\psi_\mu 0} \approx \frac{F}{\sqrt{3} M_P} \,. \tag{3.100}$$

This is the super-Higgs effect.[4] Again, higher-order terms can be included to account for the backreaction of the gravitino boundary mass, although in practice this is not necessary in the relevant regions of our parameter space. As expected, due to the universality of gravity, this matches the usual 4D result. Since the gravitational coupling is Planck-scale suppressed, the gravitino mass is lower than the characteristic soft mass scale F/Λ_{IR} by a warp factor, and the gravitino is therefore always the LSP in the relevant regions of parameter space. This is

[4]Note that a constant superpotential can also be introduced on the IR brane, as is generically expected in the context of radion stabilization. However, such a superpotential provides a positive contribution to the cosmological constant, and so it cannot be the sole source for the gravitino mass.

consistent with the partial compositeness result Eq.(3.77) in the 4D dual theory, where the gravitino is mostly an elementary state.

3.3.3.2 Gaugino masses

For a field strength superfield W^a of a vector supermultiplet V^a containing a Standard Model gauge field A^a_μ and its Majorana fermion gaugino superpartner λ_a (where a is the gauge index), we introduce the interaction

$$S_5 = \int d^5x\,\sqrt{-g}\int d^2\theta\left[\frac{1}{2}\frac{X}{\Lambda_{\rm UV}k}W^{\alpha a}W^a_\alpha + \text{h.c.}\right]\delta(y-\pi R)\,. \tag{3.101}$$

This term gives rise to a boundary Majorana mass for the gaugino field and breaks supersymmetry, shifting the masses of the Kaluza-Klein modes up such that there is no longer a massless gaugino zero-mode solution. At tree level, the lightest KK mass is

$$\hat{m}_{\lambda 0} \approx \frac{g_5^2 k}{2\pi k R}\frac{F}{\Lambda_{\rm IR}} = g^2\frac{F}{\Lambda_{\rm IR}}\,, \tag{3.102}$$

where $g_5^2 k = (2\pi kR)g^2$. This mass expression Eq.(3.102) assumes the zero-mode approximation for the profiles, where the backreaction of the boundary Majorana mass is neglected, an approximation that is valid provided $\sqrt{F}/\Lambda_{\rm IR} \lesssim 1$. In practice, we include terms higher order in $\sqrt{F}/\Lambda_{\rm IR}$. The mass for arbitrary F can be determined by solving the full KK mass quantization condition (see [40, 33]). Note that the gaugino masses are suppressed relative to $F/\Lambda_{\rm IR}$ by $g^2 \sim g_5^2/(2\pi R)$, the square of the 4D gauge coupling [62][5], and hence the gauginos in general obtain masses suppressed below those of sfermions with flat profiles ($\pm c = 1/2$). This suppression matches that found in Eq.(3.72), as expected from the AdS/CFT dictionary.

If the supersymmetry-breaking sector does not contain any singlets with large F-terms, the interaction Eq.(3.101) is forbidden. In this case, with a nonsinglet spurion X, the leading contribution to the gaugino masses is [64]

$$S_5 = \int d^5x\,\sqrt{-g}\int d^4\theta\left[\frac{1}{2}\frac{X^\dagger X}{\Lambda_{\rm UV}^3 k}W^{\alpha a}W^a_\alpha + \text{h.c.}\right]\delta(y-\pi R)\,, \tag{3.103}$$

[5]The gauge-coupling dependence arises since we assume a generic GUT symmetry that is broken by the Higgs mechanism on the UV brane, separated from the supersymmetry-breaking sector on the IR boundary.

such that

$$\hat{m}_{\lambda 0} \approx \frac{g_5^2 k}{2\pi k R} \frac{F^2}{\Lambda_{\rm IR}^3} = g^2 \frac{F^2}{\Lambda_{\rm IR}^3} \,. \tag{3.104}$$

Except in the regime $\sqrt{F} \sim \Lambda_{\rm IR}$, this mass is highly suppressed, and other supersymmetry-breaking contributions such as radion mediation may dominate.

3.3.3.3 Sfermion masses

For a chiral supermultiplet Φ containing a Weyl fermion ψ and its complex scalar superpartner ϕ, we introduce the interaction

$$S_5 \supset \int d^5x \sqrt{-g} \int d^4\theta \, \frac{X^\dagger X}{\Lambda_{\rm UV}^2 k} \Phi^\dagger \Phi \, \delta(y - \pi R) \,. \tag{3.105}$$

As with the gauginos, adding this boundary mass breaks supersymmetry. At tree level, the lightest KK mass is

$$\hat{m}^{\rm tree}_{\phi_{L,R}0} \approx \frac{F}{\Lambda_{\rm IR}} \sqrt{\frac{\frac{1}{2} \mp c}{e^{2(\frac{1}{2} \mp c)\pi k R} - 1}} \, e^{(\frac{1}{2} \mp c)\pi k R} \sim \begin{cases} \sqrt{\pm c - \frac{1}{2}} \, \dfrac{F}{\Lambda_{\rm IR}} e^{(\frac{1}{2} \mp c)\pi k R} & \pm c > \frac{1}{2} \\ \sqrt{\frac{1}{2} \mp c} \, \dfrac{F}{\Lambda_{\rm IR}} & \pm c < \frac{1}{2} \,, \end{cases} \tag{3.106}$$

where the upper (lower) signs refer to the L (R) states. As with the gauginos, the scalar mass is valid in the limit $\sqrt{F}/\Lambda_{\rm IR} \lesssim 1$, and in our numerical calculations we include terms higher order in $F/\Lambda_{\rm IR}^2$ to account for the backreaction of the sfermion boundary mass. For simplicitly, we have taken these interactions to be flavor-diagonal, although this assumption can be relaxed. Note that the UV-localized ($\pm c > 1/2$) sfermion masses are suppressed by a warp factor relative to the IR-localized sfermion masses ($\pm c < 1/2$) because supersymmetry is broken on the IR brane. Using the relations $\Lambda_{\rm IR}/\Lambda_{\rm UV} = e^{-\pi k R}$ and $\delta_i = |c_i \pm 1/2|$, the expressions Eq.(3.106) are seen to be consistent with the masses Eq.(3.69) obtained in the 4D dual theory.

Since the soft masses generated at tree level by Eq.(3.105) can be exponentially small for UV-localized bulk scalar fields, quantum corrections become significant when $\pm c$ is sufficiently large. At the one-loop level, supersymmetry breaking is transmitted to the bulk scalars via interactions with other bulk scalars and gauginos. We derived the resulting contributions to the bulk scalar masses squared in the bulk theory. From the 4D perspective, these appear as one-loop threshold corrections to the scalar soft masses squared at the

IR-brane scale, arising when the KK modes of the theory are integrated out.

3.3.3.4 Higgs sector

The Higgs sector, confined to the UV brane, does not couple directly to the supersymmetry-breaking sector, and thus the Higgs soft terms at the IR-brane scale are zero at tree level. Nevertheless, as with the sfermions, the breaking is transmitted to the Higgs fields at the quantum level. We derived the one-loop corrections to $m_{H_u}^2$, $m_{H_d}^2$, and b from the bulk theory. The origin of the μ-term on the UV brane is assumed to arise from the Kim-Nilles mechanism, as discussed in Section 3.2.4; its magnitude is determined as necessary to ensure that electroweak symmetry is broken, along with the value of $\tan\beta$.

In Figure 3.8, we plot the magnitudes of the various one-loop contributions to the Higgs soft masses as functions of hypermultiplet localization in the singlet spurion case. The U(1) (lighter green) and SU(2) (darker green) gauge-sector contributions are independent of localization. In orange, we give the maximal contribution from a single Yukawa coupling (this corresponds to $c_L = 1/2$ or $-c_R = 1/2$ for the corresponding doublet and singlet hypermultiplets), neglecting all color multiplicity factors and modulo the 5D Yukawa coupling. These contributions are negative. In yellow is the D-term contribution from a single bulk scalar, modulo the scalar hypercharge. These individual contributions can be either positive or negative depending on the relative sign between the hypercharge of the Higgs field and the hypercharge of the scalar.

3.4 What do we have at the end of the day?

The parameter space available for our partially composite supersymmetric model is in general quite large. The overall mass scale of our sparticle spectrum is jointly determined by Λ_{IR}, the scale of the IR brane, and $\sqrt{F}$, the scale of supersymmetry breaking. Together these two parameters fill the roles associated with M_{GUT}, $m_{1/2}$, and m_0 in classic universal supergravity (SUGRA) models. We do not have the usual freedom in $\tan\beta$ and the sign of μ, which are in this case determined by electroweak symmetry breaking. In addition to these universal parameters, our model features nonuniversal IR-scale boundary conditions for the sfermion soft masses, which we specify in a flavor-dependent way by choosing field localizations to explain the SM fermion mass spectrum. We choose a universal value $Y^{(5)}k$ for all 5D Yukawa couplings, such that this specification requires fixing six additional free parameters, which we take as the doublet c parameters c_{L_i} and c_{Q_i}. We consider the

Table 3.1: Selected parameter space sampling regions.

	A	B
$\Lambda_{\rm IR}$	2×10^{16} GeV	6.5×10^{6} GeV
$\sqrt{F}$	4.75×10^{10} GeV	2×10^{6} GeV
$\tan\beta$[a]	~3	~5
sign μ	-1	-1
$Y^{(5)}k$	1	1
spurion	singlet	nonsinglet
$\hat{m}_{\lambda_{U(1)}}$[a]	52.9 TeV	14.60 TeV
$\hat{m}_{\lambda_{SU(2)}}$[a]	50.7 TeV	22.9 TeV
$\hat{m}_{\lambda_{SU(3)}}$[a]	49.85 TeV	38.94 TeV
$\hat{m}_{\psi_\mu}$	535 GeV	1 keV

[a] At scale $\Lambda_{\rm IR}$.

following five phenomenological and theoretical constraints that impose limits on the set of model parameters:

1. **Gravitino dark matter**
2. **The supersymmetric flavor problem**
3. **125 GeV Higgs mass and collider exclusion limits**
4. **Gauge coupling unification**
5. **Minimal supersymmetric particle content.**

Based on these considerations, we select the regions of parameter space given in Table 3.1 as our benchmark scenarios. With these parameters we determine the sparticle mass spectrum and Higgs boson mass predicted by the partially composite supersymmetric model. The IR brane scale, $\Lambda_{\rm IR}$, and the scale of supersymmetry breaking, $\sqrt{F}$, set the overall soft mass scale, and are chosen to comply with all phenomenological constraints. $\tan\beta$ is determined by the measured Higgs boson mass and the sign of μ is set in order to achieve the correct pattern of electroweak symmetry breaking.

To explore the parameter space of the benchmark scenarios given in Table 3.1, we randomly sample over the estimated ranges of doublet c parameters (c_{L_i,Q_i}) that are consistent with all phenomenological constraints. The allowed ranges are principally determined by the flavor-changing neutral currents (FCNC) constraints on the first- and second-generation

sfermions and by the Higgs mass constraints on the third-generation squarks. EWSB and the large D-term radiative corrections impose further limits on the c parameters that can only be determined a posteriori in the numerical renormalization. These constraints can further limit the c-parameter ranges and introduce correlations among the c parameters of successful spectra. Once the doublet c parameters are specified, the singlet c parameters are fixed according to Eq.(3.96) to generate the SM fermion mass spectrum. In order to avoid introducing any new hierarchies with this mechanism, we additionally require that all the c parameters are order-one numbers. In practice, we (generously) require $\pm c \lesssim 10$, providing effective upper and lower limits on all sfermion masses that hold in the absence of stronger constraints.

In Figure 3.9 we present the resulting superpartner pole mass spectra obeying all phenomenological constraints and consistent with the measured value of the Higgs boson mass. In general, the spread in the masses is a result of the freedom in the bulk hypermultiplet localizations (c parameters) remaining after the application of all constraints, combined with the uncertainty in the numerical calculations.

The allowed mass ranges for the third-generation sfermions are relatively unconstrained on phenomenological grounds, and their limits are principally determined by the restriction of c-parameters to order-one numbers. In particular, we note that for the stops (below 100 TeV, these can be identified unequivocally with $\widetilde{u}_{1,2}$), the general mass scale ($\sqrt{\hat{m}_{\tilde{t}_1}\hat{m}_{\tilde{t}_2}}$) is broadly consistent with the observed Higgs mass throughout the allowed c-parameter ranges.

The numerical results of our benchmark scenarios, given in Table 3.1, predict a hierarchical sfermion mass spectrum. The third-generation sfermions have masses in the approximate range 10–100 TeV (20–100 TeV for the stops), while the first- and second-generation sfermions have masses in the range 100–350 TeV. We do not obtain a unique prediction because we assume that there is no relation between the $c_{L,R}$ parameters of the left- and right-handed fermions. Nevertheless, the numerical results reveal some interesting features. Most obvious is the hierarchical nature of the spectrum. Typical renormalization group equations of the MSSM cannot produce a mass spectrum with widely separated sparticle masses, and thus, with minimal particle content, the origin of the mass hierarchy must necessarily reside in the high-scale boundary conditions. Such conditions are a generic feature of our model and result in a distinctive split spectrum. The nonuniversality of the sfermion boundary conditions is also visible at a finer level, as it is responsible for the presence of sizeable D-term radiative corrections to the scalar masses. Although the sign and magnitude of these corrections are highly constrained on tachyonic grounds, they can be

favorable for EWSB and can offset negative contributions to the scalars that arise at two loops. Due to the structure of EWSB in our model (imposed by radiative corrections from the bulk), the predicted Higgs boson mass is also sensitive to D-term corrections, and the experimentally measured mass value can therefore indirectly constrain the heaviest mass scales in the theory. In fact, since the measured Higgs mass is broadly consistent with stop masses in the 10–100 TeV range (as predicted in both benchmark scenarios) it is primarily through this effect that it constrains our benchmark spectra.

The hierarchical structure of the mass spectrum is clear. The largest hierarchy occurs for $\widetilde{\tau}_1$, where we find ratios up to $\hat{m}_{\tilde{u}_6,\tilde{d}_6}/\hat{m}_{\tilde{\tau}_1} \sim 13$ in the singlet spurion case and up to $\hat{m}_{\tilde{u}_6}/\hat{m}_{\tilde{\tau}_1} \sim 35$ in the nonsinglet spurion case. The hierarchy for the stops is relatively more modest: we find ratios up to $\hat{m}_{\tilde{u}_6,\tilde{d}_6}/\hat{m}_{\tilde{t}_1} \sim 3$ in the singlet spurion case and up to $\hat{m}_{\tilde{u}_6}/\hat{m}_{\tilde{t}_1} \sim 18$ in the nonsinglet spurion case. The size of these mass splittings, which cannot be generated by MSSM running alone, is a direct consequence of the hierarchy in the sfermion IR-brane soft mass boundary conditions, and hence is ultimately a signature of the SM fermion mass spectrum, mediated by the radiative corrections of the extra dimension and the MSSM.

To summarize, after introducing the idea of partial compositeness and engineering the electroweak symmetry breaking and supersymmetry breaking in a certain way, we were able to relate the expected inverted sfermion mass hierarchy to the known fermion mass hierarchy. The four-dimensional naive model let us calculate the tree-level mass terms which are confirmed by the warped five-dimensional calculations as we can see by comparing the following equations,

$$\begin{aligned} &\text{4D} \Longleftrightarrow \text{5D} \\ \text{sfermion mass: } &\text{Eq.(3.69)} \Longleftrightarrow \text{Eq.(3.106)} \\ \text{gaugino mass: } &\text{Eq.(3.72)} \Longleftrightarrow \text{Eq.(3.102)} \\ \text{gravitino mass: } &\text{Eq.(3.77)} \Longleftrightarrow \text{Eq.(3.100)}\,. \end{aligned} \tag{3.107}$$

These are tree-level results at a high IR scale, so the five-dimensional numerical calculations were needed for the renormalization process that takes them down to lower energies. When we only considered the tree-level results in 4D setup, Figure 3.6 showed us what the sfermion mass hierarchy looks like for different IR scales. The possibility of achieving large ratios of $m_{\tilde{e}}/m_{\tilde{t}}$ was seen, however: the 5D numerical calculations, Figure 3.9, showed us that the renormalization process below IR scale makes this ratio significantly smaller for the

singlet spurion case. Moreover, we were able to derive an analytical expression for 4D one-loop radiative corrections to Higgs mass below IR scale, and the results, Figure 3.5, nicely matched the the results, Figure 3.8, from 5D computation.

Our model is not too different from the usual MSSM, where a hidden sector with strong dynamics is typically invoked to dynamically break supersymmetry (e.g., via gaugino condensation). The supersymmetry breaking is then mediated via gravity (or alternatively, gauge interactions) to the visible sector with universal boundary conditions for the sfermion masses. The difference in our model is that the first- and second-generations of matter are composites of the strong dynamics at some high scale $\Lambda_{\rm IR}$. The composite states also directly feel the supersymmetry breaking (e.g., perhaps via a nonzero F-term of the underlying constituents), thereby giving rise to strongly flavor-dependent sfermion mass boundary conditions. Furthermore, assuming that the strong dynamics is SU(5) invariant (similar to what is imposed on the messenger sector in gauge-mediated models), gauge coupling unification is still preserved at the GUT scale $\sim 10^{16}$ GeV.

In light of the Higgs boson discovery and its implications for the supersymmetric spectrum, our model thus provides a more predictive, splitlike supersymmetry scenario by explicitly relating the SM fermion mass hierarchy to the sfermion mass spectrum. It would be interesting to construct models of the nontrivial dynamics (perhaps going beyond large-N theories) that may constrain the anomalous dimensions even further, and therefore lead to exact predictions for the sparticle spectrum. Nonetheless, the partially composite supersymmetric model provides the raision d'être for the inverted sfermion hierarchy with a gravitino LSP. The NLSP is typically a Bino, Higgsino, or right-handed stau which decays to the gravitino and could eventually be probed at a future 100 TeV collider. Alternatively, the heavy first- and second-generation sfermions could be indirectly probed via rare-decay experiments, such as the flavor-violating Mu2e experiment [66], or experiments attempting to measure the electric dipole moment of the electron [67]. Of course, with heavy superpartners, our model is tuned, and the question of why the overall scale of the sparticle spectrum is much heavier than the TeV scale remains a mystery. Perhaps this is just evidence of the multiverse, as speculated in split-supersymmetric models, or a supersymmetric relaxion mechanism is at play, or, instead, the tuning could be related to the strong dynamics of the supersymmetry-breaking sector. In any case, we have attempted to provide further rationale for why low-energy supersymmetry may be lurking at a scale of 10–1000 TeV.

Au milieu de ces hommes j'ai cheminé avec sagesse et ruse...

Mani

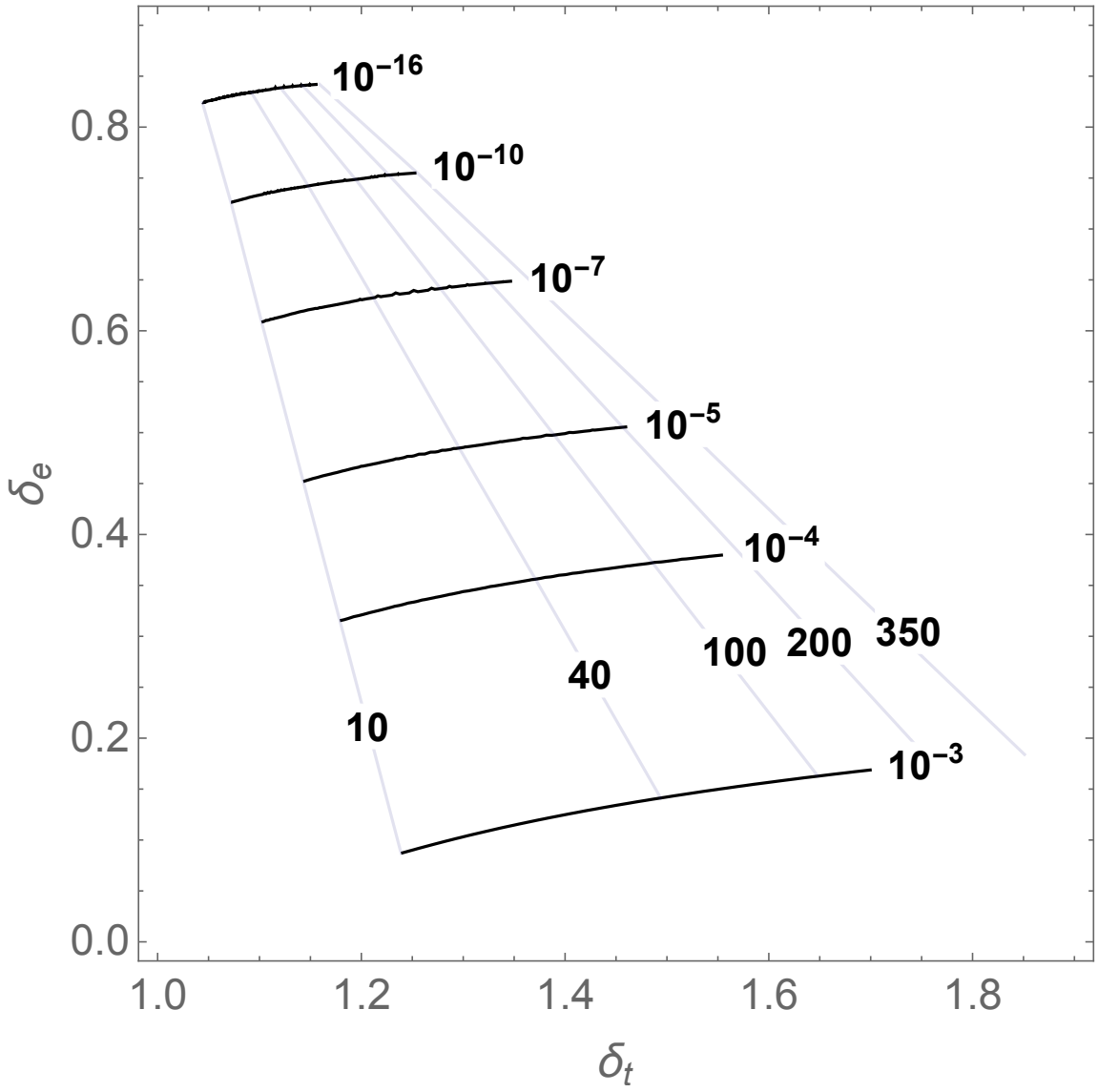

Figure 3.6: Values of the anomalous dimensions δ_e and δ_t that give rise to the electron to top-quark Yukawa coupling ratio. The approximately horizontal lines are contours of the ratio $\Lambda_{\rm IR}/\Lambda_{\rm UV}$, while the approximately vertical lines are contours of the tree-level sfermion mass ratio $\hat{m}_{\tilde{e}}/\hat{m}_{\tilde{t}}$. The running of the Yukawa couplings has been included, assuming $\Lambda_{\rm UV} = 10^{18}$ GeV, $\tan\beta = 3$, and a supersymmetric mass threshold at 50 TeV.

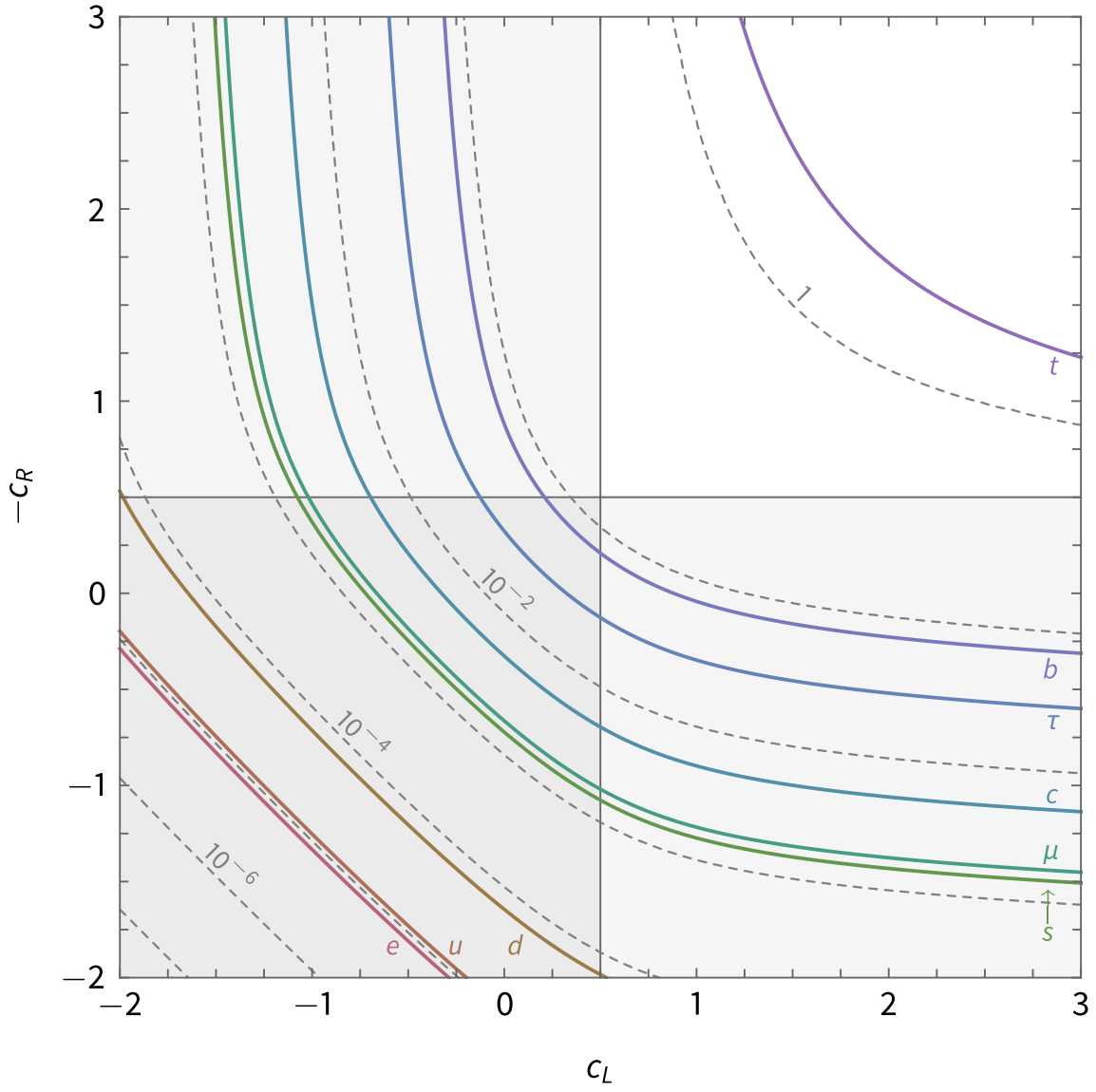

Figure 3.7: Contours of the effective 4D Yukawa coupling Eq.(3.96) at the IR-brane scale as a function of the localization parameters c_L and c_R of the bulk fermion fields for $\tan\beta = 3$, $\Lambda_{\rm IR} = 2 \times 10^{16}$ GeV, and $Y^{(5)}k = 1$. The dashed gray lines give contours of the Yukawa coupling strength. In color are contour lines corresponding to the coupling strengths of the SM Yukawa couplings at the IR-brane scale. The region in which each field is IR localized is shaded light gray and the region where both fields are IR-localized is darker gray.

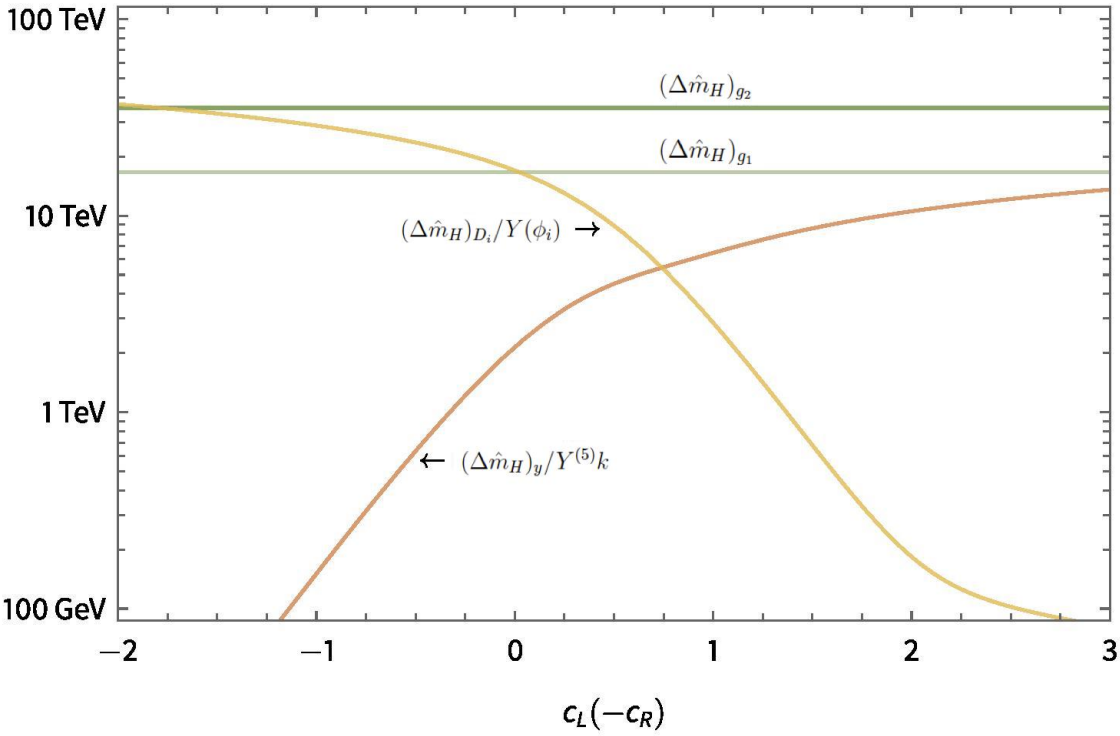

Figure 3.8: Plot of the magnitude of the one-loop radiative corrections that generate the Higgs soft masses as a function of hypermultiplet localization in the singlet spurion case. We take $\Lambda_{\rm IR} = 2 \times 10^{16}$ GeV, $\sqrt{F} = 4.75 \times 10^{10}$ GeV, and $\tan\beta = 3$. [65, 38]

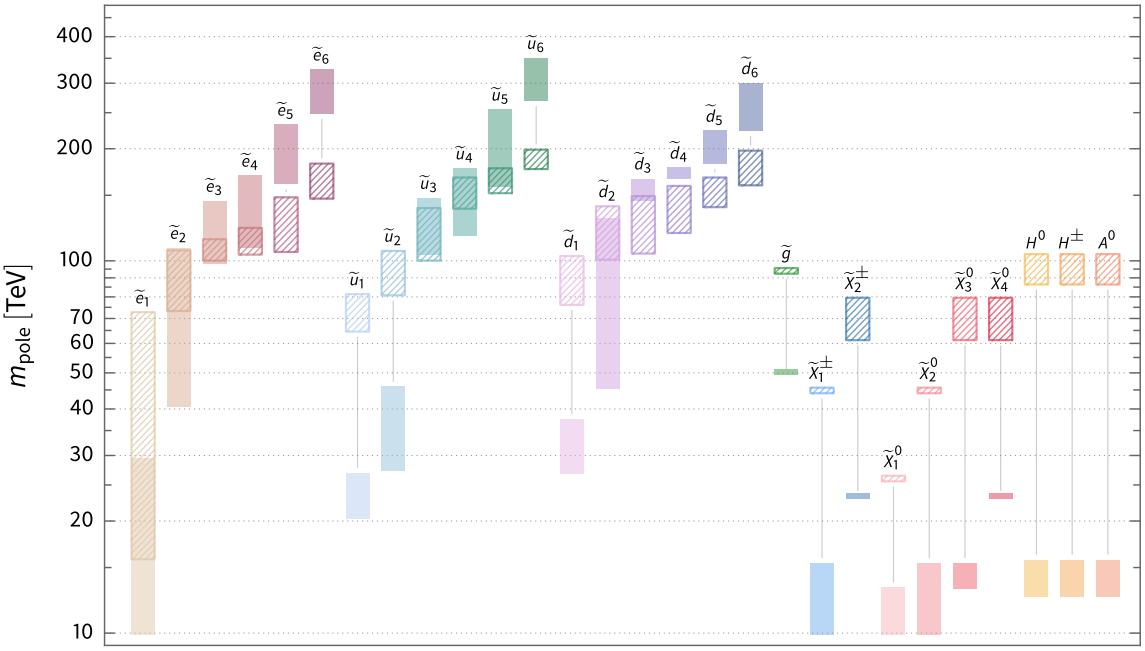

Figure 3.9: Predicted superpartner pole mass spectra for benchmark scenarios A (hatched) and B (solid) given in Table 3.1. [65, 38]

Chapter 4

Coming up with a zoo of dark matter particles

As we briefly mentioned in Chapter 1, most of the dark matter models propose a single stable dark matter particle. Since it's a stable particle or a particle with a lifetime longer than the age of the universe, it does not decay into other particles that we can observe. If it interacts with SM particles other than gravitationally, there would still be ways to detect these interactions. However, a model with dark matter particles that can decay would have a distinct signature. Stability of the dark matter sector is not a property one can give up easily without upsetting the successful cosmological predictions up to date. A multi-component dark matter model like Dynamical Dark Matter is a great way of exploiting this possibility. If one can arrange the abundances of the individual components such that the components that decay early have small enough abundances to not ruin the successful predictions of BBN, this type of more complicated approach would have promising implications on dark matter phenomenology. The required balance between the lifetimes and the abundances of the dark matter particles in the ensemble can be achieved naturally in a number of ways. The initial attempt considers a five-dimensional setup where the fifth dimension is flat. A generalization of this idea would be to work with a warped extra dimension where the zero warping limit takes one back to the flat extra dimension case. The advantage of this modification is that this model can be given a purely four-dimensional interpretation using the idea of partial compositeness similar to the supersymmetry example that we demonstrated in Chapter 3.

Now, let us consider a possible realization of the DDM framework in the context of a conformal field theory (CFT) in four dimensions. In particular, we consider a strongly-coupled theory which exhibits conformal invariance at high energies, but in which this

invariance is spontaneously broken at low energies. Below the corresponding symmetry-breaking scale, a spectrum of particle-like composite states emerges. As we will show, these composite states can acquire a spectrum of decay widths and abundances by mixing with an additional, elementary degree of freedom external to the CFT. However, since the theory is strongly coupled, it is in general not possible to calculate the masses, couplings, etc. of the physical fields of the the low-energy theory directly from first principles. It is therefore not *a priori* obvious whether these fields can collectively exhibit an appropriate balancing of decay widths against abundances for DDM.

Fortunately, the AdS/CFT correspondence [68, 69, 70] provides us with a tool for overcoming this obstacle. By studying the gravity dual of our partially composite DDM scenario we can infer information about the values of these parameters and ultimately determine how the lifetimes, abundances, etc. of the individual constituents scale across that ensemble. This dual theory involves a scalar propagating in the bulk of a spacetime orbifold which is tantamount to a slice of five-dimensional anti-de Sitter space. A spectrum of decay widths and abundances for the physical fields in the dual theory, which are admixtures of the KK modes of this bulk scalar, arises as a result of physics localized on the boundaries of this slice of AdS_5.

Moreover, the gravity dual of our partially composite DDM scenario is not only useful as a tool for gleaning information about this scenario, but is also interesting in its own right. It has been shown [14, 16] that the KK modes of an axion-like particle propagating in the bulk of a theory with a single, flat extra dimension constitute a phenomenologically viable DDM ensemble with a particular set of scaling relations. The dual of our partially composite DDM scenario can be viewed as a generalization of these flat-space bulk-scalar DDM scenarios to warped space, and thus can allow us to address a variety of questions related to such DDM scenarios. To what extent do these scenarios survive in warped space? How much warping of the space can be tolerated? As we will see, the warping has a profound effect on the phenomenology of the ensemble. Indeed, constraints on warped-space bulk-scalar DDM scenarios become increasingly stringent as the AdS curvature scale increases. Moreover, there exist interesting qualitative differences between these warped-space scenarios and their flat-space analogues. One such difference is that, in the case of a warped extra dimension, there exist regions of parameter space within which the decay widths of the ensemble constituents scale non-monotonically with their masses across the ensemble. Another difference arises due to the fact that, as a consequence of the warp factor, the effect of brane-localized dynamics on one of the boundaries of the AdS_5 slice is significantly different

from the effect of identical dynamics on the other boundary. As a result, a variety of different possible scaling behaviors can arise within the basic scenario, depending on which of the boundaries the operators responsible for establishing the abundances and decay widths of the ensemble constituents reside.

This chapter is organized as follows. In Section 4.1, we present our partially composite DDM scenario and show how a spectrum of abundances for the mass eigenstate fields in this scenario can be generated via misalignment production. In Section 4.2, we construct the gravity dual of this scenario. In Section 4.3, we calculate the total abundance and equation of state for the ensemble in this dual theory as functions of time and use this information to constrain the parameter space of our scenario. We also show that there exist substantial regions of the decay widths and abundances that exhibit the appropriate scaling relations for a DDM ensemble. In Section 4.4, we complete the dictionary which relates the parameters of the partially composite 4D theory to those of the 5D dual theory and investigate to what the flat-space limit of the dual theory corresponds in the partially composite theory.

4.1 Maybe the family of dark matter is more crowded than we thought

Partially composite scalars arise in a variety of extensions of the Standard Model. The QCD axion, for example, is an elementary scalar which mixes with with composite states such as the π^0 and η'. Models involving composite invisible axions have also been posited to explain why the allowed window for the axion decay constant lies between the grand-unification scale and the electroweak scale [71]. In this section, we consider a scenario in which a single elementary scalar mixes with a large — and potentially even infinite — number of composite states. As we will see, scenarios of this sort can be fertile ground for DDM model-building.

In constructing the elementary sector of our theory, we consider a complex scalar field Φ which is charged under a global $U(1)$ symmetry. We will assume that the potential for Φ is such that it receives a non-zero vacuum expectation value $\langle\Phi\rangle = \hat{f}_X/\sqrt{2}$, thereby spontaneously breaking this symmetry at the scale $\hat{f}_X$. At scales well below $\hat{f}_X$, this complex scalar may be parametrized as

$$\Phi \;\approx\; \frac{\hat{f}_X}{\sqrt{2}} e^{i\phi_{(0)}/\hat{f}_X} \,, \tag{4.1}$$

where $\phi_{(0)}$ is a real (CP-odd) scalar field which can be viewed as the Nambu-Goldstone

boson associated with the breaking of this symmetry. This field $\phi_{(0)}$, which could in principle be identified with the QCD axion, but could also be some additional axion-like particle, will effectively constitute the elementary sector of our theory.

Since $\phi_{(0)}$ is a Nambu-Goldstone boson, the manner in which it interacts with any other fields present in the theory is in this case dictated in part by a global shift symmetry under which $\phi_{(0)} \to \phi_{(0)} + C$, where C is an arbitrary real constant. For example, in the presence of an additional non-Abelian gauge group G, the action for $\phi_{(0)}$ takes the form

$$\mathcal{S}_\phi \;=\; \int d^4x \left[\frac{1}{2} \partial_\mu \phi_{(0)} \partial^\mu \phi_{(0)} + \frac{g_G^2 c_g \phi_{(0)}}{32\pi^2 \hat{f}_X} G_{\mu\nu} \widetilde{G}^{\mu\nu} \right] , \tag{4.2}$$

where g_G is the gauge coupling associated with the gauge group G, $G_{\mu\nu}$ is the corresponding field-strength tensor, $\widetilde{G}^{\mu\nu} \equiv \epsilon^{\mu\nu\rho\sigma} G_{\rho\sigma}/2$ is the corresponding dual field-strength tensor, and c_g is a model-dependent coefficient that parametrizes the interaction between $\phi_{(0)}$ and the gauge fields.

Strict invariance under the classical shift symmetry of Eq.(4.2) would imply that the potential for $\phi_{(0)}$ vanishes. However, this classical symmetry is broken dynamically at the quantum level by non-perturbative instanton effects associated with the gauge group G which become significant at scales around or below the scale Λ_G at which G becomes confining. Thus, $\phi_{(0)}$ is effectively massless at scales above Λ_G, while at lower scales it generically acquires a mass as a consequence of these instanton effects. The implications of this dynamically generated mass term will be discussed in greater detail below.

We now turn to discuss the composite sector of the theory. We take the fields $\widetilde{\phi}_n$ of this sector to be the composite states of a $SU(N)$ gauge theory with $N \gg 1$ which appear in the spectrum of the infrared theory at scales below the confinement scale $\Lambda_{\rm IR}$. We emphasize that this $SU(N)$ group is distinct from the non-Abelian gauge group G discussed above. At scales above $\Lambda_{\rm IR}$, the unconfined theory rapidly approaches an ultraviolet fixed point and effectively behaves as a CFT up to some ultraviolet scale $\Lambda_{\rm UV}$. At higher scales, the approximate conformal invariance of the theory is explicitly broken by the presence of additional fields Ψ with masses of order $M_\Psi \sim \Lambda_{\rm UV}$ which transform non-trivially under the same $SU(N)$ gauge group — fields which are integrated out of the effective theory below $\Lambda_{\rm UV}$. We will also assume that this $SU(N)$ gauge theory is vector-like and therefore yields no contribution to the chiral anomaly.

We will assume that the quantum numbers of the $\widetilde{\phi}_n$ are such that they can mix with $\phi_{(0)}$. Moreover, the shift symmetry once again dictates that this mixing occurs as the result of

Lagrangian terms linear in $\phi_{(0)}$. For concreteness, we will consider the simple case in which this mixing arises as the result of a coupling between $\phi_{(0)}$ and an operator $\mathcal{O}^c$ with dim $[\mathcal{O}^c] = 4$ constructed from the fundamental degrees of freedom of the unconfined $SU(N)$ theory. At the scale $\Lambda_{\rm UV}$, the action for $\phi_{(0)}$ therefore takes the form

$$\mathcal{S}_\phi = \int d^4x \Big[\frac{1}{2} \partial_\mu \phi_{(0)} \partial^\mu \phi_{(0)} + \left(\frac{\Phi}{\Lambda_{\rm UV}} \mathcal{O}^c + h.c. \right) + \frac{g_G^2 c_g \phi_{(0)}}{32\pi^2 \hat{f}_X} G_{\mu\nu} \widetilde{G}^{\mu\nu} + \dots \Big] \,. \tag{4.3}$$

We will assume that the operator $\mathcal{O}^c$ transforms non-trivially under the global $U(1)$ symmetry in such a way that the action is invariant under this symmetry. At scales $\Lambda_{\rm IR} < \mu \leq \Lambda_{\rm UV}$, radiative corrections to the kinetic term for $\phi_{(0)}$ arise as a result of the interaction in Eq.(4.3). The effect of these corrections can be interpreted as a renormalization of the kinetic term for $\phi_{(0)}$. Thus, at an arbitrary scale $\Lambda_{\rm IR} < \mu \leq \Lambda_{\rm UV}$, the kinetic term in Eq.(4.3) takes the form [70, 72]

$$\mathcal{L}_\phi \;\ni\; \frac{Z(\mu)}{2} \partial_\mu \phi_{(0)} \partial^\mu \phi_{(0)} \,, \tag{4.4}$$

where $Z(\Lambda_{\rm UV}) = 1$. The renormalization-group equation for $Z(\mu)$ in the presence of the $SU(N)$ operator $\mathcal{O}^c$, where $\langle \mathcal{O}^c \mathcal{O}^c \rangle \propto N/16\pi^2$ for large-N, takes the form

$$\frac{\partial Z(\mu)}{\partial \log \mu} \;\approx\; -2\gamma \frac{N}{16\pi^2} \left(\frac{\mu}{\Lambda_{\rm UV}} \right)^2 \,, \tag{4.5}$$

where γ is an order-one constant. In the large-N limit, the solution to this equation at low scales $\mu \ll \Lambda_{\rm UV}$ is approximately

$$Z\,(\mu) \;\approx\; \gamma \frac{N}{16\pi^2} \,. \tag{4.6}$$

In the confined phase of the theory at scales $\mu < \Lambda_{\rm IR}$, there exists a tower of composite states $\widetilde{\phi}_n$ with the masses, $\widetilde{m}_n \sim n\Lambda_{\rm IR}$. The precise mass spectrum of these states and the extent to which each of them mixes with the elementary field $\phi_{(0)}$ cannot in general be determined in a straightforward manner from the properties of the theory in the unconfined phase, due to the strong dynamics involved. Thus, for the moment, we simply seek to parametrize the Lagrangian for the fields of the confined phase in a meaningful way, given certain reasonable assumptions about the symmetry structure of the theory and certain results which are known to hold for $SU(N)$ gauge theories in the large-N limit. As we will see, however, whenever these assumptions hold, it will be possible for us to determine the properties of the physical

fields of the theory using other means.

In parametrizing the Lagrangian for the confined phase, we choose to work in a basis in which the kinetic terms for all physical fields are canonical, and mixing between these fields occurs only via the mass matrix. In this basis, it can be shown that in the large-N limit, the matrix element of the operator O^c between the vacuum and each scalar $\widetilde{\phi}_n$ takes the form [73]

$$\langle 0|O^c|\widetilde{\phi}_n\rangle \;\propto\; \frac{\sqrt{N}}{4\pi}\,. \tag{4.7}$$

The corresponding operator-field identity takes the form

$$O^c \;=\; \frac{N}{16\pi^2}\frac{\Lambda_{\rm IR}^4}{\sqrt{2}}\sum_{n=1}^{\infty}\tilde{\xi}_n^2 e^{\frac{4\pi i}{\sqrt{N}}\frac{\widetilde{\phi}_n}{\Lambda_{\rm IR}}}\,, \tag{4.8}$$

where $\tilde{\xi}_n$ is a dimensionless order-one coefficient. We now turn to consider what the action for the theory looks like in the confined phase. Given that the $SU(N)$ gauge group in our scenario is assumed to be vector-like, no coupling between the Chern-Simons term and $\phi_{(0)}$ is generated. We therefore expect that the global shift symmetry of the original action in Eq.(4.2) is not disturbed by the confining phase transition at $\mu \sim \Lambda_{\rm IR}$ and remains intact within the confined phase. This implies that a massless degree of freedom should likewise be present in the spectrum of the theory within the confined phase. To remove the constant potential that appears when we expand Eq.(4.3), we add the appropriate terms at the IR scale. It therefore follows that the Lagrangian at scales $\mu \lesssim \Lambda_{\rm IR}$ takes the form

$$\mathcal{L}_\phi = \frac{1}{2}\partial_\mu\phi_{(0)}\partial^\mu\phi_{(0)} + \sum_{n=1}^{\infty}\frac{1}{2}\partial_\mu\widetilde{\phi}_n\partial^\mu\widetilde{\phi}_n + \frac{g_G^2 c_g\phi_{(0)}}{32\pi^2\hat{f}_X}G_{\mu\nu}\widetilde{G}^{\mu\nu} + \frac{1}{2}\Lambda_{\rm IR}^2\sum_{n=1}^{\infty}\left(\varepsilon_n\phi_{(0)} + g_n\widetilde{\phi}_n\right)^2\,, \tag{4.9}$$

where the g_n and ε_n are dimensionless parameters which cannot, in general, be calculated from first principles. Indeed, we observe that the corresponding action is invariant under the combined transformations

$$\begin{aligned}\phi_{(0)} &\;\to\; \phi_{(0)} + C\\ \widetilde{\phi}_n &\;\to\; \widetilde{\phi}_n - \frac{\varepsilon_n}{g_n}C\,.\end{aligned} \tag{4.10}$$

The parameters $g_n \equiv \widetilde{m}_n/\Lambda_{\rm IR}$ in Eq.(4.9) can be viewed as a convenient parametrization for

the mass $\widetilde{m}_n$ that the field $\widetilde{\phi}_n$ would have had in the absence of mixing. By contrast, the ε_n, each of which determines the degree of mixing between $\phi_{(0)}$ and the corresponding $\widetilde{\phi}_n$, arise as a consequence of the operator $\mathcal{O}^c$ and may be viewed as a convenient reparameterization of the corresponding coefficients $\tilde{\xi}_n$ in Eq.(4.8). Indeed, through use of this operator-field identity, we see that

$$\varepsilon_n \;=\; \frac{\xi_n}{\sqrt{\gamma}}\frac{\Lambda_{\rm IR}}{\Lambda_{\rm UV}}\,, \tag{4.11}$$

where $\xi_n \equiv \tilde{\xi}_n\sqrt{\Lambda_{\rm UV}/\hat{f}_X}$. Of course, if $\varepsilon_n \neq 0$ for one or more of the $\widetilde{\phi}_n$, the mass eigenstates of the theory are not $\phi_{(0)}$ and the $\widetilde{\phi}_n$, but rather linear combinations of these fields. The mass-squared matrix which follows from the Lagrangian in Eq.(4.9) is

$$\mathcal{M}^2 \;=\; \begin{pmatrix} \sum_{n=1}^{\infty}\varepsilon_n^2 & \varepsilon_1 g_1 & \varepsilon_2 g_2 & \cdots \\ \varepsilon_1 g_1 & g_1^2 & 0 & \cdots \\ \varepsilon_2 g_2 & 0 & g_2^2 & \cdots \\ \vdots & \vdots & \vdots & \ddots \end{pmatrix}\Lambda_{\rm IR}^2\,. \tag{4.12}$$

Within the regime in which $\Lambda_{\rm IR} \ll \Lambda_{\rm UV}$, a hierarchy among the parameters develops in which $\varepsilon_n \ll 1 \lesssim g_n$ for each of the $\widetilde{\phi}_n$. Within this regime, the eigenvalues and eigenvectors of $\mathcal{M}^2$ can be reliably calculated using a perturbation expansion in the ε_n. In particular, to $\mathcal{O}(\varepsilon_n^2)$, the squared masses are

$$m_n^2 \;\approx\; \begin{cases} 0 & n = 0 \\ (\varepsilon_n^2 + g_n^2)\Lambda_{\rm IR}^2 & n > 0\,, \end{cases} \tag{4.13}$$

and the corresponding mass eigenstate fields are approximately

$$|\phi_n\rangle \;\approx\; \begin{cases} \left(1 - \displaystyle\sum_{m=1}^{\infty}\frac{\varepsilon_m^2}{2g_m^2}\right)|\phi_{(0)}\rangle - \displaystyle\sum_{m=1}^{\infty}\frac{\varepsilon_m}{g_m}|\widetilde{\phi}_m\rangle & n = 0 \\ \left(1 - \dfrac{\varepsilon_n^2}{2g_n^2}\right)|\widetilde{\phi}_n\rangle + \dfrac{\varepsilon_n}{g_n}|\phi_{(0)}\rangle + \displaystyle\sum_{m\neq 0,n}\frac{\varepsilon_n\varepsilon_m g_m}{g_n(g_n^2 - g_m^2)}|\widetilde{\phi}_m\rangle & n > 0\,. \end{cases} \tag{4.14}$$

The presence of a massless physical degree of freedom is a direct consequence of the global shift symmetry. Indeed, ϕ_0 transforms under the corresponding symmetry transformation according to the relation

$$\phi_0 \;\to\; \phi_0 + C\left(1 + \sum_{n=1}^{\infty} \frac{\varepsilon_n^2}{g_n^2}\right)^{1/2} \;\approx\; \phi_0 + C\,, \tag{4.15}$$

while $\phi_n \to \phi_n$ for all $n > 0$. Since ϕ_0 transforms non-trivially under this symmetry transformation, a mass term for this field is forbidden as long as the shift symmetry remains intact.

While we have assumed that the shift symmetry is preserved, at least approximately, during the confining phase transition at $\Lambda_{\rm IR}$, this classical symmetry is in general broken at the quantum level by instanton effects associated with the gauge group G, as discussed above. At early times, when the temperature T of the thermal bath greatly exceeds the scale Λ_G at which G becomes confining — a scale which we will assume is much smaller than $\Lambda_{\rm IR}$ —, these effects are negligible. However, when the temperature of the universe falls to around $T \sim \Lambda_G$ these effects dynamically generate a potential for $\phi_{(0)}$, which generically includes a temperature-dependent mass term $m_{\rm dyn}(T)$. Exactly how $m_{\rm dyn}(T)$ behaves as a function of T at temperatures $T \sim \Lambda_G$ depends on the details of the instanton dynamics. Nevertheless, we generically expect that $m_{\rm dyn}(T) \approx 0$ at temperatures $T \gg \Lambda_G$, while $m_{\rm dyn}(T)$ asymptotically approaches a constant value $m_\phi \equiv \lim_{T\to 0} m_{\rm dyn}(T)$ at temperatures $T \ll \Lambda_G$. Provided that the phase transition is sufficiently rapid, it is reasonable to work in the "rapid-turn-on" approximation in which we approximate the phase transition as infinitely rapid and model $m_{\rm dyn}(T)$ with a step function of the form

$$m_{\rm dyn}(T) \;\approx\; \begin{cases} 0 & T > \Lambda_G \\ m_\phi & T \leq \Lambda_G\,. \end{cases} \tag{4.16}$$

In this approximation, the mass matrix in Eq.(4.12) is modified at temperatures $T \leq \Lambda_G$ to

$$\mathcal{M}^2 \;=\; \begin{pmatrix} \frac{m_\phi^2}{\Lambda_{\rm IR}^2} + \sum_{n=1}^{\infty} \varepsilon_n^2 & \varepsilon_1 g_1 & \varepsilon_2 g_2 & \cdots \\ \varepsilon_1 g_1 & g_1^2 & 0 & \cdots \\ \varepsilon_2 g_2 & 0 & g_2^2 & \cdots \\ \vdots & \vdots & \vdots & \ddots \end{pmatrix} \Lambda_{\rm IR}^2\,. \tag{4.17}$$

Since we are assuming $\Lambda_G \ll \Lambda_{\rm IR}$, we are primarily interested in the regime within which $m_\phi^2 \ll \varepsilon_n^2 \Lambda_{\rm IR}^2$. Within this regime, the additional dynamical contribution to the mass matrix in Eq.(4.17) represents a small perturbation to the original mass matrix in Eq.(4.12). Within the regime in which $\Lambda_{\rm IR} \ll \Lambda_{\rm UV}$, the squared masses $\hat{m}_n^2$ of the theory at temperatures

$T \leq \Lambda_G$ are to $O(\varepsilon_n^2)$ given by

$$\hat{m}_n^2 \;\approx\; \begin{cases} m_\phi^2 & n = 0 \\ \left(\varepsilon_n^2 + g_n^2\right)\Lambda_{\rm IR}^2 + \dfrac{\varepsilon_n^2}{g_n^2} m_\phi^2 & n > 0\,, \end{cases} \tag{4.18}$$

while the corresponding mass eigenstate fields $\hat{\phi}_n$ are

$$|\hat{\phi}_n\rangle \;\approx\; \begin{cases} \left(1 - \displaystyle\sum_{m=1}^{\infty} \frac{\varepsilon_m^2}{2g_m^2} - \sum_{m=1}^{\infty} \frac{\varepsilon_m^2}{g_m^4}\frac{m_\phi^2}{\Lambda_{\rm IR}^2}\right)|\phi_{(0)}\rangle - \displaystyle\sum_{m=1}^{\infty}\left(\frac{\varepsilon_m}{g_m} + \frac{\varepsilon_m}{g_m^3}\frac{m_\phi^2}{\Lambda_{\rm IR}^2}\right)|\widetilde{\phi}_m\rangle & n = 0 \\ \left(1 - \dfrac{\varepsilon_n^2}{2g_n^2} - \dfrac{\varepsilon_n^2}{g_n^4}\dfrac{m_\phi^2}{\Lambda_{\rm IR}^2}\right)|\widetilde{\phi}_n\rangle + \left(\dfrac{\varepsilon_n}{g_n} + \dfrac{\varepsilon_n}{g_n^3}\dfrac{m_\phi^2}{\Lambda_{\rm IR}^2}\right)|\phi_{(0)}\rangle & \\ \qquad + \displaystyle\sum_{m\neq 0,n} \frac{\varepsilon_n \varepsilon_m g_m}{g_n(g_n^2 - g_m^2)}\left(1 + \frac{1}{g_n^2}\frac{m_\phi^2}{\Lambda_{\rm IR}^2}\right)|\widetilde{\phi}_m\rangle & n > 0\,. \end{cases} \tag{4.19}$$

We now turn to assess whether the partially composite states $\hat{\phi}_n$ which emerge in this scenario at $T \leq \Lambda_G$ can collectively play the role of a DDM ensemble. In order for this to be the case, these states must exhibit an appropriate balancing of decay widths against abundances across the ensemble as a whole. On the other hand, without additional information about the values of the constants ξ_n and g_n, we cannot at this point make any more rigorous assessment as to whether such a balancing in fact arises. On the other hand, there are many qualitative features of this partially composite theory which are auspicious from a DDM perspective. The theory includes a potentially vast number of particle species with a broad spectrum of masses, all of which are neutral under the SM gauge group. Moreover, as we will discuss in further detail below, there exists a natural mechanism — namely, misalignment production — for generating a spectrum of abundances for the $\hat{\phi}_n$ in this scenario.

The consequences of a bulk axion acquiring a misaligned vacuum value were investigated in [15]. Since ϕ_0 is forbidden from acquiring a potential at $T \gtrsim \Lambda_G$ by the shift symmetry, the VEV $\langle\phi_0\rangle$ of this field at such temperatures is arbitrary. We may parametrize this VEV in terms of a misalignment angle θ as

$$\langle\phi_0\rangle \;=\; \theta \hat{f}_X\,. \tag{4.20}$$

By contrast, $\langle\phi_n\rangle = 0$ for all ϕ_n with $n > 0$ at $T \gtrsim \Lambda_G$, since these fields already have non-zero masses $m_n \sim O(\Lambda_{\rm IR})$. After the mass-generating phase transition occurs, however,

the mass eigenstates of the theory are no longer the ϕ_n, but rather the $\hat{\phi}_n$. These latter fields can be expressed as linear combinations of the ϕ_n. In general, we may write

$$|\hat{\phi}_n\rangle \;=\; \sum_{n=0}^{\infty} U_{n\ell}|\phi_\ell\rangle\,, \tag{4.21}$$

where the $U_{n\ell} \equiv \langle\phi_\ell|\hat{\phi}_n\rangle$ are the elements of the mixing matrix between these two sets of basis states. Of particular significance for the phenomenology of the $\hat{\phi}_n$ are the *mixing coefficients* $A_n \;\equiv\; U_{n0}$ between these states and the massless state ϕ_0. Indeed, since ϕ_0 is the only one of the ϕ_n which acquires a non-zero VEV from the misalignment mechanism, the mixing coefficient A_n determines the VEV $\langle\hat{\phi}_n\rangle$ of each $\hat{\phi}_n$. In particular, in the rapid-turn-on approximation, Eq.(4.20) implies that at the time t_G at which the phase transition occurs [15], we have

$$\langle\hat{\phi}_n(t_G)\rangle \;=\; \theta A_n \hat{f}_X\;. \tag{4.22}$$

As a result, each $\hat{\phi}_n$ acquires an energy density at $t = t_G$, given by

$$\rho_n(t_G) \;=\; \frac{1}{2}\hat{m}_n^2\langle\hat{\phi}_n(t_G)\rangle^2\,, \tag{4.23}$$

and hence also a cosmological abundance. Similarly, in order to assess whether our ensemble of $\hat{\phi}_n$ constitute a viable DDM ensemble, we must also evaluate the corresponding decay widths Γ_n of these particles. One way in which the $\hat{\phi}_n$ can decay is through interactions with fields outside the composite sector — interactions which these fields inherit from the elementary field $\phi_{(0)}$. Such interactions are typically suppressed by powers of the scale $\hat{f}_X$. Since these interactions are a consequence of mixing with $\phi_{(0)}$, the matrix element for any process by which one of the $\hat{\phi}_n$ decays necessarily includes one or more factors of the *projection coefficient* $A'_n \equiv \langle\phi_{(0)}|\hat{\phi}_n\rangle$ which quantifies the extent of this mixing.

Another way in which contributions to the Γ_n might arise is through intra-ensemble decays — processes in which one of the $\widetilde{\phi}_n$ decays to a final state involving one or more other, lighter ensemble constituents. However, given that our composite sector consists of the meson-like bound states of a large-N $SU(N)$ gauge theory, we expect the collective contribution to each Γ_n from such processes to be suppressed relative to the contribution from decays inherited from $\phi_{(0)}$ into final states consisting solely of particles external to the ensemble. In a large-N gauge theory of this sort, the three-point functions for meson-like states scale as $\sim 1/\sqrt{N}$, while correlation functions with larger numbers of external lines are

suppressed by higher powers of N [73]. The amplitudes for two-body decay processes in which one such state decays to a pair of other, lighter meson-like states therefore also scale as $\sim 1/\sqrt{N}$. Thus, in the $N \to \infty$ limit, these meson-like states become free particles and their decay widths vanish, while for large but finite values of N they are heavily suppressed. An alternative way of understanding this suppression is to note that if we were to model the flux tubes of our $SU(N)$ theory as strings, as was done in the "dark-hadron" DDM model presented [18, 19], the string coupling which governs the interactions of these flux tubes with each other scales as $g_s \sim 1/N$. For these reasons, we will assume that decays to states external to the ensemble dominate the decay width of each $\hat{\phi}_n$ and neglect the effect of intra-ensemble decays in what follows.

For concreteness, we will focus on the case in which the dominant contribution to each Γ_n arises due to two-body decay processes associated with Lagrangian operators of mass dimension $d = 5$. Such an assumption is well motivated, given that $\phi_{(0)}$ is an axion-like particle and therefore naturally couples to fermion and gauge fields through such operators. In the regime in which the decay products of $\hat{\phi}_n$ are much lighter than $\hat{\phi}_n$ itself for all ensemble constituents, the decay width of each constituent is

$$\Gamma_n \;\sim\; \frac{\hat{m}_n^3}{\hat{f}_X^2} A_n'^2 \; . \tag{4.24}$$

Within the $\Lambda_{\rm IR} \ll \Lambda_{\rm UV}$ regime, Eq.(4.14) and Eq.(4.19) together imply that

$$A_n \;\approx\; \begin{cases} 1 & n = 0 \\ \frac{\xi_n}{g_n^3 \sqrt{\gamma}} \frac{m_\phi^2}{\Lambda_{\rm IR} \Lambda_{\rm UV}} & n > 0 \; . \end{cases} \tag{4.25}$$

Likewise, in this same regime, the projection coefficients are well approximated by

$$A_n' \;\approx\; \begin{cases} 1 & n = 0 \\ \frac{\xi_n}{g_n \sqrt{\gamma}} \frac{\Lambda_{\rm IR}}{\Lambda_{\rm UV}} & n > 0 \; . \end{cases} \tag{4.26}$$

However, without additional information about the constants ξ_n and g_n, we cannot determine how the A_n, and by extension the cosmological abundances of the $\hat{\phi}_n$, scale across the ensemble. Nevertheless, as we will see in the next section, we can glean the information we require in order to determine whether or not this partially composite DDM scenario is phenomenologically viable by exploiting certain aspects of the AdS/CFT correspondence.

4.2 The extra dimension comes to the rescue once again

Our ignorance of strong dynamics prevents us from being able to determine directly the manner in which the decay widths and cosmological abundances of our partially composite scalars scale across the ensemble. Nevertheless, inspired by AdS/CFT correspondence [68], we may hope to glean additional information about these scaling exponents by examining the gravity dual of our partially composite DDM scenario. As discussed at the beginning of this chapter, this dual theory involves a higher-dimensional scalar ϕ which propagates throughout the bulk of a five-dimensional spacetime orbifold which is tantamount to a slice of AdS_5. While ϕ propagates through the entirety of the bulk, the fields of the SM are assumed to be localized on the UV brane. Consistency also requires that an additional non-Abelian gauge group G is also assumed to be present in the dual theory, the gauge fields of which are likewise localized on the UV brane. Like the corresponding gauge group in the 4D theory, this gauge group is assumed to become confining at temperatures $T \lesssim \Lambda_G$, or equivalently, at times $t \gtrsim t_G$.

The bulk scalar which appears in the gravity dual of the theory presented in Section 4.1 is the axion or axion-like particle associated with a global $U(1)$ symmetry which is broken by some bulk dynamics at the scale f_X. The action for the dual theory is therefore invariant under a global shift symmetry under which $\phi \rightarrow \phi + C$, where C is an arbitrary real constant. In particular, this action takes the form

$$\mathcal{S}_\phi = -\int d^5x\sqrt{-g}\left[\frac{1}{2}\partial_M\phi\partial^M\phi + \frac{g_G^2 c_g \phi}{32\pi^2 f_X^{3/2}} G_{\mu\nu}\widetilde{G}^{\mu\nu}\delta(y)\right], \tag{4.27}$$

where g is the metric determinant, and g_G, $G_{\mu\nu}$, $\widetilde{G}^{\mu\nu}$, and c_g are defined as in Eq.(4.2). We note that according to the AdS/CFT dictionary, the 5D scalar ϕ corresponds to an operator of mass dimension $d = 4$ in the 4D CFT [74]. We also note that since a potential for ϕ is forbidden by the shift symmetry, the VEV $\langle\phi\rangle$ of this field at times $t \ll t_G$ is arbitrary. We parametrize this VEV in terms of a misalignment angle θ as follows:

$$\langle\phi(x^\mu, y)\rangle \;=\; \theta f_X^{3/2}\,. \tag{4.28}$$

In analyzing the implications of this setup, we begin by performing a KK decomposition of our bulk scalar. In particular, we write

$$\phi(x^\mu, y) \;=\; \sum_{n=0}^{\infty} \phi_n(x^\mu)\zeta_n(y)\,, \tag{4.29}$$

where $\phi_n(x^\mu)$ is the four-dimensional KK mode of $\phi(x^\mu, y)$ with KK number n, and $\zeta_n(y)$ is the bulk profile of the corresponding KK mode. We note that since the potential for our bulk scalar ϕ vanishes at times $t \lesssim t_G$, the only contribution to the mass matrix for the ϕ_n at such times is the contribution from the KK masses. Thus, the ϕ_n are also mass eigenstates of the theory at such times. The masses m_n and profiles $\zeta_n(y)$ of these fields can be determined by solving the equation of motion for $\phi(x^\mu, y)$ which follows from the action in Eq.(4.27) with the boundary conditions

$$\partial_y \phi(x^\mu, y)\big|_{y=0,\pi R} \;=\; 0\,. \tag{4.30}$$

In particular, one finds that the KK spectrum contains one massless mode ϕ_0 with a flat profile [75]

$$\zeta_0(y) \;=\; \sqrt{\frac{2k}{1 - e^{-2\pi k R}}}\,, \tag{4.31}$$

as well as a tower of massive modes with masses which are solutions to the transcendental equation

$$J_1\left(\frac{m_n}{m_{\rm KK}}\right) Y_1\left(\frac{m_n}{k}\right) \;=\; Y_1\left(\frac{m_n}{m_{\rm KK}}\right) J_1\left(\frac{m_n}{k}\right)\,, \tag{4.32}$$

where $J_\alpha(x)$ and $Y_\alpha(x)$ respectively denote the Bessel functions of the first and second kind, and we have defined

$$m_{\rm KK} \;\equiv\; k e^{-\pi k R}\,. \tag{4.33}$$

The corresponding bulk profiles of these massive modes are given by

$$\zeta_n(y) \;=\; \mathcal{N}_n e^{2ky}\left[J_2\left(\frac{m_n}{k e^{-ky}}\right) + b_n Y_2\left(\frac{m_n}{k e^{-ky}}\right)\right]\,, \tag{4.34}$$

where b_n is a constant whose value is specified by the boundary conditions for $\phi(x^\mu, y)$ at $y = 0$ and $y = \pi R$ and the normalization constant $\mathcal{N}_n$ is determined by the orthogonality relation

$$\int_0^{\pi R} e^{-2ky}\zeta_m(y)\zeta_n(y)dy \;=\; \delta_{mn}\;. \tag{4.35}$$

For the boundary conditions given in Eq.(4.30), we have

$$b_n \;=\; \frac{J_1\left(\frac{m_n}{m_{\rm KK}}\right)}{Y_1\left(\frac{m_n}{m_{\rm KK}}\right)}\;. \tag{4.36}$$

The massless mode ϕ_0, which has a flat profile in the extra dimension, inherits the VEV in Eq.(4.28) from the bulk scalar. Thus, we have

$$\langle\phi_0\rangle \;=\; \theta\sqrt{\frac{1-e^{-2\pi kR}}{2k}}f_X^{3/2} \;\equiv\; \theta\hat{f}_X\,, \tag{4.37}$$

while $\langle\phi_n\rangle = 0$ for all of the ϕ_n with $n > 0$. At times $t \sim t_G$, instanton effects associated with the gauge group G give rise to a potential for ϕ on the UV brane. We focus here on the consequences of the brane-localized mass term m_B for ϕ which generically appears in this potential. In the presence of such a mass term, the action in Eq.(4.27) is modified at times $t \gtrsim t_G$ to

$$\mathcal{S}_\phi \;=\; -\int d^5x\sqrt{-g}\left[\frac{1}{2}\partial_M\phi\partial^M\phi + m_B\phi^2\delta(y)\right]. \tag{4.38}$$

The corresponding boundary condition for ϕ on the UV brane at late times is

$$\left(\partial_y - m_B\right)\phi(x^\mu, y)\big|_{y=0} \;=\; 0\,, \tag{4.39}$$

while the boundary condition on the IR brane remains unchanged. As a result of this modification, the mass eigenstates $\hat{\phi}_n$ of the four-dimensional theory at $t \gtrsim t_G$ are no longer the KK-number eignenstates ϕ_n, but rather admixtures of these fields. The masses $\hat{m}_n$ of these fields are the solutions to the equation

$$J_1\left(\frac{\hat{m}_n}{m_{\rm KK}}\right)\left[\frac{m_B}{\hat{m}_n}Y_2\left(\frac{\hat{m}_n}{k}\right) - Y_1\left(\frac{\hat{m}_n}{k}\right)\right] \;=\; Y_1\left(\frac{\hat{m}_n}{m_{\rm KK}}\right)\left[\frac{m_B}{\hat{m}_n}J_2\left(\frac{\hat{m}_n}{k}\right) - J_1\left(\frac{\hat{m}_n}{k}\right)\right]\;. \tag{4.40}$$

The bulk profiles $\hat{\zeta}_n(y)$ of the $\hat{\phi}_n$ are given by an expression identical in form to the expression appearing in Eq.(4.34), but with $\hat{m}_n$ in place of m_n and a constant $\hat{b}_n$ which reflects the modified boundary condition on the UV brane in place of b_n. In particular, $\hat{b}_n$ turns out to have the same form as in Eq.(4.36), but with $\hat{m}_n$ in place of m_n. We note that in the presence

of a non-zero mass term m_B, all of the $\hat{\phi}_n$ — including even the lightest such state $\hat{\phi}_0$ — are massive.

We now turn to examine how the brane-localized mass term m_B affects the physics of these mass eigenstate fields. In doing so, we will find it convenient to adopt an alternative parametrization for this mass term. In particular, without loss of generality, we choose to parametrize the brane-localized mass term m_B in terms of a "brane-mass parameter" m_ϕ, which we define such that

$$m_B \;=\; \frac{m_\phi^2}{2k}\left(1 - e^{-2\pi k R}\right) \;. \tag{4.41}$$

We note that parameter m_ϕ has a straightforward physical interpretation. In particular, given the normalization for the KK zero mode in Eq.(4.31), we observe that m_ϕ^2 represents the element $\mathcal{M}^2_{00}$ of the mass-squared matrix $\mathcal{M}^2$ in the basis of the unmixed KK modes ϕ_n. In this way, the parameter m_ϕ can be viewed as the warped-space analogue of the similarly-named parameter in [13].

As discussed above, the late-time mass eigenstates $\hat{\phi}_n$ of the theory can be represented as linear combinations of the KK-number eigenstates ϕ_ℓ. In particular, one finds that [76]

$$|\hat{\phi}_n\rangle \;=\; \sum_{\ell=0}^{\infty} U_{n\ell}|\phi_\ell\rangle \,, \tag{4.42}$$

where the elements $U_{n\ell}$ of the mixing matrix which relates these two sets of states are given by

$$\begin{aligned} U_{n\ell} \;&\equiv\; \langle \phi_\ell | \hat{\phi}_n \rangle \\ &=\; \int_0^{\pi R} e^{-2ky} \zeta_\ell(y) \hat{\zeta}_n(y) dy \;. \end{aligned} \tag{4.43}$$

We will once again find it useful here, as we did when analyzing our partially composite theory in Section 4.1, to define a set of mixing coefficients $A_n \;\equiv\; U_{n0}$, which in the dual theory represent the mixing between these mass eigenstates and the KK zero-mode ϕ_0. Indeed, these mixing coefficients once again play an important role in the phenomenology of the $\hat{\phi}_n$. Since ϕ_0 is the only one of the KK-number eigenstates which acquires a non-zero VEV, A_n determines the VEV $\langle \hat{\phi}_n \rangle$ of $\hat{\phi}_n$ from the misalignment mechanism. In particular, in the rapid-turn-on approximation, Eq.(4.37) implies that [15]

$$\langle \hat{\phi}_n(t_G) \rangle \;=\; \theta A_n \hat{f}_X \;. \tag{4.44}$$

The mixing coefficients A_n can be obtained from the general expression for $U_{n\ell}$ in Eq.(4.43), which holds regardless of the relationship between m_ϕ, k, and R. However, a simple analytic approximation for A_n may also be obtained within one of the regimes of greatest phenomenological interest, which is the regime in which m_ϕ is small compared to the other relevant scales in the theory. In particular, in the regime in which $m_\phi \ll m_{\rm KK}$, the mixing coefficient A_0 for the lightest mass eigenstate $\hat{\phi}_0$ is approximately unity. Moreover, within this same regime, the mixing coefficients for all $\hat{\phi}_n$ with masses in the regime $k \gg \hat{m}_n \gg m_{\rm KK}$ are approximately given by

$$A_n \;\approx\; \sqrt{\frac{\pi}{2}} e^{-\pi k R} \left(\frac{m_\phi}{m_{\rm KK}}\right)^2 \left(\frac{m_{\rm KK}}{\hat{m}_n}\right)^{3/2} \;, \tag{4.45}$$

while the masses themselves are well approximated by

$$\hat{m}_n \;\approx\; \left(n + \frac{1}{4}\right) \pi m_{\rm KK} \;. \tag{4.46}$$

We note that since this analytic approximation is valid in the regime in which $k \gg \hat{m}_n \gg m_{\rm KK}$, the greatest degree of agreement between the values of A_n obtained from this approximation and the exact result obtained from Eq.(4.43) occurs for intermediate values of n.

In Section 4.1, we saw that a second set of coefficients, namely the projection coefficients A'_n, also played a crucial role in the phenomenology of our partially composite DDM scenario. The analogous quantity in the dual theory for each $\hat{\phi}_n$ is the coefficient $A'_n \equiv \sqrt{1 - e^{-2\pi k R}} \langle \phi(x^\mu, 0) | \hat{\phi}_n \rangle / \sqrt{2k}$ which describes the projection of this state onto the UV brane at $y = 0$. Indeed, since the fields of the SM are also assumed to be localized on the UV brane, all interactions between the $\hat{\phi}_n$ and any SM field necessarily include one or more factors of A'_n. In general, these projection coefficients are given by

$$\begin{aligned} A'_n \;&\equiv\; \sqrt{\frac{1 - e^{-2\pi k R}}{2k}} \sum_{\ell=0}^{\infty} \zeta_\ell(0) \int_0^{\pi R} e^{-2ky} \zeta_\ell(y) \hat{\zeta}_n(y) dy \\ &=\; \sqrt{\frac{1 - e^{-2\pi k R}}{2k}} \hat{\zeta}_n(0) \;, \end{aligned} \tag{4.47}$$

where in going from the first to the second line, we have used the completeness relation

$$\sum_{n=0}^{\infty} \zeta_n(y)\zeta_n(y') \;=\; e^{2ky}\delta(y-y') \;. \tag{4.48}$$

Once again, while the expression in Eq.(4.47) is completely general, simple analytic approximations for the A'_n may also be obtained within our regime of phenomenological interest — i.e., the regime in which m_ϕ is much smaller than the other relevant scales in the theory. Indeed, we find that within this regime, the A'_n for those $\hat{\phi}_n$ with masses which satisfy $k \gg \hat{m}_n \gg m_{\rm KK}$ are well approximated by

$$A'_n \;\approx\; \sqrt{\frac{\pi}{2}} e^{-\pi kR} \left(\frac{\hat{m}_n}{m_{\rm KK}}\right)^{1/2} \;. \tag{4.49}$$

4.3 Organize the family to satisfy the experimental constraints

Thus far, we have analyzed the properties of the mass eigenstate fields $\hat{\phi}_n$ which emerge in the gravity dual of our partially composite DDM scenario. We will now show that an appropriate balancing of decay widths against abundances can emerge across this collection of fields such that the $\hat{\phi}_n$ collectively constitute a viable DDM ensemble.

Cosmological constraints on dark matter decays arise primarily as a consequence of two considerations. First, such decays lead to a modification of the total dark matter abundance and the effective dark matter equation of state, and thus to a departure from the standard cosmology. Second, observational limits constrain the production rate of SM particles which might appear in the final states into which the dark matter particles decay. Since the corresponding constraints on DDM scenarios depend sensitively on the mass scales involved and on the particular channels through which the different dark matter species decay, we focus here on the constraints on the total abundance and equation of state for our ensemble of $\hat{\phi}_n$.

4.3.1 Total abundance and effective equation of state

In order to determine how the total abundance and effective equation of state for our ensemble evolve in time, we begin by assessing how the cosmological abundances Ω_n of the individual

$\hat{\phi}_n$ scale across the ensemble as a function of $\hat{m}_n$ immediately after these abundances are established. In general, $\Omega_n = \rho_n/\rho_{\rm crit}$ represents the ratio of the energy density ρ_n of $\hat{\phi}_n$ to the critical density $\rho_{\rm crit} \equiv 3M_P^2H^2$ of the universe, where M_P is the reduced Planck mass and H is the Hubble parameter. We focus here on the contribution to each of the Ω_n from misalignment production, which arises as a consequence of dynamics associated with the mass-generating phase transition described in Section 4.2. We have seen that each of the $\hat{\phi}_n$ acquires a misaligned VEV as a consequence of this phase transition. As a result, each of these fields acquires an energy density $\rho_n(t_G)$ given by Eq.(4.23). In the rapid-turn-on approximation, $\langle\hat{\phi}_n(t_G)\rangle$ is given by Eq.(4.44) and the corresponding initial abundance $\Omega_n(t_G)$ of each $\hat{\phi}_n$ at $t = t_G$ is

$$\Omega_n(t_G) \;=\; \frac{\theta^2 A_n^2 \hat{m}_n^2 \hat{f}_X^2}{6M_P^2H^2(t_G)}\,. \tag{4.50}$$

It is also important to note that the Ω_n do not necessarily all evolve with t in the same way for all $t > t_G$. Indeed, at any particular t, only those $\hat{\phi}_n$ for which $2\hat{m}_n \gtrsim 3H(t)$ experience underdamped oscillations, whereas the $\hat{\phi}_n$ for which $2\hat{m}_n \lesssim 3H(t)$ remain overdamped. We may therefore associate an oscillation-onset time t_n with each such field. At any given time t, the energy densities of those fields for which $t_n < t$ evolve in time like massive matter, whereas, the energy densities of those $\hat{\phi}_n$ with $t_n > t$ scale like vacuum energy. Since successively lighter fields begin oscillating at successively later times, we may consider the time t_0 at which the lightest ensemble constituent $\hat{\phi}_0$ begins oscillating as the time at which the initial abundance for the DDM ensemble is effectively established, since at all subsequent times $t \geq t_0$ all of the ensemble constituents behave like massive matter. Of course, the manner in which the initial abundances $\Omega_n^0 \equiv \Omega_n(t_0)$ at this time scale with $\hat{m}_n$ over some range of n depends on whether the $\hat{\phi}_n$ all begin oscillating instantaneously at $t = t_G$, or whether the t_n are staggered in time. As a result, the overall scaling behavior of Ω_n^0 with $\hat{m}_n$ turns out to be [13]

$$\Omega_n^0 \;\propto\; \begin{cases} \hat{m}_n^2 A_n^2 & \text{instantaneous} \\ \hat{m}_n^{1/2} A_n^2 & \text{staggered (RD era)} \\ A_n^2 & \text{staggered (MD era)}\,, \end{cases} \tag{4.51}$$

where in cases in which the oscillation-onset times are staggered, the manner in which Ω_n^0 scales with $\hat{m}_n$ depends on whether these oscillation-onset times occur during a radiation-dominated (RD) or matter-dominated (MD) epoch. While the expressions in Eq.(4.51) do

not account for the decays of shorter-lived ensemble constituents at times $t < t_0$, we note that these expressions are nevertheless valid either if $t_0 \ll \tau_n$ for all of the $\hat{\phi}_n$ in an ensemble with a finite number of constituents, or else if the $\hat{\phi}_n$ with $\tau_n \lesssim t_0$ collectively contribute only a negligible fraction of the total abundance of the ensemble at t_0.

At times $t \geq t_0$, all of the $\hat{\phi}_n$ behave like massive matter. Thus, their energy densities are all affected by Hubble expansion in exactly the same way. In particular, each ρ_n evolves according to an equation of the form

$$\frac{d\rho_n}{dt} \;=\; -(3H + \Gamma_n)\rho_n \,, \tag{4.52}$$

where Γ_n is the decay width of $\hat{\phi}_n$. Within either a radiation-dominated or matter-dominated era, H is well approximated by

$$H \;\approx\; \frac{\kappa}{3t} \,, \tag{4.53}$$

where κ is constant and given by

$$\kappa \;=\; \begin{cases} 3/2 & \text{RD} \\ 2 & \text{MD} \,. \end{cases} \tag{4.54}$$

Solving Eq.(4.52) for H of this form and using the fact that the critical density scales with the scale factor a like $\rho_{\text{crit}} \propto a^{-\frac{6}{\kappa}}$ within a RD or MD era, we find that

$$\Omega_n(t) \;=\; \Omega_n^* \left(\frac{a}{a_*}\right)^{\frac{6}{\kappa}-3} e^{-\Gamma_n(t-t_*)} \,, \tag{4.55}$$

where t_* is an arbitrary fiducial time within the same era and $\Omega_n^* = \Omega_n(t_*)$ and $a_* = a(t_*)$ respectively denote the values of Ω_n and a at this fiducial time. The total abundance Ω_{tot} of the ensemble, which is simply the sum of the individual Ω_n, is therefore given by

$$\Omega_{\text{tot}}(t) \;=\; \sum_{n=0}^{\infty} \Omega_n^* \left(\frac{a}{a_*}\right)^{\frac{6}{\kappa}-3} e^{-\Gamma_n(t-t_*)} \,. \tag{4.56}$$

The effective dark matter equation of state for a DDM ensemble can be characterized by a time-dependent parameter $w_{\text{eff}}(t)$, which is defined by the relation $p_{\text{tot}}(t) = w_{\text{eff}}(t)\rho_{\text{tot}}(t)$, where $p_{\text{tot}}(t)$ is the total momentum density of the ensemble as a whole at time t and $\rho_{\text{tot}}(t)$ is the corresponding energy density. This equation-of-state parameter can be written in the general form [13]

$$w_{\rm eff} \;=\; \frac{1}{3H}\frac{d\log\rho_{\rm tot}}{dt}\;. \tag{4.57}$$

Within a RD or MD era, this expression reduces to

$$w_{\rm eff} \;=\; -\frac{t}{\kappa\Omega_{\rm tot}}\frac{d\Omega_{\rm tot}}{dt}+\frac{2}{\kappa}-1\;. \tag{4.58}$$

The time derivative of the expression for $\Omega_{\rm tot}$ in Eq.(4.55) is simply

$$\frac{d\Omega_{\rm tot}}{dt} \;=\; \sum_{n=0}^{\infty}\left[\frac{2-\kappa}{t}-\Gamma_n\right]\Omega_n^*\left(\frac{a}{a_*}\right)^{\frac{6}{\kappa}-3} e^{-\Gamma_n(t-t_*)}\;. \tag{4.59}$$

Thus, we find that with the assumptions outlined above, the expression for $w_{\rm eff}$ in Eq.(4.58) simplifies to

$$\begin{aligned} w_{\rm eff} &= \frac{\sum_{n=0}^{\infty}\Omega_n^*[\Gamma_n t-(2-\kappa)]e^{-\Gamma_n(t-t_*)}}{\kappa\sum_{n=0}^{\infty}\Omega_n^* e^{-\Gamma_n(t-t_*)}}+\frac{2}{\kappa}-1 \\ &= \frac{\sum_{n=0}^{\infty}\Omega_n^*\Gamma_n t e^{-\Gamma_n(t-t_*)}}{\kappa\sum_{n=0}^{\infty}\Omega_n^* e^{-\Gamma_n(t-t_*)}}\;. \end{aligned} \tag{4.60}$$

We now turn to assess how the Γ_n scale with $\hat{m}_n$ across the ensemble. Since the fields of the SM are assumed to be localized on the UV brane, the partial width for any tree-level process in which one of the $\hat{\phi}_n$ decays directly into a final state involving these fields necessarily involves the projection coefficients A'_n. In particular, in situations in which two-body decays directly to a pair of much lighter SM particles dominate the width of $\hat{\phi}_n$, one finds that [13]

$$\Gamma_n \;\sim\; \frac{\hat{m}_n^3}{\hat{f}_X^2}A_n'^2\;. \tag{4.61}$$

In principle an additional contribution to Γ_n for each of the $\hat{\phi}_n$ can arise as a result of intra-ensemble decays. In the case of a flat extra dimension [13, 14], KK-number conservation serves to suppress such contributions, which arise in this case only through brane-localized operators. In the case of a warped extra dimension, no such conservation principle holds. Nevertheless, we expect any bulk interactions which could give rise to intra-ensemble decays to be suppressed, based on the general arguments advanced in Section 4.1 concerning the scaling properties of the decay amplitudes of the $\hat{\phi}_n$ in the 4D dual picture. We will therefore neglect the contribution from intra-ensemble decays in what follows.

4.3.2 Constraining deviations from the standard cosmology

Having derived general expressions for $\Omega_{\rm tot}$ and $w_{\rm eff}$ for our ensemble within a RD or MD era, we now turn to consider how these quantities are constrained by data. First of all, consistency with observation requires that $\Omega_{\rm tot}$ not differ significantly from the abundance of a stable, cold dark matter candidate over the range of time scales extending from the time $t_{\rm BBN}$ at which Big-Bang nucleosynthesis begins until the present time $t_{\rm now}$. Motivated by this consideration, at all times $t_0 \leq t \leq t_{\rm now}$, we will impose the bound

$$\frac{\Omega_{\rm tot}(t)}{\widetilde{\Omega}_{\rm tot}(t)} \;>\; 0.95\,, \tag{4.62}$$

where $\widetilde{\Omega}_{\rm tot}(t)$ represents the total abundance that the ensemble *would* have had at a given time t if all of the ensemble constituents had been absolutely stable. The value 0.95 has been chosen in accord with the value adopted in [18] in order to ensure that the total abundance of the ensemble does not deviate significantly from the case of a stable CDM candidate.

In addition to imposing this constraint on $\Omega_{\rm tot}$, we must also ensure that $w_{\rm eff}$ does not deviate significantly from that of a stable CDM candidate at any time during the recent cosmological past. For the case of a flat extra dimension, it was shown in [13] that this bound on $w_{\rm eff}$ could be phrased primarily as a constraint on the scaling relations which govern how the abundances, decay widths, etc. of the individual ensemble constituents scale in relation to one another across the ensemble. Indeed, in the flat-space limit, one finds that the decay widths Γ_n of the ensemble constituents increase monotonically with $\hat{m}_n$. As a result, within the regime which the spectrum of decay widths Γ_n within the ensemble is reasonably dense, one may sensibly approximate the spectrum of abundances $\Omega(\Gamma)$ and the density of states per unit decay width $n_\Gamma(\Gamma)$ within the ensemble as functions of a continuous variable Γ. Without loss of generality, one may parametrize these functions as

$$\begin{aligned} \Omega(\Gamma) &= A\Gamma^{\alpha(\Gamma)} \\ n_\Gamma(\Gamma) &= B\Gamma^{\beta(\Gamma)}\,, \end{aligned} \tag{4.63}$$

where A and B are constants and the scaling exponents $\alpha(\Gamma)$ and $\beta(\Gamma)$ are functions of Γ. Moreover, for the DDM ensembles considered in [13], $\alpha(\Gamma) \approx \alpha$ and $\beta(\Gamma) \approx \beta$ are typically roughly constant either across the entire ensemble or else across a large range of Γ. Under these assumptions, it was shown that at times $t \gtrsim t_{\rm MRE}$ after the time of matter-radiation

equality, $w_{\rm eff}$ is well approximated by

$$w_{\rm eff}(t) \;\approx\; w_{\rm eff}(t_{\rm now}) \left(\frac{t}{t_{\rm now}}\right)^{-1-x} \tag{4.64}$$

where $x \equiv \alpha + \beta$. Thus, constraints on $w_{\rm eff}$ for the case of a flat extra dimension can be phrased as bound on x and $w_{\rm eff}(t_{\rm now})$. In particular, ensembles which are likely to be phenomenologically viable are those for which $w_{\rm eff}(t_{\rm now})$ is fairly small and $x \leq -1$. The former criterion ensures that the equation-of-state parameter for the ensemble does not differ significantly from the constant value $w = 0$ associated with a stable CDM candidate at present time, while the latter criterion ensures that $0 \leq w_{\rm eff}(t) \leq w_{\rm eff}(t_{\rm now})$ for all $t \leq t_{\rm now}$.

By contrast, for the case of a warped extra dimension, constraints on $w_{\rm eff}$ cannot always be characterized in this way. The reason is that within certain regions of the parameter space of our scenario, Γ_n is not a monotonic function of $\hat{m}_n$. A non-monotonicity of this sort implies that ensemble constituents with significantly different $\hat{m}_n$ — and hence, in general, significantly different individual abundances Ω_n — can have similar or identical values of Γ_n. When this is the case, the function $\Omega(\Gamma)$ in Eq.(4.63) cannot be sensibly defined and indeed may not even be single-valued. Thus, within any region of parameter space in which such non-monotonicities in the spectrum of decay widths develop, there is no meaning to the parameter x.

In Figure 4.1, in order to show how and where such non-monotonicities can arise within the parameter space of our scenario, we display the decay-width spectra obtained for several different choices of model parameters. The dots of each color indicate the actual Γ_n values of the $\hat{\phi}_n$, and the continuous solid curve connecting these dots is included simply to guide the eye. In order to facilitate comparison between the different spectra, we normalize the decay width of each state in a given ensemble to the maximum decay width

$$\Gamma_{\rm max} \;\equiv\; \max_{\hat{m}_n \leq \Lambda_{\rm UV}} \{\Gamma_n\}, \tag{4.65}$$

obtained for any ensemble constituent with a mass in the range $\hat{m}_n \leq \Lambda_{\rm UV}$. The four decay-width spectra shown in the left panel illustrate the effect of varying the AdS_5 curvature scale in the regime in which m_ϕ is large. For all spectra shown in the panel, we have fixed $m_\phi/\Lambda_{\rm UV} = 0.398$ (indicated by the black dashed vertical line) and $\Lambda_{\rm UV} R = 3$. The four decay-width spectra shown in the right panel illustrate the effect of varying m_ϕ with $\pi k R = 4.94$ and $\Lambda_{\rm UV} R = 3$ held fixed. For each of these four spectra, the dashed vertical line of the same color indicates the corresponding value of $m_\phi/\Lambda_{\rm UV}$.

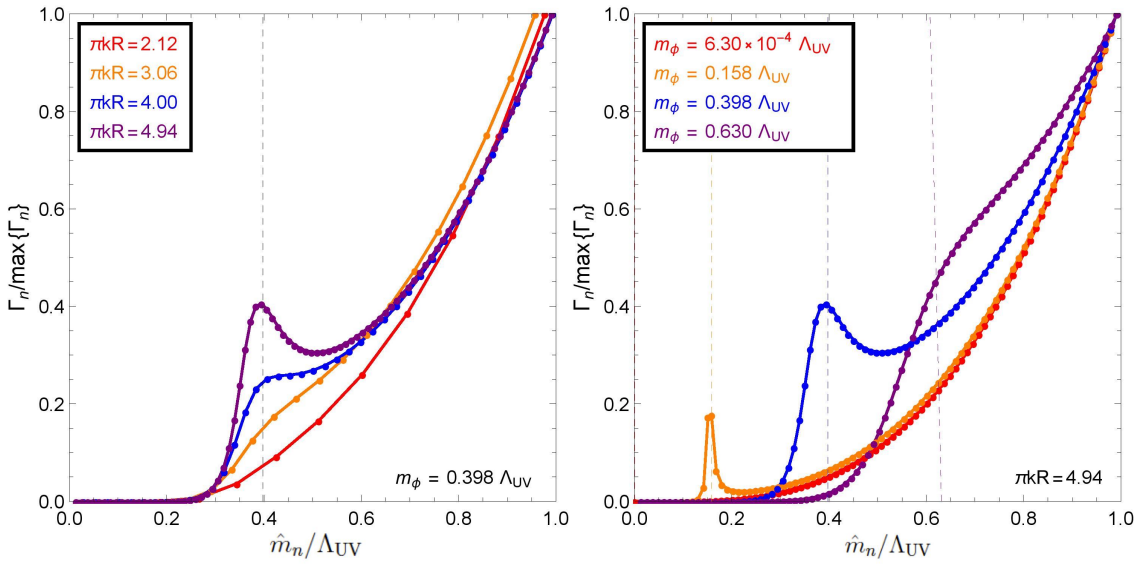

(a) (b)

Figure 4.1: The decay-width spectra obtained for several different choices of our model parameters. The dots of each color indicate the decay widths Γ_n of the ensemble constituents, normalized to the maximum width $\Gamma_{\rm max}$ obtained for any ensemble constituent with a mass in the range $\hat{m}_n \leq \Lambda_{\rm UV}$. The continuous solid curve which connects each set of dots is included simply to guide the eye. The four decay-width spectra shown in the panel (a) illustrate the effect of varying the AdS curvature scale in the regime in which m_ϕ is large with $\Lambda_{\rm UV}R = 3$ and $m_\phi/\Lambda_{\rm UV} = 0.398$ held fixed. We observe that as πkR increases, a non-monotonicity emerges in the spectrum wherein a local maximum in Γ_n occurs around $\hat{m}_n \sim m_\phi$. The four decay-width spectra shown in the panel (b) illustrate the effect of varying m_ϕ with $\pi kR = 4.94$ and $\Lambda_{\rm UV}R = 3$ held fixed.

We observe from the left panel of Figure 4.1 that for small values of πkR, the decay-width spectrum of the ensemble rises monotonically with $\hat{m}_n$, just as it does in the flat-space limit. However, as πkR increases, a local maximum in Γ_n develops around $\hat{m}_n \sim m_\phi$. This non-monotonicity, which is a consequence of the warping of the extra dimension, is an example of a qualitative feature which does not arise in flat-space DDM scenarios. This behavior is a consequence of the manner in which the projection coefficient A'_n, which is proportional to the value $\hat{\zeta}_n(0) = \hat{\mathcal{N}}_n[J_2(\hat{m}_n/k) + \hat{b}_n Y_2(\hat{m}_n/k)]$ of the bulk profile of the corresponding field on the UV brane, varies across the ensemble. Since $|J_2(\hat{m}_n/k)| \ll |Y_2(\hat{m}_n/k)|$ in the regime in which $\hat{m}_n \ll k$, the magnitude of A'_n will be maximized in this regime when the constant $\hat{b}_n$ is large. While it is not immediately obvious from the form of the expression in Eq.(4.34) that the value of $\hat{b}_n$ is enhanced for ensemble constituents with masses $\hat{m}_n \sim m_\phi$, we note that this expression can also be recast in the alternative form

$$\hat{b}_n \;=\; -\left[\frac{m_B J_2\left(\frac{\hat{m}_n}{k}\right) - \hat{m}_n J_1\left(\frac{\hat{m}_n}{k}\right)}{m_B Y_2\left(\frac{\hat{m}_n}{k}\right) - \hat{m}_n Y_1\left(\frac{\hat{m}_n}{k}\right)}\right], \tag{4.66}$$

which is obtained applying the boundary condition at $y = 0$ in Eq.(4.39) to $\phi(x^\mu, y)$ instead of the boundary condition at $y = \pi R$ in Eq.(4.30). For $\hat{m}_n \ll k$, we may approximate $J_\alpha(x)$ and $Y_\alpha(x)$ using the standard asymptotic expansions for $x \ll 1$. After some algebra, we find that

$$\hat{b}_n \;\approx\; \frac{\pi \hat{m}_n^4}{32k^4}\left[\frac{m_\phi^2(1 - e^{-2\pi kR}) - 8k^2}{m_\phi^2(1 - e^{-2\pi kR}) - \hat{m}_n^2}\right]. \tag{4.67}$$

We see that within the regime in which πkR is large, the denominator in this expression is quite small for $\hat{m}_n \sim m_\phi$. Indeed, the expression for $\hat{b}_n$ in Eq.(4.67) exhibits a singularity at $\hat{m}_n = m_\phi(1 - e^{-2\pi kR})^{1/2}$, though none of the physical masses for the ensemble constituents ever takes precisely this singular value. As a result, $\hat{b}_n$ — and therefore also A'_n — is sharply peaked for $\hat{\phi}_n$ with masses near m_ϕ in this regime. By contrast, within the regime in which πkR is small or vanishing, the asymptotic expansions which led from Eq.(4.66) to Eq.(4.67) are not valid.

In order to make contact with the results obtained in [15, 13] for the case of a flat extra dimension, now we derive the corresponding expressions valid in the regime in which $\hat{m}_n \gg k$ and then demonstrate that these expressions reduce to the expected results in the $k \to 0$ limit.

We begin by considering the mass spectrum of the theory at early times $t \lesssim t_G$, before

the phase transition occurs. The mass spectrum of the ϕ_n in this phase of the theory consists of the solutions to Eq.(4.32). In the regime in which $\pi kR \ll 1$, this equation reduces to

$$\sin(\pi m_n R) \approx 0\,, \tag{4.68}$$

which implies that $m_n \approx n/R$, in accord with the expected flat-space result. We now consider the mass spectrum of the theory at times $t \gtrsim t_G$, after the brane mass has been generated. Since the action in the flat-space limit is symmetric under the coordinate transformation $y \to \pi R - y$, the mass spectrum of the $\hat{\phi}_n$ in this limit is the same regardless of whether the dynamics that generates m_ϕ is localized on the UV or IR brane. We therefore focus on the case in which this dynamics is localized on the UV brane. The mass spectrum of the $\hat{\phi}_n$ in this phase of the theory consists of the solutions to Eq.(4.40). In the regime in which $\hat{m}_n \gg k$, regardless of the value of πkR, the Bessel functions in this equation are well approximated by

$$\begin{aligned} J_\alpha(x) &\approx \sqrt{\frac{2}{\pi x}}\cos\left(x - \frac{\alpha\pi}{2} - \frac{\pi}{4}\right) \\ Y_\alpha(x) &\approx \sqrt{\frac{2}{\pi x}}\sin\left(x - \frac{\alpha\pi}{2} - \frac{\pi}{4}\right)\,. \end{aligned} \tag{4.69}$$

One therefore finds that, in this regime, Eq.(4.40) reduces to

$$\frac{m_\phi^2}{2k}\left(1 - e^{-2\pi kR}\right)\cot\left[\frac{\hat{m}_n}{k}\left(e^{\pi kR} - 1\right)\right] \approx \hat{m}_n\,. \tag{4.70}$$

In the regime in which $\pi kR \ll 1$, this equation further reduces to

$$\pi m_\phi^2 R\cot(\pi\hat{m}_n R) \approx \hat{m}_n\,. \tag{4.71}$$

This result — and therefore the mass spectrum of the $\hat{\phi}_n$ obtained in this regime — agrees with the corresponding flat-space expression in [13, 15]. The solutions for $\hat{m}_n$ are given by $\hat{m}_n \approx (n + 1/2)/R$ for $n \ll \pi m_\phi^2 R^2$ and $\hat{m}_n \approx n/R$ for $n \gg \pi m_\phi^2 R^2$ and interpolate smoothly between these asymptotic expressions.

In order to derive the corresponding analytic approximations for A_n and A_n', we begin by noting that for $m_n \gg k$, the expression for the bulk profile $\zeta_n(y)$ of the early-time mass eigenstate ϕ_n in Eq.(4.34) reduces to

$$\zeta_n(y) \;\approx\; \frac{r_n}{\sqrt{\pi R}} e^{3ky/2} \cos\left[\frac{m_n}{k}(e^{ky} - e^{\pi kR})\right] , \tag{4.72}$$

where we have defined

$$r_n \;\equiv\; \sqrt{\frac{4\pi m_n R}{\frac{2m_n}{k}(e^{\pi kR} - 1) + \sin\left[\frac{2m_n}{k}(e^{\pi kR} - 1)\right]}} . \tag{4.73}$$

The expression for the bulk profile $\hat{\zeta}_n$ of the late-time mass eigenstate $\hat{\phi}_n$ is identical in form to the expression for $\zeta_n(y)$ in Eq.(4.72), but with $\hat{m}_n$ in place of m_n. In the regime in which $\pi kR \ll 1$, Eq.(4.72) reduces to

$$\zeta_n(y) \;\approx\; \frac{r_n}{\sqrt{\pi R}} \cos\left[m_n(y - \pi R)\right] , \tag{4.74}$$

where

$$r_n \;\approx\; \sqrt{\frac{2}{1 + \frac{\sin(2\pi m_n R)}{2\pi m_n R}}} . \tag{4.75}$$

We note that for either $m_n \approx n/R$ or $m_n \approx (n + 1/2)/R$ with $n \in \mathbb{Z}$, this quantity is well approximated by

$$r_n \;\approx\; \begin{cases} 1 & n \;=\; 0 \\ \sqrt{2} & n \;>\; 0 \,. \end{cases} \tag{4.76}$$

Taking into account the difference in normalization conventions, these results agree with those derived in [13]. Since A_n and A'_n are derived directly from $\zeta_0(y)$ and the corresponding bulk profile $\hat{\zeta}_n(y)$, it therefore follows that the mixing and projection coefficients obtained in the $k \to 0$ limit of our warped-space scenario reproduce those obtained in [15, 13] as well.

Substituting our analytic approximation for $\hat{\zeta}_n(y)$ into Eq.(4.43), we find that the elements of the mixing matrix are

$$A_n \approx \sqrt{\frac{2k}{1 - e^{-2\pi kR}}} \frac{\hat{r}_n}{\sqrt{\pi R}} \int_0^{\pi R} e^{-ky/2} \cos\left[\frac{\hat{m}_n}{k}(e^{ky} - e^{\pi kR})\right] dy , \tag{4.77}$$

where $\hat{r}_n$ is given by Eq.(4.73), but with $\hat{m}_n$ in place of m_n. In order to simplify this expression further, we observe that the integral over y can be written in terms of the Fresnel integrals

$$
\begin{aligned}
C(x) &\equiv \int_0^x \cos\left(\frac{\pi t^2}{2}\right) dt \\
S(x) &\equiv \int_0^x \sin\left(\frac{\pi t^2}{2}\right) dt \ .
\end{aligned}
\tag{4.78}
$$

In particular, we find that

$$
\begin{aligned}
A_n \approx\ & \frac{1}{\sqrt{\hat{m}_n R(1-e^{-2\pi k R})}} \left(\frac{4\hat{m}_n \hat{r}_n}{k}\right) \left\{ \sin\left(\tfrac{\hat{m}_n}{m_{\rm KK}}\right) \left[C\left(\sqrt{\tfrac{2\hat{m}_n}{\pi m_{\rm KK}}}\right) - C\left(\sqrt{\tfrac{2\hat{m}_n}{\pi k}}\right)\right] \right. \\
& \left. - \cos\left(\tfrac{\hat{m}_n}{m_{\rm KK}}\right) \left[S\left(\sqrt{\tfrac{2\hat{m}_n}{\pi m_{\rm KK}}}\right) - S\left(\sqrt{\tfrac{2\hat{m}_n}{\pi k}}\right)\right] + \sqrt{\frac{k}{2\pi\hat{m}_n}} \cos\left(\tfrac{\hat{m}_n}{m_{\rm KK}} - \tfrac{\hat{m}_n}{k}\right) - \sqrt{\frac{m_{\rm KK}}{2\pi\hat{m}_n}} \right\} .
\end{aligned}
\tag{4.79}
$$

Since we are working within the regime in which $\hat{m}_n \gg k$, we may simplify this expression by making use of the well-known asymptotic expansions for $C(x)$ and $S(x)$. In particular, for large arguments $x \gg 1$, these integrals are well approximated by

$$
\begin{aligned}
C(x) &\approx \frac{1}{2} + \frac{1}{\pi x}\sin\left(\frac{\pi x^2}{2}\right) - \frac{1}{\pi^2 x^3}\cos\left(\frac{\pi x^2}{2}\right) \\
S(x) &\approx \frac{1}{2} - \frac{1}{\pi x}\cos\left(\frac{\pi x^2}{2}\right) - \frac{1}{\pi^2 x^3}\sin\left(\frac{\pi x^2}{2}\right) \ .
\end{aligned}
\tag{4.80}
$$

With these approximations, we find that Eq.(4.79) reduces to

$$
A_n \approx \sqrt{\frac{2k}{\pi \hat{m}_n^2 R(1-e^{-2\pi k R})}}\, \hat{r}_n \sin\left[\frac{\hat{m}_n}{k}(e^{\pi k R}-1)\right] \ . \tag{4.81}
$$

Using Eq.(4.70) in order to eliminate the trigonometric functions, we arrive at our final expression for A_n in the $\hat{m}_n \gg k$ regime. After some algebra, we find that

$$
A_n \approx \sqrt{\frac{\frac{m_\phi^2}{\hat{m}_n^2}\left(\frac{1-e^{-2\pi k R}}{e^{\pi k R}-1}\right)}{\frac{\hat{m}_n^2}{m_\phi^2} + \frac{m_\phi^2}{4k^2}(1-e^{-2\pi k R})^2 + \frac{(1-e^{-2\pi k R})}{2(e^{\pi k R}-1)}}} \ . \tag{4.82}
$$

We note that for $\pi k R \ll 1$, this expression reduces to

$$A_n \;\approx\; \frac{\sqrt{2} m_\phi}{\hat{m}_n} \frac{1}{\sqrt{\frac{\hat{m}_n^2}{m_\phi^2} + \pi^2 m_\phi^2 R^2 + 1}} \,, \tag{4.83}$$

which once again agrees with the corresponding result in [15, 13]. The analytic approximation for A'_n in the $\hat{m}_n \gg k$ regime, obtained by substituting Eq.(4.74) into Eq.(4.47), is

$$A'_n \;\approx\; \sqrt{\frac{1 - e^{-2\pi k R}}{2\pi k R}} \hat{r}_n \cos\left[\frac{\hat{m}_n}{k}(e^{\pi k R} - 1)\right] \,. \tag{4.84}$$

Using Eq.(4.70) in order to eliminate trigonometric functions, we find that this expression simplifies to

$$A'_n \;\approx\; \sqrt{\frac{\frac{\hat{m}_n^2}{m_\phi^2}\left(\frac{1-e^{-2\pi k R}}{e^{\pi k R}-1}\right)}{\frac{\hat{m}_n^2}{m_\phi^2} + \frac{m_\phi^2}{4k^2}(1 - e^{-2\pi k R})^2 + \frac{(1-e^{-2\pi k R})}{2(e^{\pi k R}-1)}}} \,. \tag{4.85}$$

Comparing this result with Eq.(4.82), we observe that $A'_n \approx (\hat{m}_n/m_\phi)^2 A_n$ within this regime, in accord with the relationship between the mixing and projection coefficients obtained in [15, 13]. Moreover, we observe that the expression in Eq.(4.85) increases monotonically with $\hat{m}_n$. Thus, in the regime in which the AdS curvature is sufficiently small that the criterion $\hat{m}_n \gg k$ is satisfied for all $\hat{\phi}_n$ within the ensemble, the A'_n — and therefore also the decay widths Γ_n — do not exhibit the non-monotonicities discussed earlier, which can arise when the ensemble includes states with masses $\hat{m}_n \lesssim k$.

If we return to our case in which there are some states with $\hat{m}_n \lesssim k$, as m_ϕ is further increased, the peak in Γ_n around $\hat{m}_n \sim m_\phi$ becomes higher and broader. However, for sufficiently large m_ϕ, the decrease in A'_n with $\hat{m}_n$ beyond this peak is more than compensated for by the $\hat{m}_n^2$ factor in Eq.(4.61). As a result, the decay-width spectrum once again becomes monotonic in $\hat{m}_n$. Thus, we see that both in the regime in which $m_\phi \ll m_{\rm KK}$ and in the regime in which $m_\phi \sim \Lambda_{\rm UV}$, the scaling relation $\Omega(\Gamma)$ in Eq.(4.63) can still be meaningfully defined, even for large $\pi k R$. Rather, it is for intermediate values of m_ϕ that this description breaks down when the warping of the space becomes significant. Note that while Γ_n scales non-monotonically with $\hat{m}_n$, the abundances Ω_n nevertheless scale monotonically. Interestingly, this is the converse of the situation in [77], where it is the abundances which scale non-monotonically with mass while the decay widths are monotonic.

Since the parameter x is not well defined across the entire parameter space of our warped-space DDM scenario, we must establish a different method for constraining deviations of the effective equation-of-state parameter $w_{\rm eff}$ of the ensemble from the constant value $w = 0$ which characterizes a stable CDM candidate during the recent cosmological past. In particular, at all times $t_0 \leq t \leq t_{\rm now}$, we will impose an upper bound,

$$w_{\rm eff}(t) \ < \ 0.05 \ . \tag{4.86}$$

Once again, the value 0.05 has been chosen in accord with the value adopted in [18] in order to ensure that the equation of state for the ensemble does not deviate significantly from that of a stable CDM candidate.

4.3.3 Case study: small brane mass, strong warping

Before embarking on a general exploration of the parameter space of our 5D scenario, we begin by focusing on a particular region of interest within that parameter space. In particular, we consider the region in which the AdS curvature scale is large, in the sense that $\pi kR \gg 1$, while m_ϕ is small in comparison with all other relevant scales in the theory — a criterion which, in the highly-warped regime, is tantamount to requiring that $m_\phi \ll m_{\rm KK}$. This region is interesting for several reasons. On the one hand, the region in which $\pi kR \gg 1$ represents the greatest degree of departure from the flat-space limit investigated as a context for DDM model-building in [13, 14, 16]. Moreover, this highly-warped regime corresponds to the regime in the 4D dual theory within which $\Lambda_{\rm UV}/\Lambda_{\rm IR} = e^{\pi kR}$ is large and a significant hierarchy exists between the UV and IR scales. On the other hand as discussed above, the scaling relation $\Omega(\Gamma)$ is nevertheless sensibly defined within the regime in which $m_\phi \ll m_{\rm KK}$. Thus, within this region we may compare our results to those obtained in these previous studies in a straightforward manner. Indeed, as we will demonstrate, the scaling exponents $\alpha(\Gamma)$ and $\beta(\Gamma)$ in Eq.(4.63) are roughly constant across the range of Γ values associated with the lighter constituents in the ensemble which carry the majority of the abundance. Thus, within this region, we can meaningfully define a single value of x with the ensemble.

Within this parameter-space region of interest, the low-lying states within the ensemble include a single extremely light state $\hat{\phi}_0$ with a mass $\hat{m}_0 \sim m_\phi$, as well as a large number of additional $\hat{\phi}_n$ with masses $k \gg \hat{m}_n \gtrsim m_{\rm KK}$. While of course heavier states with $\hat{m}_n \geq k$ are also present within the ensemble, the collective abundance of these states is typically so small that the phenomenology of the ensemble is not terribly sensitive to how Ω_n and Γ_n

scale with $\hat{m}_n$ across this set of states. Thus, we will focus on the lighter $\hat{\phi}_n$ in deriving a value of x for the ensemble. The expressions for A_n and A'_n for the light states with $n > 0$ are given by Eq.(4.45) and Eq.(4.47), respectively. Each of these expressions scales with $\hat{m}_n$ according to a simple power law. Thus, we find that the abundances of the $\hat{\phi}_n$ in our 5D dual theory scale with $\hat{m}_n$ according to the relation

$$\Omega_n \;\propto\; \begin{cases} \hat{m}_n^{-1} & \text{instantaneous} \\ \hat{m}_n^{-5/2} & \text{staggered (RD era)} \\ \hat{m}_n^{-3} & \text{staggered (MD era)}\,, \end{cases} \tag{4.87}$$

while the decay widths of these states scale with $\hat{m}_n$ according to the relation

$$\Gamma_n \;\propto\; \hat{m}_n^4\,. \tag{4.88}$$

Given the results in Eq.(4.87) and Eq.(4.88), we find that the functional form for $\Omega(\Gamma)$ in this case is

$$\Omega(\Gamma) \;\propto\; \begin{cases} \Gamma^{-1/4} & \text{instantaneous} \\ \Gamma^{-5/8} & \text{staggered (RD era)} \\ \Gamma^{-3/4} & \text{staggered (MD era)}\,. \end{cases} \tag{4.89}$$

We emphasize that the scaling relation in Eq.(4.89) was derived from asymptotic expressions for A_n and A'_n valid only for $n > 0$. Within the region of parameter space in which m_ϕ is much smaller than all other relevant scales in the theory, the abundance Ω_0 and decay width Γ_0 of $\hat{\phi}_0$ do not accord with this scaling relation. Moreover, within this region of parameter space, Ω_0 typically dominates the abundance of the ensemble, while Γ_0 is typically significantly smaller than the decay widths of all of the remaining Γ_n. Indeed, this behavior arises not only in the case of a warped extra dimension, but in the corresponding $mR \ll 1$ regime in the case of a flat extra dimension as well [13]. Nevertheless, since Ω_0 represents a significant fraction of $\Omega_{\rm tot}$ within this region, $\hat{\phi}_0$ is typically required to be sufficiently long-lived that its decays at $t < t_{\rm now}$ have a negligible effect on the phenomenology of the ensemble. Rather, it is primarily the $\hat{\phi}_n$ with $n > 0$ which dictate that phenomenology. Thus, in what follows, we will focus on the $\hat{\phi}_n$ with $n > 0$ in deriving an effective value of x for our warped-space DDM ensembles — as was done in the analysis in [13].

In order to determine the scaling relation for $n_\Gamma(\Gamma)$, we begin by noting that the splitting $\hat{m}_{n+1} - \hat{m}_n$ between the masses of any two adjacent states $\hat{\phi}_{n+1}$ and $\hat{\phi}_n$ is approximately

uniform across the ensemble for $n > 0$. We are once again primarily interested in the regime in which the mass spectrum is sufficiently dense that we may approximate the density of states per unit mass $n_m(m)$ within the ensemble as a function of the continuous variable m. Within this regime, a uniform mass splitting implies that $n_m(m)$ is approximately constant across the ensemble. The corresponding density of states per unit Γ is therefore

$$n_\Gamma(\Gamma) \;=\; n_m(m) \left(\frac{d\Gamma}{dm}\right)^{-1} \;\sim\; \Gamma^{-3/4} \,. \tag{4.90}$$

Combining the results in Eq.(4.89) and Eq.(4.90), we find that within the parameter-space region in which $\pi k R \gg 1$ and $m_\phi \ll m_{\rm KK}$, the value of x obtained for our ensemble of $\hat{\phi}_n$ is

$$x \;\approx\; \begin{cases} -1 & \text{instantaneous} \\ -11/8 & \text{staggered (RD era)} \\ -3/2 & \text{staggered (MD era)} \,. \end{cases} \tag{4.91}$$

These results indicate that within this region of parameter space, our ensemble satisfies the rough consistency criterion $x \lesssim -1$ independent of the details of when the individual constituents begin oscillating. Thus, we find that ensembles of this sort indeed exhibit an appropriate balancing of decay widths against abundances for DDM. The values of x appearing in Eq.(4.91), along with the corresponding values of α and β obtained in each case, are collected in Table 4.1 for ease of reference.

4.3.4 Generalizing the scenario

It is possible to generalize the results of the previous section in several ways, even if we wish to restrict our focus to the region of parameter space within which m_ϕ is much smaller than all other relevant scales in the problem and x is well defined.

Thus far, we have focused on the case in which the fields of the SM and the dynamics which generates m_ϕ are both localized on the UV brane. However, we are also free to consider alternative possibilities in which this dynamics, the SM fields, or both are instead localized on the IR brane. Such modifications of our scenario can have a significant impact on $\Omega(\Gamma)$ and $n_\Gamma(\Gamma)$. For example, if the SM fields are localized on the IR brane, it is not the projection coefficients A'_n which determine the decay widths of our ensemble constituents, but rather a different set of coefficients $A''_n \equiv e^{-4\pi k R}\sqrt{1 - e^{-2\pi k R}}\langle\phi(x, \pi R)|\hat{\phi}_n\rangle/\sqrt{2k}$ which represent the projection of the $\hat{\phi}_n$ onto the IR brane at $y = \pi R$. A detailed derivation of the

Model		Instantaneous			Staggered (RD Era)			Staggered (MD Era)		
Brane Mass	SM Fields	α	β	x	α	β	x	α	β	x
UV	UV	$-1/4$	$-3/4$	-1	$-5/8$	$-3/4$	$-11/8$	$-3/4$	$-3/4$	$-3/2$
UV	IR	$-1/3$	$-2/3$	-1	$-5/6$	$-2/3$	$-3/2$	-1	$-2/3$	$-5/3$
IR	UV	$-1/2$	$-3/4$	$-5/4$	$-7/8$	$-3/4$	$-13/8$	-1	$-3/4$	$-7/4$
IR	IR	$-2/3$	$-2/3$	$-4/3$	$-7/6$	$-2/3$	$-11/6$	$-4/3$	$-2/3$	-2

Table 4.1: The scaling exponents α and β and the parameter $x = \alpha + \beta$ obtained for the four different possible combinations of locations for the brane mass and the SM fields in our 5D scenario within the regime in which $\pi kR \gg 1$ and $m_\phi \ll m_{\rm KK}$. Within this regime, x is well defined and approximately constant across a large number of the lower-lying $\hat{\phi}_n$ with $n > 0$ within the ensemble. Results are shown for three different possible scenarios depending on whether all of the ensemble constituents begin oscillating (and thus behaving as matter rather than as vacuum energy) instantaneously at the time of the mass-generating phase transition, or whether different constituents begin oscillating at different times in staggered fashion after the phase transition has occurred, during either a RD or MD epoch.

values of α and β for each of the four possible combinations of locations for the brane mass and the SM fields is provided as follows. Once again, in deriving these scaling exponents, we focus on the regime in which $\pi kR \gg 1$ and $m_\phi \ll m_{\rm KK}$.

In Section 4.2 we derived expressions for the mixing and projection coefficients A_n and A'_n for the ensemble constituents for the case in which the dynamics which generates the mass term m_ϕ and the SM particles into which these ensemble constituents decay are both localized on the UV brane. In this section, we derive the corresponding expression for A_n for the case in which the dynamics that generates m_ϕ is localized on the IR brane and the corresponding expression for A'_n for the case in which the SM is localized on the IR brane. From these results and those appearing in Eq.(4.45) and Eq.(4.47), the scaling exponents α and β for all possible combinations of locations for the mass-generating dynamics and the SM can be determined in a straightforward manner.

4.3.4.1 Mass-generating dynamics on the IR brane

We begin by deriving the mixing coefficients A_n for the case in which the dynamics that generates m_ϕ is localized on the IR brane. At times $t \lesssim t_G$ before the scale at which the mass-generating phase transition occurs, the action is essentially the same as it is in the case in which m_ϕ is localized on the UV brane. The lightest state is likewise massless, with a profile given by Eq.(4.31), while the remaining states have masses given by the solutions of Eq.(4.32) and profiles given by Eqs.(4.34). However, at times $t \gtrsim t_G$, however, the action in this case is given not by Eq.(4.38), but rather by

$$\mathcal{S}_\phi \;=\; -\int d^5x\sqrt{-g}\left[\frac{1}{2}\partial_M\phi\partial^M\phi - m_B\phi^2\delta(y-\pi R)\right]. \tag{4.92}$$

The masses and bulk profiles of the mass eigenstates $\hat{\phi}_n$ can be determined by solving the equation of motion derived from Eq.(4.92) with the boundary conditions

$$\begin{aligned}\partial_y\phi(x^\mu,y)\big|_{y=0} &= 0\\ \left(\partial_y - m_B\right)\phi(x^\mu,y)\big|_{y=\pi R} &= 0\,.\end{aligned} \tag{4.93}$$

In particular, the masses $\hat{m}_n$ are the solutions to the equation

$$J_1\left(\frac{\hat{m}_n}{k}\right)\left[\frac{m_B}{\hat{m}_n e^{\pi kR}}Y_2\left(\frac{\hat{m}_n}{m_{\rm KK}}\right) - Y_1\left(\frac{\hat{m}_n}{m_{\rm KK}}\right)\right] = Y_1\left(\frac{\hat{m}_n}{k}\right)\left[\frac{m_B}{\hat{m}_n e^{\pi kR}}J_2\left(\frac{\hat{m}_n}{m_{\rm KK}}\right) - J_1\left(\frac{\hat{m}_n}{m_{\rm KK}}\right)\right], \tag{4.94}$$

while the bulk profiles once again take the form

$$\hat{\zeta}_n(y) \;=\; \hat{\mathcal{N}}_n e^{2ky}\left[J_2\left(\frac{\hat{m}_n}{ke^{-ky}}\right) + \hat{b}_n Y_2\left(\frac{\hat{m}_n}{ke^{-ky}}\right)\right], \tag{4.95}$$

where $\hat{\mathcal{N}}_n$ is a normalization coefficient. However, due to the difference in boundary conditions in this case relative to the case in which m_ϕ is localized on the UV brane, the constant $\hat{b}_n$ is given not by Eq.(4.36), but rather by

$$\hat{b}_n \;=\; -\frac{J_1\left(\frac{\hat{m}_n}{k}\right)}{Y_1\left(\frac{\hat{m}_n}{k}\right)}\,. \tag{4.96}$$

For any given choice of m_ϕ, k, and R, evaluating $A_n = U_{n0}$ for the case in which m_ϕ is localized on the IR brane is simply a matter of substituting the expression for $\hat{\zeta}_n(y)$ in Eq.(4.95) into Eq.(4.43). However, we note that simple analytic expressions for the A_n can be derived within the regime in which $m_\phi \ll m_{\rm KK}$. As in the case in which m_ϕ is localized on the UV brane, we find that A_0 is approximately unity. Moreover, within the same regime, we find that the mixing coefficients for all $\hat{\phi}_n$ with masses within the regime $k \gg \hat{m}_n \gg m_{\rm KK}$ are well approximated by

$$A_n \;\approx\; e^{-3\pi kR}\left(\frac{m_\phi}{m_{\rm KK}}\right)^2\left(\frac{m_{\rm KK}}{\hat{m}_n}\right)^2, \tag{4.97}$$

while the $\hat{m}_n$ themselves are once again well approximated by the expression in Eq.(4.46). The initial abundances Ω_n^0 for the ensemble constituents with masses within the regime $k \gg \hat{m}_n \gg m_{\rm KK}$ in the case in which the mass-generating dynamics is localized on the IR brane may be obtained simply by substituting our result for A_n in Eq.(4.97) into Eq.(4.51). This yields

$$\Omega_n^0 \sim \begin{cases} \hat{m}_n^{-2} & \text{instantaneous} \\ \hat{m}_n^{-\frac{7}{2}} & \text{staggered (RD era)} \\ \hat{m}_n^{-4} & \text{staggered (MD era)} \, . \end{cases} \tag{4.98}$$

4.3.4.2 SM on the IR brane

We have seen in cases in which the SM fields into which the $\hat{\phi}_n$ decay are localized on the UV brane, the quantity A'_n plays a crucial role in determining how Γ_n scales with $\hat{m}_n$ across the ensemble. By contrast, in cases in which the SM fields are localized on the IR brane, it is the quantity A''_n, which describes the projection of $\hat{\phi}_n$ onto the IR brane at $y = \pi R$, which plays this same role. In general, these projection coefficients are given by

$$\begin{aligned} A''_n &\equiv e^{-4\pi kR} \sqrt{\frac{1-e^{-2\pi kR}}{2k}} \sum_{\ell=0}^{\infty} \zeta_\ell(\pi R) \int_0^{\pi R} dy \; e^{-2ky} \zeta_\ell(y) \hat{\zeta}_n(y) \\ &= e^{-4\pi kR} \sqrt{\frac{1-e^{-2\pi kR}}{2k}} \hat{\zeta}_n(\pi R) \, , \end{aligned} \tag{4.99}$$

where in going from the first to the second line, we have once again used the completeness relation in Eq.(4.48).

As was the case with our expression for A'_n in Eq.(4.47), the expression for A''_n in Eq.(4.99) turns out to have a simple analytic form within the regime in which $m_\phi \ll m_{\rm KK}$ and $k \gg \hat{m}_n \gtrsim m_{\rm KK}$. In particular, we find that

$$A''_n \approx e^{-3\pi kR} \, . \tag{4.100}$$

The scaling relation for the decay widths in this regime may be obtained by substituting this result for A''_n into Eq.(4.61), which yields

$$\Gamma_n \propto \hat{m}_n^3 \, . \tag{4.101}$$

The density of states per unit Γ in this case is therefore

$$n_\Gamma \;\sim\; n_m(m)\left(\frac{d\Gamma}{dm}\right)^{-1} \;\sim\; \Gamma^{-2/3}. \tag{4.102}$$

Given these results above, it is straightforward to evaluate the values of α and β obtained in the $m_\phi \ll m_{\rm KK}$ regime for any of the four possible configurations for the brane mass and the SM fields. These values are tabulated in Table 4.1.

It is also interesting to consider how the results in Table 4.1 are modified when we depart from the $\pi kR \gg 1$ regime. However, while the parameter x is always well defined within the region of parameter space wherein m_ϕ is much smaller than all other relevant scales in the problem, regardless of the value of πkR, it is not always constant. Thus, in assessing how our results for x generalize for arbitrary values of πkR, we must first identify the regions of parameter space within which x is constant across a large number of the lower-lying $\hat{\phi}_n$ with $n > 0$ within the ensemble, since it is only within these regions where we can meaningfully associate a single value of x with the ensemble. We have already seen that this is the case within the regime wherein $\pi kR \gg 1$. For πkR outside this regime, however, the number of states with masses $k \gg \hat{m}_n \gtrsim m_{\rm KK}$ is far smaller. When this is the case, x is not necessarily constant even across the lightest several $\hat{\phi}_n$ with $n > 0$ in the ensemble. That said, we also note that for $\pi kR \lesssim 1$, all of the low-lying $\hat{\phi}_n$ with $n > 0$ have $\hat{m}_n \gtrsim k$. As a result, x is approximately constant across this portion of the ensemble within this regime. Thus, it is once again sensible from a DDM perspective to identify this value of x as the effective value of x for the ensemble.

Given these considerations, we adopt the following procedure in analyzing how x varies as a function of πkR. We calculate a value of x only for those ensembles for which the masses of the $\hat{\phi}_n$ with $1 \leq n \leq 10$ either all satisfy the condition $\hat{m}_n \leq k$ or else all satisfy the condition $\hat{m}_n \geq k$. We then calculate x by performing linear fits of both $\log(A_n)$ and $\log(A'_n)$ to $\log(\hat{m}_n)$ for the set of ensemble constituents $\hat{\phi}_n$ with $2 \leq n \leq 9$. In this way, we may define an effective value of x for all πkR either above or below the rough range $1 \lesssim \pi kR \lesssim 3$.

In Figures 4.2, 4.3 and 4.4, we plot this effective value of x as a function of $\pi kR = \log(\Lambda_{\rm UV}/\Lambda_{\rm IR})$ for all four possible combinations of locations for the brane mass and the SM fields. The results shown in Figures 4.2, 4.3 and 4.4 correspond respectively to the case in which the $\hat{\phi}_n$ all begin oscillating instantaneously at $t_n = t_G$, the case in which the t_n are staggered in time during a RD epoch, and the case in which the t_n are staggered in time during a MD epoch. All points displayed in these figures correspond to the same value for

the dimensionless product $m_\phi R \approx 3.5 \times 10^{-4}$ — a value chosen such that $m_\phi = m_{\rm KK}$ for the largest value of $\pi k R$ within the range $0 \leq \pi k R \leq 9$ included in each plot. This parameter choice ensures that $m_\phi \ll m_n$ for all $n > 1$ across this entire range of $\pi k R$. While we have connected these points in order to guide the eye, we emphasize that we have only included x values for $\pi k R$ within the ranges $\pi k R \lesssim 1$ and $\pi k R \gtrsim 3$ wherein this quantity is sensibly defined.

For all of the curves shown in Figures 4.2, 4.3 and 4.4, we observe that the value of x rapidly approaches the corresponding asymptotic value quoted in Table 4.1 as $\pi k R \gtrsim 1$. Moreover, we see that the values of x obtained for $\pi k R = 9$ accord well with this asymptotic value in all cases. By contrast, we see in each figure that as $\pi k R \to 0$, the values of x obtained for all possible combinations of brane-mass and SM-field locations asymptote to a single, common value. This common value is precisely the value of x obtained in [13] for the corresponding oscillation-onset behavior in the flat-space limit: $x = -4/3$ for an instantaneous turn-on, $x = -11/10$ and for a staggered turn-on during a RD epoch, and $x = -2$ for a staggered turn-on during a MD epoch.

4.3.5 Surveying the parameter space

We now turn to examine how the bounds in Eq.(4.62) and Eq.(4.86) constrain the full parameter space of our ensemble. We will assume that the lightest ensemble constituent begins oscillating well before the beginning of the BBN epoch — *i.e.*, that $t_0 \ll t_{\rm BBN}$. When evaluating $\Omega_{\rm tot}$ and $w_{\rm eff}$ during the RD era prior to $t_{\rm MRE}$, we take our fiducial time t_* in Eq.(4.56) and Eq.(4.60) to be some early time $t_0 \leq t_* \ll t_{\rm BBN}$. Thus, for all $t_{\rm BBN} \leq t \leq t_{\rm MRE}$, we may approximate $t - t_* \approx t$. For simplicity, at all times $t > t_{\rm MRE}$, we ignore the effect of dark energy on H at late times $t \sim t_{\rm now}$ and approximate the universe as strictly MD. We also ignore any back-reaction on H which results from the decay of the ensemble itself during this MD era, even though $\rho_{\rm tot}$ dominates the energy density of the universe at this time, given that we will be imposing the bound in Eq.(4.62) and thereby mandating that $\rho_{\rm tot}$ does not differ significantly from the prediction of the ΛCDM cosmology. With these approximations, $\Omega_{\rm tot}$ and $w_{\rm eff}$ are given by Eq.(4.56) and Eq.(4.60) at times $t < t_{\rm MRE}$, but with $\kappa = 2$ rather than $\kappa = 3/2$. When evaluating $\Omega_{\rm tot}$ and $w_{\rm eff}$ during this MD era, we take $t_* = t_{\rm MRE}$. However, since $\Omega_n(t_{\rm MRE}) \propto \Omega_n^0 e^{-\Gamma_n (t - t_0)}$, where the constant of proportionality is the same for all $\hat{\phi}_n$ and is independent of the background cosmology, we find that the ratio $\Omega_{\rm tot}/\widetilde{\Omega}_{\rm tot}$ at any time $t_{\rm BBN} < t \leq t_{\rm now}$, regardless of the relationship between t and $t_{\rm MRE}$, is given by

$$\frac{\Omega_{\rm tot}}{\widetilde{\Omega}_{\rm tot}} \;\approx\; \frac{\sum_{n=0}^{\infty}\Omega_n^0 e^{-\Gamma_n t}}{\sum_{n=0}^{\infty}\Omega_n^0}\,. \tag{4.103}$$

By contrast, the effective equation-of-state parameter for the ensemble is given by

$$w_{\rm eff} \;\approx\; \frac{\sum_{n=0}^{\infty}\Omega_n^0\Gamma_n t e^{-\Gamma_n t}}{\sum_{n=0}^{\infty}\Omega_n^0 e^{-\Gamma_n t}} \times \begin{cases} 2/3 & t < t_{\rm MRE} \\ 1/2 & t > t_{\rm MRE}\,. \end{cases} \tag{4.104}$$

We note that while our expressions for $w_{\rm eff}$ before and after matter-radiation equality are not equal at $t = t_{\rm MRE}$, this apparent discontinuity in $w_{\rm eff}$ is simply a reflection of the fact that we are approximating the transition from the RD era to the MD era as an instantaneous event occurring at time $t = t_{\rm MRE}$, at which point the Hubble parameter leaps discontinuously from $H = 1/(2t)$ to $H = 2/(3t)$. In reality, of course, H transitions continuously between these asymptotic values at $t \sim t_{\rm MRE}$. In order to describe the evolution of $w_{\rm eff}$ during this transition, one would need to treat the parameter κ as a function of t. However, since we are only interested in bounding $w_{\rm eff}$ and not its time derivatives, approximating this transition as instantaneous is sufficient for our purposes.

In assessing how the constraints in Eq.(4.62) and Eq.(4.86) impact the parameter space of our scenario, we begin by noting that the expression for $\Omega_{\rm tot}/\widetilde{\Omega}_{\rm tot}$ in Eq.(4.103) depends on the physical scales Γ_0 and t only through the dimensionless quantity $\sigma \equiv \Gamma_0 t$. Indeed, we observe that

$$\frac{\Omega_{\rm tot}}{\widetilde{\Omega}_{\rm tot}} \;\approx\; \frac{\sum_{n=0}^{\infty}\Omega_n^0 e^{-\frac{\Gamma_n}{\Gamma_0}\sigma}}{\sum_{n=0}^{\infty}\Omega_n^0}\,, \tag{4.105}$$

which depends on σ and on the ratios $\Gamma_n/\Gamma_0 = \hat{m}_n^3 A_n'^2/(\hat{m}_0^3 A_0'^2)$ of the decay widths of the ensemble constituents, but not on the value of Γ_0 itself. Likewise, our expression for $w_{\rm eff}$ in Eq.(4.104) can be written as

$$w_{\rm eff} \;\approx\; \frac{\sum_{n=0}^{\infty}\Omega_n^0\frac{\Gamma_n}{\Gamma_0}\sigma e^{-\frac{\Gamma_n}{\Gamma_0}\sigma}}{\sum_{n=0}^{\infty}\Omega_n^0 e^{-\frac{\Gamma_n}{\Gamma_0}\sigma}} \times \begin{cases} 2/3 & \sigma < \Gamma_0 t_{\rm MRE} \\ 1/2 & \sigma > \Gamma_0 t_{\rm MRE}\,, \end{cases} \tag{4.106}$$

which depends on the value of Γ_0 only in that this parameter determines the value of σ at the time of matter-radiation equality. Moreover, we note that the expression for $w_{\rm eff}$ at times $t < t_{\rm MRE}$ is always larger than the corresponding expression at times $t > t_{\rm MRE}$ by an overall multiplicative factor of precisely $4/3$. Given this, we will hereafter adopt a conservative

approach in establishing bounds on $w_{\rm eff}$ in which we always treat $w_{\rm eff}$ as being given by the expression valid during the RD era prior to matter-radiation equality, regardless of the actual relationship between t and $t_{\rm MRE}$. With this modification, our expressions for both $\Omega_{\rm tot}$ and $w_{\rm eff}$ depend only on σ, and not on Γ_0 and t independently. In other words, these expressions are invariant under any simultaneous rescaling of Γ_0 and t which leaves their product invariant.

The utility of this invariance is perhaps best conveyed in the context of a graphical example. In Figure 4.5, we show how $w_{\rm eff}(\sigma)$ and $\Omega_{\rm tot}(\sigma)$ actually evolve as functions of σ for four different choices of $m_\phi R$ and $\pi k R$. These four choices are intended to exemplify different possible regimes for these two parameters. In particular, these choices are representative of the regimes in which $\pi k R$ and $m_\phi R$ are both small (first row), in which $\pi k R$ is small but $\pi k R$ is large (second row), in which $\pi k R$ is large but $m_\phi R$ is small (third row), and in which $\pi k R$ and $m_\phi R$ are both large (fourth row). In all cases, we have taken $\Lambda_{\rm UV} R = 3$ and assumed that all of the $\hat{\phi}_n$ begin oscillating instantaneously at $t = t_0$. In each panel, the blue line indicates the value of the quantity $w_{\rm eff}(\sigma)$ or $\Omega_{\rm tot}(\sigma)$ itself, while the black dashed line indicates the corresponding constraint from either Eq.(4.86) or Eq.(4.62). The vertical red lines indicate the values $\sigma_n \equiv \Gamma_0 \tau_n$ of the dimensionless time variable σ which correspond to the lifetimes of the $\hat{\phi}_n$ with $\hat{m}_n \leq \Lambda_{\rm UV}$.

In interpreting the results shown in Figure 4.5, we begin by observing that while reciprocal rescalings of Γ_0 and t do not affect the overall *shapes* of the curves representing $w_{\rm eff}$ and $\Omega_{\rm tot}/\widetilde{\Omega}_{\rm tot}$ as functions of σ, such rescalings do change the value $\sigma_{\rm now} \equiv \Gamma_0 t_{\rm now}$ of σ which corresponds to present time. In particular, the smaller Γ_0 is, the smaller the corresponding value of $\sigma_{\rm now}$. Consistency with the constraints in Eq.(4.62) and Eq.(4.86) requires only that these constraints be satisfied for $\sigma < \sigma_{\rm now}$. The results shown in each row of Figure 4.5 therefore suggest that these constraints can generally be satisfied by choosing a sufficiently small value for Γ_0 that the blue curves for both $w_{\rm eff}$ and $\Omega_{\rm tot}$ never enter the respective gray regions for all σ within the range $\sigma < \sigma_{\rm now}$. Indeed, we observe that consistency with these constraints can always be achieved by taking Γ_0 to be sufficiently small, provided either that the number of $\hat{\phi}_n$ in the ensemble is finite and that their lifetimes satisfy $t_0 \ll \tau_0$, or else that the $\hat{\phi}_n$ with lifetimes $\tau_n \lesssim t_0$ collectively contribute only a negligible fraction of the total abundance of the ensemble at $t = t_0$.

Thus, when this is the case, we see that the constraints in Eq.(4.86) and Eq.(4.62) do not simply serve to exclude particular combinations of the model parameters $\pi k R$, m_ϕ, and $\Lambda_{\rm UV} R$ outright, but rather to establish an upper bound on Γ_0 — or, equivalently, a lower

bound on τ_0 — for any such combination of these parameters. More explicitly, the maximum value $\sigma_{\rm now}^{\rm max}$ of $\sigma_{\rm now}$ for which these constraints are simultaneously satisfied determines the minimum possible lifetime $\tau_0^{\rm min}$ for the lightest ensemble constituent through the relation

$$\tau_0^{\rm min} \;=\; \frac{t_{\rm now}}{\sigma_{\rm now}^{\rm max}} \;. \tag{4.107}$$

We stress that τ_0 is indeed an independent degree of freedom in this scenario. Although the overall normalization factors for both the abundances and lifetimes of the $\hat{\phi}_n$ both depend on $\hat{f}_X$, the normalization factor for the Ω_n depends not only on additional model parameters, such as the misalignment angle θ, but also on the details of the cosmological history at times $t > t_0$.

It is also worth remarking that the results shown in the top two rows of Figure 4.5 are qualitatively similar to those obtained in the $k \to 0$ limit studied in [13]. The last two rows of the figure correspond to cases in which $\pi k R$ is large and therefore represent departures from the flat-space case. We observe that it is when $\pi k R$ and $m_\phi R$ are both large that the deviations from the CDM limit are the most dramatic.

We now survey the parameter space of our model, using the criterion in Eq.(4.107) in order to establish a bound on τ_0 at each point within that parameter space. In particular, we hold $\Lambda_{\rm UV} R$ fixed and vary both $\pi k R$ and $m_\phi R$. In Figures 4.6, 4.7 and 4.8 we show contours in $(\pi k R, m_\phi R)$-space of $\tau_0^{\rm min}$ for the parameter choice $\Lambda_{\rm UV} R = 3$. These figures correspond to the three different behaviors for the oscillation-onset times delineated in Eq.(4.51).

Generally speaking, we observe that in each panel of the figure, the bound on τ_0 tends to become more stringent as $\pi k R$ is increased for a fixed value of $m_\phi R$. This implies that for a given choice of the parameter τ_0, there is a maximum degree of AdS warping for which a phenomenologically consistent dark sector can emerge for any fixed value of $m_\phi R$. Moreover, we observe that the bound on the AdS curvature scale generally becomes more and more stringent as $m_\phi R$ is increased, in agreement with the results shown in Figure 4.5. Indeed, the regime in which $\pi k R$ and $m_\phi R$ are both large is the regime in which a significant number of low-lying states with similar abundances and comparable lifetimes are present within the ensemble. Moreover, comparing results across the three panels of the figure, we see that the bounds are more stringent for the case of an instantaneous turn-on than they are for the case of a staggered turn-on during either a RD or MD era. Indeed, this is expected, since the Ω_n^0 for the lighter $\hat{\phi}_n$ are enhanced relative to the Ω_n^0 for the heavier $\hat{\phi}_n$ in the case of a staggered turn-on. These lighter modes, which typically have longer lifetimes, therefore carry a larger fraction of $\Omega_{\rm tot}$ in this case than in the case of an instantaneous turn-on, and as

a result the ensemble as a whole is more stable.

While the results in Figures 4.6, 4.7 and 4.8 provide a great deal of information about the ensembles which arise within the parameter space of our warped-space scenario, there are other considerations which we must also take into account in assessing which regions of that parameter space are phenomenologically of interest. In particular, from a DDM perspective, we are interested in ensembles which are not only consistent with observational constraints, but which also represent a significant departure from traditional dark matter scenarios — scenarios in which a single particle species contributes essentially the entirety of the dark matter abundance. The degree to which the contribution from the most abundant individual constituent dominates in $\Omega_{\rm tot}$ at any given time can be be parametrized by the "tower fraction" η, defined by the relation [13]

$$\eta(t) \;\equiv\; \frac{\Omega_{\rm tot} - \max_n\{\Omega_n\}}{\Omega_{\rm tot}}\,, \tag{4.108}$$

the range of which is $0 \leq \eta < 1$. If the most abundant individual ensemble constituent contributes essentially the entirety of $\Omega_{\rm tot}$, with the other $\hat{\phi}_n$ contributing negligibly to this total abundance, then $\eta \ll 1$ and this individual ensemble constituent is for all intents and purposes a single-particle dark matter candidate. By contrast, if η is order-one, multiple $\hat{\phi}_n$ contribute meaningfully to $\Omega_{\rm tot}$ and the ensemble is truly DDM-like.

In Figures 4.9, 4.10 and 4.11 we show contours of the initial value $\eta(t_0)$ of the tower fraction at the time at which the abundances Ω_n are effectively established within the same region of parameter space as in Figures 4.6, 4.7 and 4.8, and for the same choice of $\Lambda_{\rm UV}R$. While the present-day tower fraction $\eta(t_{\rm now})$ differs from $\eta(t_0)$ as a result of $\hat{\phi}_n$ decays, this difference is generally not terribly significant for ensembles which satisfy the constraint on $\Omega_{\rm tot}$ in Eq.(4.62).

One important feature that emerges upon comparing Figures 4.6, 4.7, 4.8 and Figures 4.9, 4.10, 4.11 is that the conditions which make $\eta(t_0)$ large are also those which make the bound on τ_0 quite stringent. In other words, there is an increasing tension between these two figures as πkR gets large. Indeed, if we impose an upper bound on τ_0 (so that our DDM ensemble continues to be dynamical throughout up to and including the present epoch) as well as a lower bound on $\eta(t_0)$ (so that our scenario remains "DDM-like," with a significant fraction of the total dark matter abundance shared across many ensemble constituents), then for any value of $m_\phi R$ there exists a *maximum value of warping* which may be tolerated. Fortunately, however, we also observe that it is nevertheless possible to achieve a reasonably large value of $\eta(t_0)$ without requiring the value of τ_0 to be extreme.

We also note that for $\pi k R \ll 1$, the values of $\eta(t_0)$, expressed as functions of $m_\phi R$, are in complete agreement with the flat-space results previously found in [13]. Thus, in this sense, we may view the contour plots in Figures 4.9, 4.10 and 4.11 as illustrating the structure that emerges as we move away from the flat-space limit and increase $\pi k R$.

4.4 Warped vs. flat from the dual perspective

Thus far, we have examined a 5D theory involving a bulk scalar propagating within a slice of AdS_5 and have shown that the mixed KK modes of this bulk scalar are capable of satisfying the basic criteria for a phenomenologically viable DDM ensemble in which multiple constituents contribute meaningfully to $\Omega_{\rm tot}$. This in turn implies that the ensemble of partially composite scalars which arises in the 4D dual of this warped-space theory can likewise serve as a DDM ensemble as well. Thus, we have demonstrated what we set out to demonstrate in this chapter — namely that scenarios involving such ensembles are a viable context for model-bulding within the DDM framework.

There are, however, certain aspects of the AdS/CFT dictionary that relates the two dual theories which deserve further comment. Within the regime in which the AdS curvature scale is large, this dictionary is reasonably transparent. In general, the two dimensionful parameters k and R which characterize the 5D theory at times $t \lesssim t_G$ are related to the physical scales $\Lambda_{\rm UV}$ and $\Lambda_{\rm IR}$ of the strongly-coupled 4D theory by

$$\Lambda_{\rm IR} \;=\; \Lambda_{\rm UV}\, e^{-\pi k R}\,. \tag{4.109}$$

Thus, as briefly mentioned in Section 4.3, the regime in which $\pi k R \gg 1$ corresponds to a large hierarchy between $\Lambda_{\rm IR}$ and $\Lambda_{\rm UV}$. The lightest mass eigenstate $\hat{\phi}_0$ in the 5D theory corresponds to a state in the 4D theory which is primarily elementary. The rest of the low-lying $\hat{\phi}_n$ in the 5D theory correspond to states in the 4D theory which are primarily composite.

By contrast, within the regime in which $\pi k R \ll 1$ and the theory approaches the flat-space limit considered in [13], the relationship between the states of the 4D and 5D theories is more subtle. The corresponding regime in the 4D theory is that in which $\Lambda_{\rm IR} \approx \Lambda_{\rm UV}$. The KK eigenstates $\hat{\phi}_n^{(k=0)}$ which emerge in the flat-space limit of our warped DDM scenario do not correspond to composite states of the CFT in the dual 4D theory. Rather, these states correspond to a tower of elementary fields $\phi_{(n)}$ with masses $M_n \sim n/R$ which are also generically present in the theory and mix with the $\widetilde{\phi}_n$. Indeed, the elementary scalar $\phi_{(0)}$

introduced in Section 4.1 may be viewed as the lightest of these fields. The $\phi_{(n)}$ with $n > 0$ typically do not play a significant role in the phenomenology of the partially composite theory when $\Lambda_{\rm IR} \ll \Lambda_{\rm UV}$. The reason is that within this regime a large number of light states are present in the ensemble with masses $\hat{m}_n \ll 1/R$. These light states have negligible wavefunction overlap with any of the $\phi_{(n)}$ other than $\phi_{(0)}$. However, in the opposite regime in which $\Lambda_{\rm IR} \approx \Lambda_{\rm UV}$, no such hierarchy exists between the mass scales of the elementary and composite states of the 4D theory. Within this regime, the $\phi_{(n)}$ do indeed play an important role in the phenomenology of the model.

In order to understand how the $\phi_{(n)}$ affect the properties of the DDM ensemble in the $\Lambda_{\rm IR} \approx \Lambda_{\rm UV}$ regime, it is illustrative to compare the structure of the mass matrix which emerges in this regime to the structure which emerges in the $\Lambda_{\rm IR} \ll \Lambda_{\rm UV}$ regime. In situations in which the $\widetilde{\phi}_n$ are all significantly heavier than at least the lightest several $\phi_{(n)}$, the mass eigenstates ϕ_n of the theory at times $t \lesssim t_G$ are simply the $\phi_{(n)}$, with the corresponding masses $m_0 = 0$ for $n = 0$ and $m_n = M_n$ for $n > 0$. By contrast, at times $t \gtrsim t_G$, the mass-squared matrix in the $\phi_{(n)}$ basis has the rough overall structure

$$\mathcal{M}^2 = \begin{pmatrix} m_\phi^2 & m_\phi^2 & m_\phi^2 & \dots \\ m_\phi^2 & M_1^2 + m_\phi^2 & m_\phi^2 & \dots \\ m_\phi^2 & m_\phi^2 & M_2^2 + m_\phi^2 & \dots \\ \vdots & \vdots & \vdots & \ddots \end{pmatrix} . \tag{4.110}$$

In the regime in which $m_\phi \ll M_n$ for all $n > 0$, the mass eigenstates $\hat{\phi}_n$ are, to $O(m_\phi^2/M_n^2)$, given by

$$|\hat{\phi}_n\rangle \approx \begin{cases} |\phi_{(0)}\rangle - \sum_{\ell=1}^{\infty} \frac{m_\phi^2}{M_\ell^2} |\phi_{(\ell)}\rangle & n = 0 \\ \frac{m_\phi^2}{M_n^2} |\phi_{(0)}\rangle + |\phi_{(n)}\rangle + \sum_{\ell \neq 0,n}^{\infty} \frac{m_\phi^2}{M_n^2 - M_\ell^2} |\phi_{(\ell)}\rangle & n > 0 \, . \end{cases} \tag{4.111}$$

To the same order, the corresponding mass eigenvalues are $\hat{m}_0^2 \approx m_\phi^2$ for $n = 0$ and $\hat{m}_n^2 \approx M_n^2 + m_\phi^2$ for $n > 0$. Since all of the ϕ_n with $n > 0$ are massive prior to the phase transition, only ϕ_0 can acquire a misaligned vacuum value. Thus, the mixing coefficients $A_n = \langle \phi_0 | \hat{\phi}_n \rangle$ play the same phenomenological role in the $\Lambda_{\rm IR} \approx \Lambda_{\rm UV}$ regime as they do in the $\Lambda_{\rm IR} \ll \Lambda_{\rm UV}$ regime. In our truncated theory, these coefficients are given by

$$A_n \;=\; \langle \phi_{(0)} | \hat{\phi}_n \rangle \;\approx\; \begin{cases} 1 & n = 0 \\ \frac{m_\phi^2}{M_n^2} & n > 0 \,. \end{cases} \tag{4.112}$$

The projection coefficients A'_n in this same regime are

$$A'_n \;=\; \sum_{\ell=0}^{\infty} \langle \phi_{(\ell)} | \hat{\phi}_n \rangle \;\approx\; \langle \phi_{(n)} | \hat{\phi}_n \rangle \;\approx\; 1 \,, \tag{4.113}$$

up to corrections of $\mathcal{O}(m_\phi^2/M_n^2)$. These results agree with those in [13] for the $m_\phi \ll M_n$ regime, up to order-one numerical factors. Of course, for m_ϕ outside this regime, the full, infinite-dimensional mass matrix is required in order to obtain the corresponding expressions for A_n and A'_n.

The structure of the mass-squared matrix in Eq.(4.110) clearly differs in several ways from the structure of the mass-squared matrix in Eq.(4.17) for the corresponding truncated theory within the $\Lambda_{\rm IR} \ll \Lambda_{\rm UV}$ regime. However, the mass-squared matrices in Eq.(4.110) and Eq.(4.17) cannot meaningfully be compared because the former is expressed with respect to the basis of mass eigenstates prior to the phase transition, whereas the latter is expressed in the $\{\phi_{(0)}, \widetilde{\phi}_n\}$ basis. Rather, the mass-squared matrix in Eq.(4.110) must be compared to the mass-squared matrix $\widetilde{\mathcal{M}}^2$ obtained in the $\Lambda_{\rm IR} \ll \Lambda_{\rm UV}$ regime *after* the phase transition is expressed in the basis of the states ϕ_n which are mass eigenstates of the theory *before* the phase transition. This matrix is given by $\widetilde{\mathcal{M}}^2 = \mathcal{U}\mathcal{M}^2\mathcal{U}^\dagger$, where $\mathcal{M}^2$ is the matrix appearing in Eq.(4.17) and $\mathcal{U}$ is the unitary matrix which represents the transformation from the $\{\phi_{(0)}, \widetilde{\phi}_n\}$ basis to the ϕ_n basis. The results in Eq.(4.14) imply that to $\mathcal{O}(\varepsilon_n^2)$, this latter matrix is given by

$$\mathcal{U} \;\approx\; \begin{pmatrix} 1 - \sum_{m=1}^{\infty} \frac{\varepsilon_m^2}{2g_m^2} & -\frac{\varepsilon_1}{g_1} & -\frac{\varepsilon_2}{g_2} & \cdots \\ \frac{\varepsilon_1}{g_1} & 1 - \frac{\varepsilon_1^2}{2g_1^2} & \frac{\varepsilon_1\varepsilon_2 g_2}{g_1(g_1^2 - g_2^2)} & \cdots \\ \frac{\varepsilon_2}{g_2} & \frac{\varepsilon_2\varepsilon_1 g_1}{g_2(g_2^2 - g_1^2)} & 1 - \frac{\varepsilon_2^2}{2g_2^2} & \cdots \\ \vdots & \vdots & \vdots & \ddots \end{pmatrix} . \tag{4.114}$$

As a result, to the same order in ε_n, we find that

$$\widetilde{\mathcal{M}}^2 \approx \begin{pmatrix} m_\phi^2\left(1+\sum_{m=1}^{\infty}\frac{\varepsilon_m^2}{g_m^2}\right) & \frac{\varepsilon_1}{g_1}m_\phi^2 & \frac{\varepsilon_2}{g_2}m_\phi^2 & \dots \\ \frac{\varepsilon_1}{g_1}m_\phi^2 & (g_1^2+\varepsilon_1^2)\Lambda_{\rm IR}^2+\frac{\varepsilon_1^2}{g_1^2}m_\phi^2 & \frac{\varepsilon_1\varepsilon_2}{g_1 g_2}m_\phi^2 & \dots \\ \frac{\varepsilon_2}{g_2}m_\phi^2 & \frac{\varepsilon_1\varepsilon_2}{g_1 g_2}m_\phi^2 & (g_2^2+\varepsilon_2^2)\Lambda_{\rm IR}^2+\frac{\varepsilon_2^2}{g_2^2}m_\phi^2 & \dots \\ \vdots & \vdots & \vdots & \ddots \end{pmatrix}. \tag{4.115}$$

Comparing the results in Eq.(4.110) and Eq.(4.115), we see that the crucial difference between the structures of these two mass-squared matrices is due to the factors of ε_n/g_n that appear in both the diagonal and off-diagonal contributions to $\widetilde{\mathcal{M}}^2$ which arise a result of the phase transition. These factors arise in the $\Lambda_{\rm IR} \ll \Lambda_{\rm UV}$ regime as a consequence of the coupling between $\phi_{(0)}$ and the composite sector engendered by the operator O^c. The fact that ε_n/g_n varies with n in a non-trivial manner for $\pi kR \gg 1$ accounts for the differences in the resulting mass spectra.

We now turn to examine how the structural differences between the matrices in Eq.(4.110) and Eq.(4.115) affect the actual mass spectra of the theory. In Figure 4.12, we show how the mass spectrum of the 5D gravity dual of our partially composite DDM theory varies as a function of k for two representative choices of m_ϕ. The results shown in the left panel correspond to the choice of $m_\phi = 10^{-4}\Lambda_{\rm UV}$, while the results shown in the the right panel correspond to the choice of $m_\phi = \Lambda_{\rm UV}$. In both panels, we have taken $R = 3/\Lambda_{\rm UV}$. Each of the solid curves shown in each panel corresponds to a particular value of the index n and indicates the mass $\hat{m}_n$ of the corresponding ensemble constituent. Thus, the set of points obtained by taking a vertical "slice" through either panel collectively represent the mass spectrum of the theory for the corresponding value of k. The color at any given point along each curve provides information about the degree to which the corresponding state in the partially composite theory is elementary or composite. In particular the color indicates the absolute value of the projection coefficient A_n' at that point, normalized to the absolute value of the projection coefficient $A_n'^{(k=0)}$ obtained for the same choice of m_ϕ and R, but with $k = 0$.

In order to motivate why this quantity is a useful proxy for compositeness, we note once again that the flat-space limit of the 5D dual theory corresponds to the limit in which all of the states of the corresponding 4D theory are purely elementary. As discussed in Section 4.3.2, the bulk profile of each state in this limit reduces to

$$\hat{\zeta}_n^{(k=0)}(y) \;=\; \frac{r_n}{\sqrt{\pi R}} \cos\left(\frac{n\pi y}{R}\right), \tag{4.116}$$

where we have defined

$$r_n \;\equiv\; \begin{cases} 1 & n = 0 \\ \sqrt{2} & n > 0\,. \end{cases} \tag{4.117}$$

Using the completeness relation in Eq.(4.48) for these flat-space bulk profiles with $y' = 0$, we may express A'_n for general k in the more revealing form

$$\begin{aligned} A'_n &= \sqrt{\frac{1-e^{-2\pi kR}}{2k}} \int_0^{\pi R} \hat{\zeta}_n(y)\delta(y)dy \\ &= \sqrt{\frac{1-e^{-2\pi kR}}{2k}} \int_0^{\pi R} \hat{\zeta}_n(y) \sum_{m=0}^{\infty} \frac{r_m^2}{\pi R} \cos\left(\frac{m\pi y}{R}\right) dy \\ &= \sqrt{\frac{1-e^{-2\pi kR}}{2\pi kR}} \sum_{m=0}^{\infty} r_m \int_0^{\pi R} \hat{\zeta}_m^{(k=0)}(y)\hat{\zeta}_n(y)dy\,, \end{aligned} \tag{4.118}$$

where in going from the first to the second line, we have used the completeness relation

$$\sum_{n=0}^{\infty} \hat{\zeta}_n^{(k=0)}(y)\hat{\zeta}_n^{(k=0)}(y') \;=\; \delta(y-y') \tag{4.119}$$

with $y' = 0$. Thus, up to an overall normalization coefficient and an additional factor of r_n which appears in each term of the sum, A'_n can be viewed as a sum of the overlap integrals between the state $\hat{\phi}_n$ within the ensemble and the individual mass eigenstate fields $\hat{\phi}_m^{(k=0)}$ of a theory with $k = 0$ and the same values of m_ϕ and R. We choose to normalize this quantity to $A_n'^{(k=0)}$ because $0 \leq |A'_n/A_n'^{(k=0)}| \leq 1$, with $|A'_n/A_n'^{(k=0)}| = 1$ occurring in the $k = 0$ limit. A value of $|A'_n/A_n'^{(k=0)}|$ near unity therefore suggests that the degree of overlap between $\hat{\phi}_n$ and the $\hat{\phi}_m^{(k=0)}$ is large and that the corresponding state in the partially composite theory is mostly elementary. By contrast, a value near zero suggests that the degree of overlap is small and that the corresponding state is mostly composite.

The results shown in the left panel of the Figure 4.12 are characteristic of the regime in which m_ϕ is considerably smaller than all of the other relevant scales in the problem. In this regime, for $k = 0$, the spectrum consists of one light state $\hat{\phi}_0$ with a mass $\hat{m}_0 \ll 1/R$

and several additional states with masses $\hat{m}_n \approx n/R$, all of which are elementary. As k is increased, $\hat{m}_0$ remains approximately constant and $\hat{\phi}_0$ remains approximately elementary. By contrast, the masses of the additional $\hat{\phi}_n$ decrease while the degree of compositeness for each of these states increases. Furthermore, additional $\hat{\phi}_n$ whose masses descend from infinity successively appear in the spectrum of the theory below $\Lambda_{\rm UV}$ as k increases. The process continues as k is further increased until we enter the $\pi k R \gg 1$ regime in which the spectrum includes a large number of low-lying states with masses in the range $k \gg \hat{m}_n \gtrsim m_{\rm KK}$, all of which exhibit a high degree of compositeness, as expected.

By contrast, the results shown in the right panel of Figure 4.12, which are characteristic of the regime in which m_ϕ is significantly larger than both k and $1/R$, differ from those in the left panel primarily for small k. Most notably, the masses of the states obtained for $k = 0$ are not given by $\hat{m}_n \approx n/R$ as they are in the left panel, but rather by $\hat{m}_n \approx (n + 1/2)/R$. Once again, this accords with the expected behavior of the $\hat{m}_n$ in flat-space limit [13]. For larger k, the only qualitative difference between the mass spectra obtained in the small-m_ϕ and large-m_ϕ regimes is that the spectrum in the latter regime lacks the single, primarily elementary state with $\hat{m}_0 \ll m_{\rm KK}$ present in the former regime. Indeed, for large m_ϕ, we see that all of the low-lying states within the ensemble are primarily composite when k is large.

To summarize, in this approach, the individual components of the DDM ensemble are the composite states which emerge below the confinement scale of the strongly coupled field theory. Mixing these composite states with an additional, elementary scalar $\phi_{(0)}$ can generate abundances and decay widths for these ensemble constituents. It yields a spectrum of partially composite mass eigenstates whose degree of compositeness varies across the ensemble. Using the AdS/CFT dictionary, we derived the masses, decay widths, and cosmological abundances for these partially composite states within the context of the gravity dual of this scenario. This dual theory involves a scalar field propagating in the bulk of a slice of AdS_5. We showed that decay widths and abundances can be balanced appropriately for a DDM ensemble within large regions of that parameter space, even when the degree of warping in the dual theory is significant. A significantly high degree of warping is a regime in which there exists a significant hierarchy of scales $\Lambda_{\rm IR} \ll \Lambda_{\rm UV}$ in the partially composite theory. However, we also showed that constraints on the ensemble become increasingly stringent as the degree of warping increases. In any case, we have attempted to demonstrate how rich the phenomenology of a multi-component dark matter model can become.

Mon espoir est parvenu jusqu'à l'orient du monde, et en tous endroits de la terre habitée.Mani

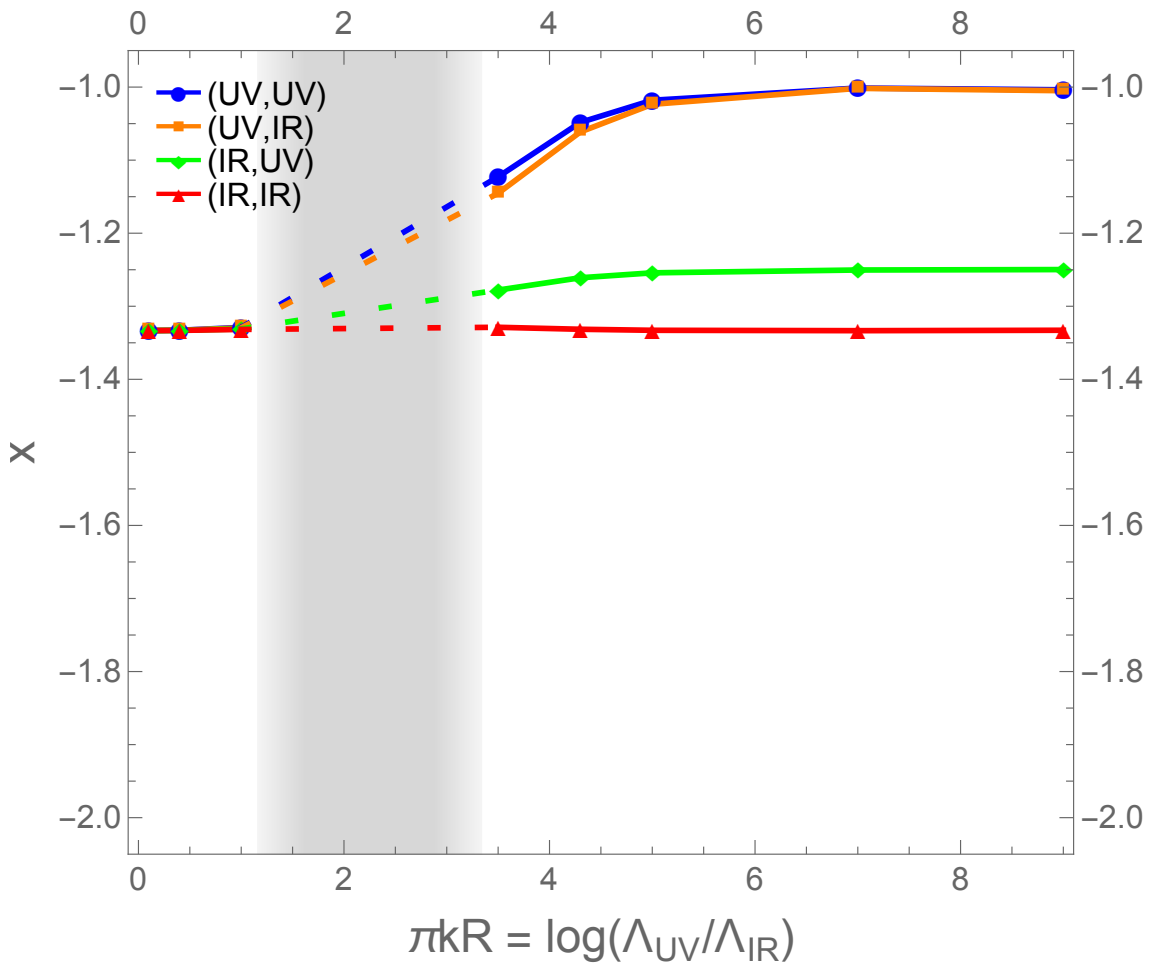

Figure 4.2: The scaling exponent $x = \alpha + \beta$, plotted as a function of the ratio $\pi kR = \log(\Lambda_{\rm UV}/\Lambda_{\rm IR})$ for the four different possible combinations of locations for the brane mass and the SM fields [78]. All curves of the figure correspond to the same value for the dimensionless product $m_\phi R \approx 3.5 \times 10^{-4}$. This figure corresponds to the case in which the $\hat{\phi}_n$ all begin oscillating instantaneously at the time of the mass-generating phase transition. We observe that all of the curves approach a common x value in the flat-space limit, which corresponds to taking $\pi kR \to 0$.

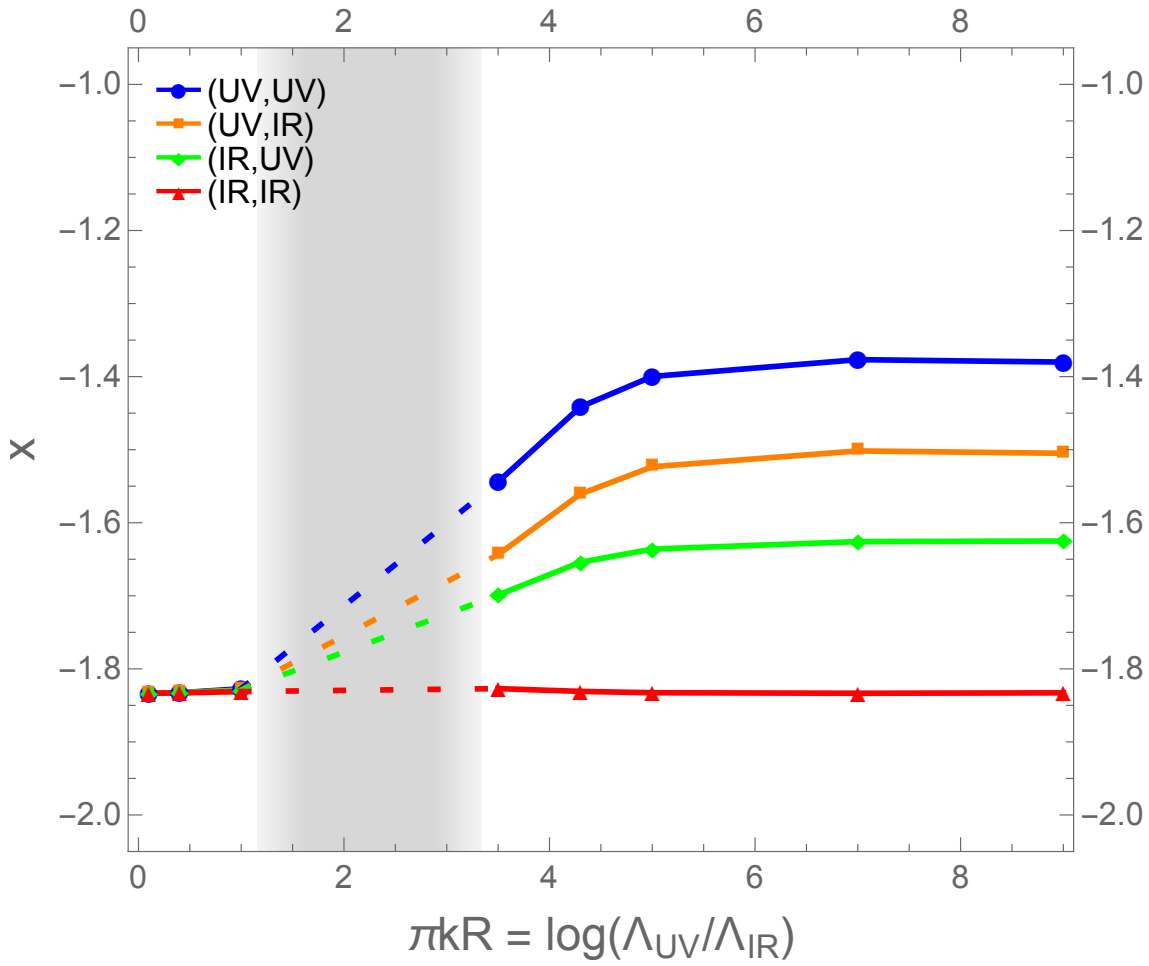

Figure 4.3: The same as in Figure 4.2, however, this figure corresponds to the case in which the t_n are staggered in time during a RD epoch.

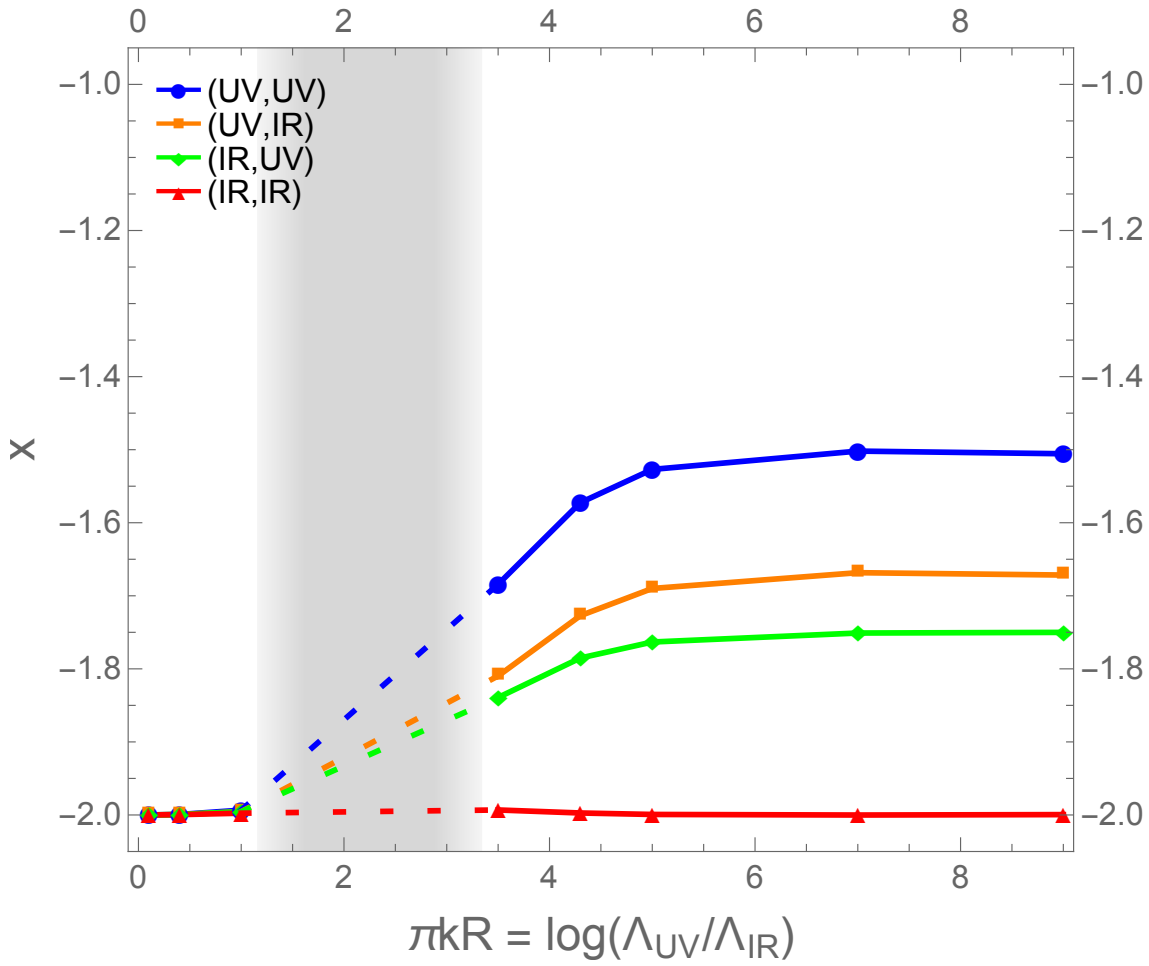

Figure 4.4: The same as in Figure 4.2, however, this figure corresponds to the case in which the t_n are staggered in time during a MD epoch.

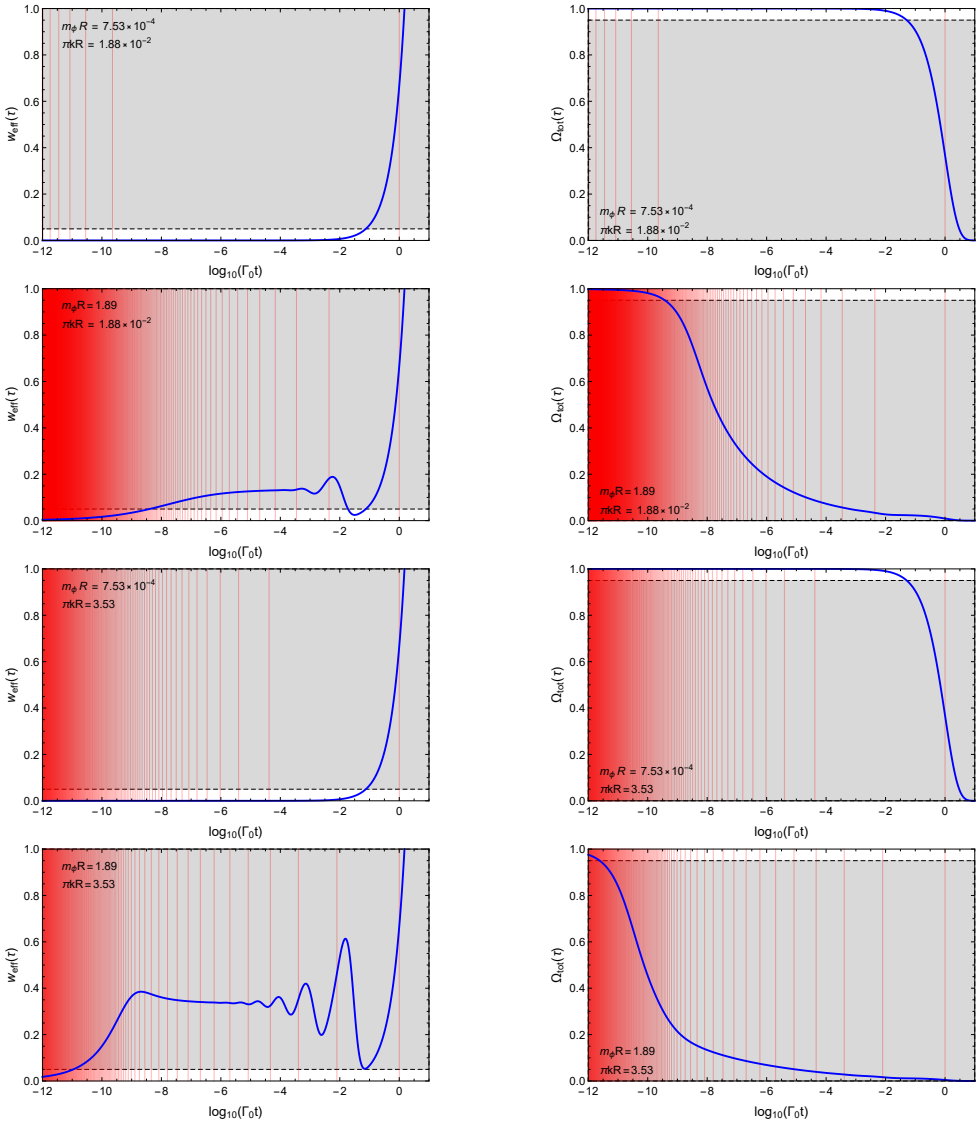

Figure 4.5: The effective ensemble equation-of-state parameter $w_{\rm eff}(\sigma)$ (left panel in each row) and total ensemble abundance $\Omega_{\rm tot}(\sigma)$ (right panel in each row), plotted as functions of $\sigma \equiv \Gamma_0 t$. Each row of the figure corresponds to a particular choice of πkR and $m_\phi R$. These choices are representative of the regimes in which πkR and $m_\phi R$ are both small (first row), πkR is small but πkR is large (second row), πkR is large but $m_\phi R$ is small (third row), and πkR and $m_\phi R$ are both large (fourth row). In all cases, we have taken $\Lambda_{\rm UV} R = 3$ and assumed that all of the $\hat{\phi}_n$ begin oscillating instantaneously at $t = t_0$. In each panel, the blue line is the value of the quantity $w_{\rm eff}$ or $\Omega_{\rm tot}$ itself, while the black dashed line indicates the corresponding constraint from either Eq.(4.86) or Eq.(4.62). The red vertical lines indicate the values $\sigma_n = \Gamma_0 \tau_n$ of σ at which the various $\hat{\phi}_n$ decay. The gray regions are excluded by the constraints. In particular, for any given ensemble, consistency with these constraints requires that Γ_0 be taken sufficiently small that for all σ within the range $\sigma < \sigma_{\rm now} \equiv \Gamma_0 t_{\rm now}$, the blue curves for both $w_{\rm eff}$ and $\Omega_{\rm tot}$ do not enter the gray region.

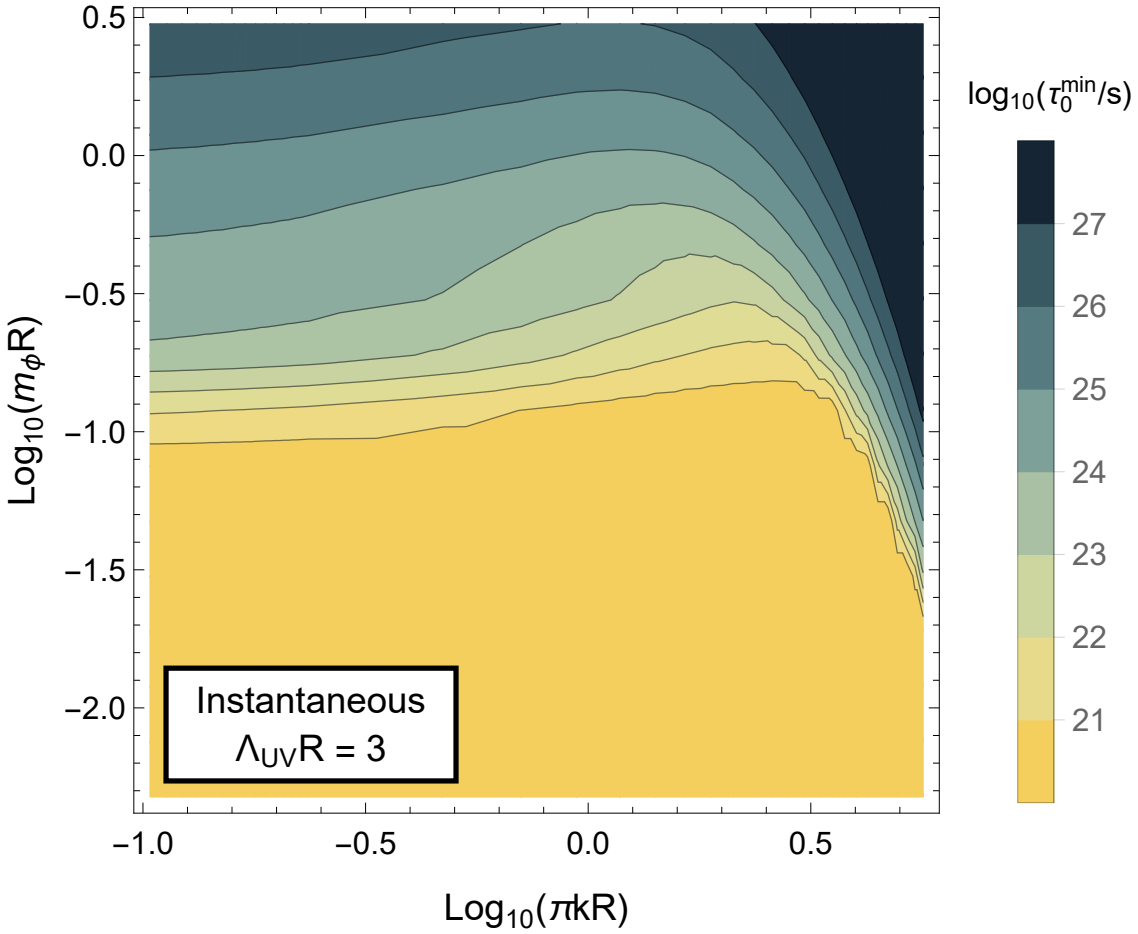

Figure 4.6: Contours of the minimum lifetime $t_0^{\min}$ consistent with the constraints in Eq.(4.86) and Eq.(4.62), plotted within the $(\pi kR, m_\phi R)$-plane. For this plot, we take $\Lambda_{\rm UV}R = 3$. This figure corresponds to the case of an instantaneous turn-on. We see that the bound on τ_0 becomes increasingly stringent as the degree of warping is increased for fixed $m_\phi R$.

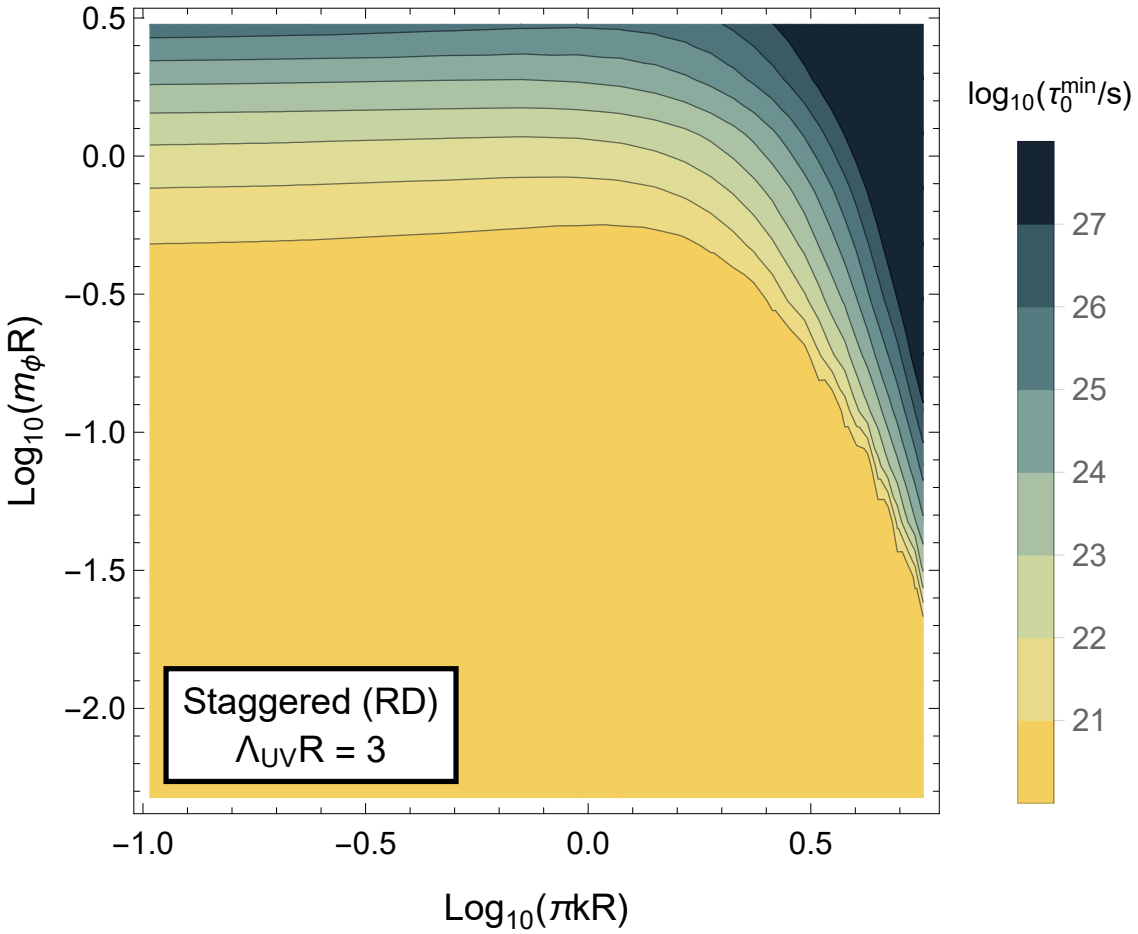

Figure 4.7: The same as in Figure 4.6, however, this figure corresponds to the case of a staggered turn-on during a radiation-dominated era.

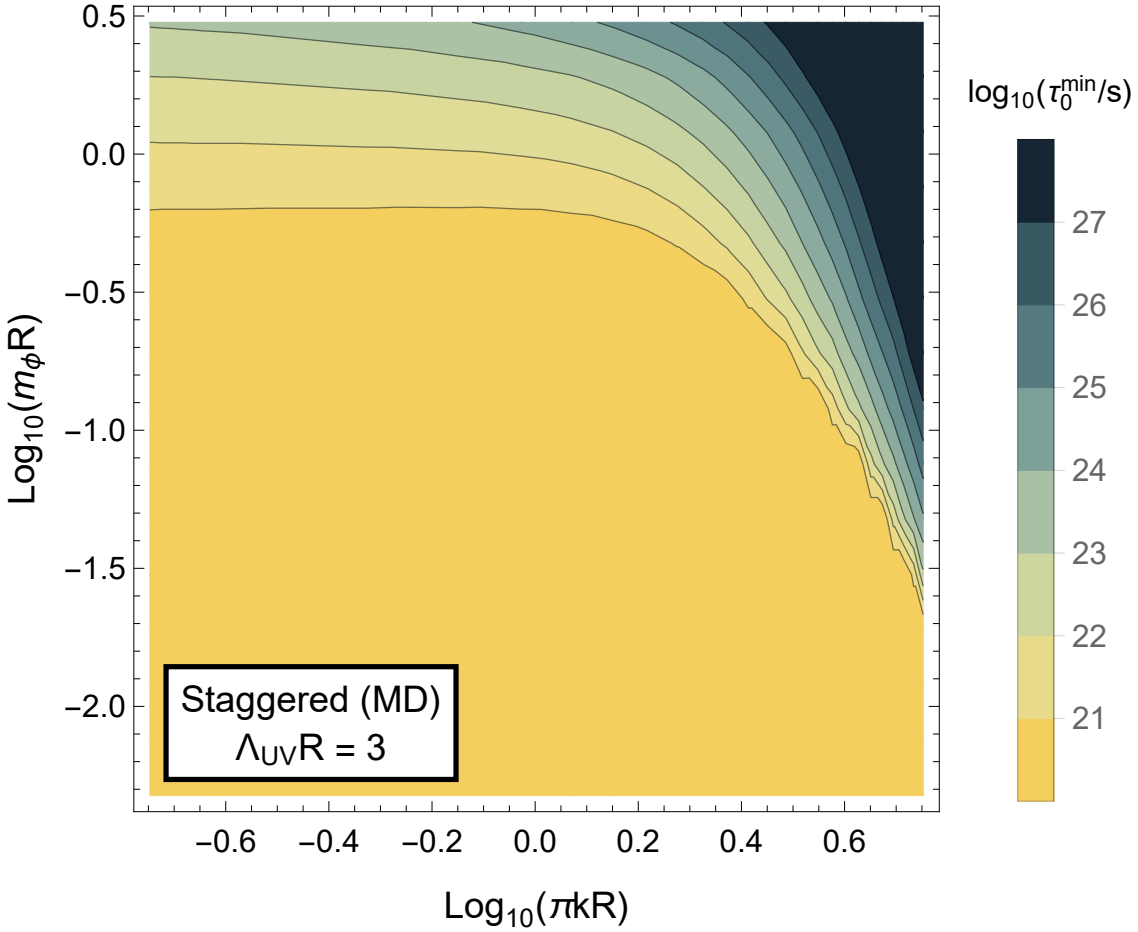

Figure 4.8: The same as in Figure 4.6, however, this figure corresponds to the case of a staggered turn-on during a matter-dominated era.

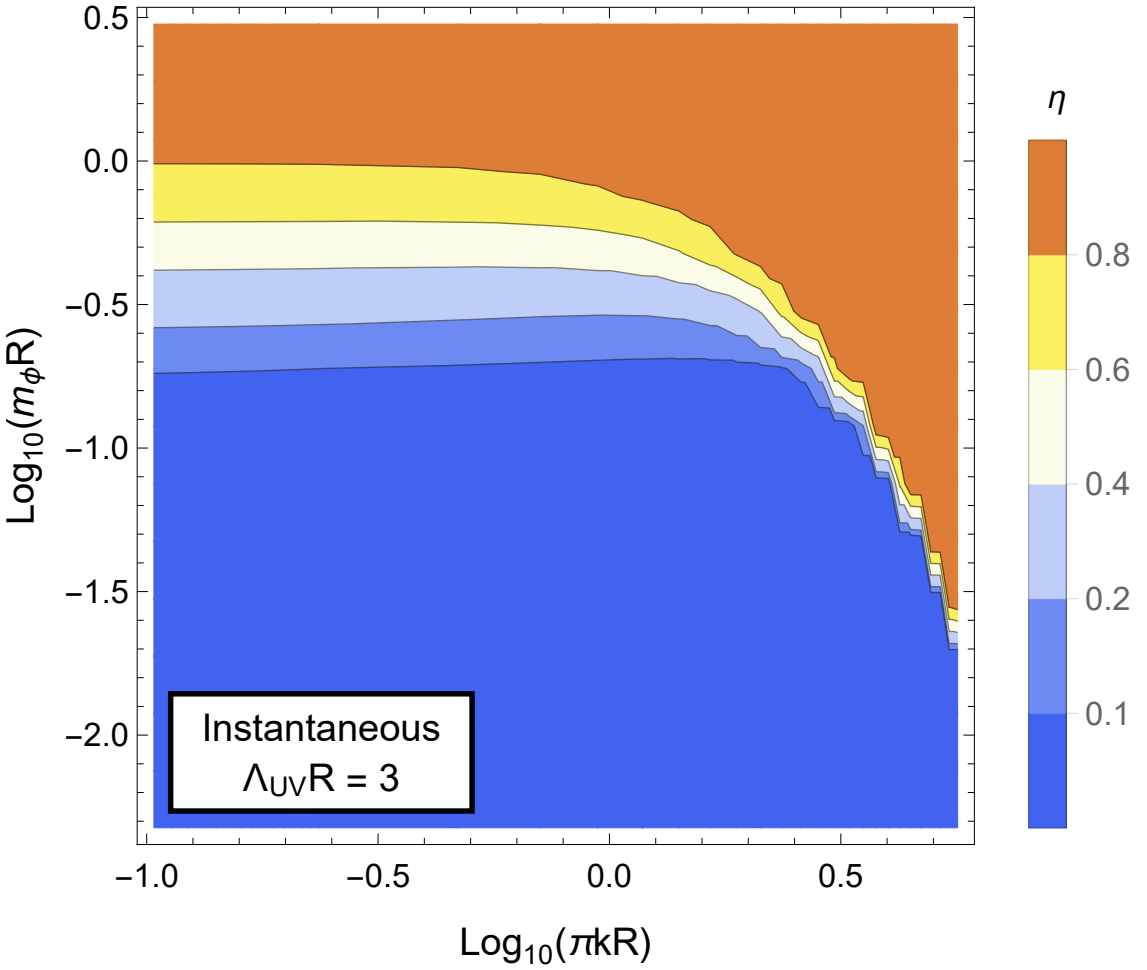

Figure 4.9: Contours of the initial value $\eta(t_0)$ of the DDM tower fraction, plotted within the same $(\pi kR, m_\phi R)$-plane shown in Figure 4.6. Once again, we take $\Lambda_{\rm UV}R = 3$.

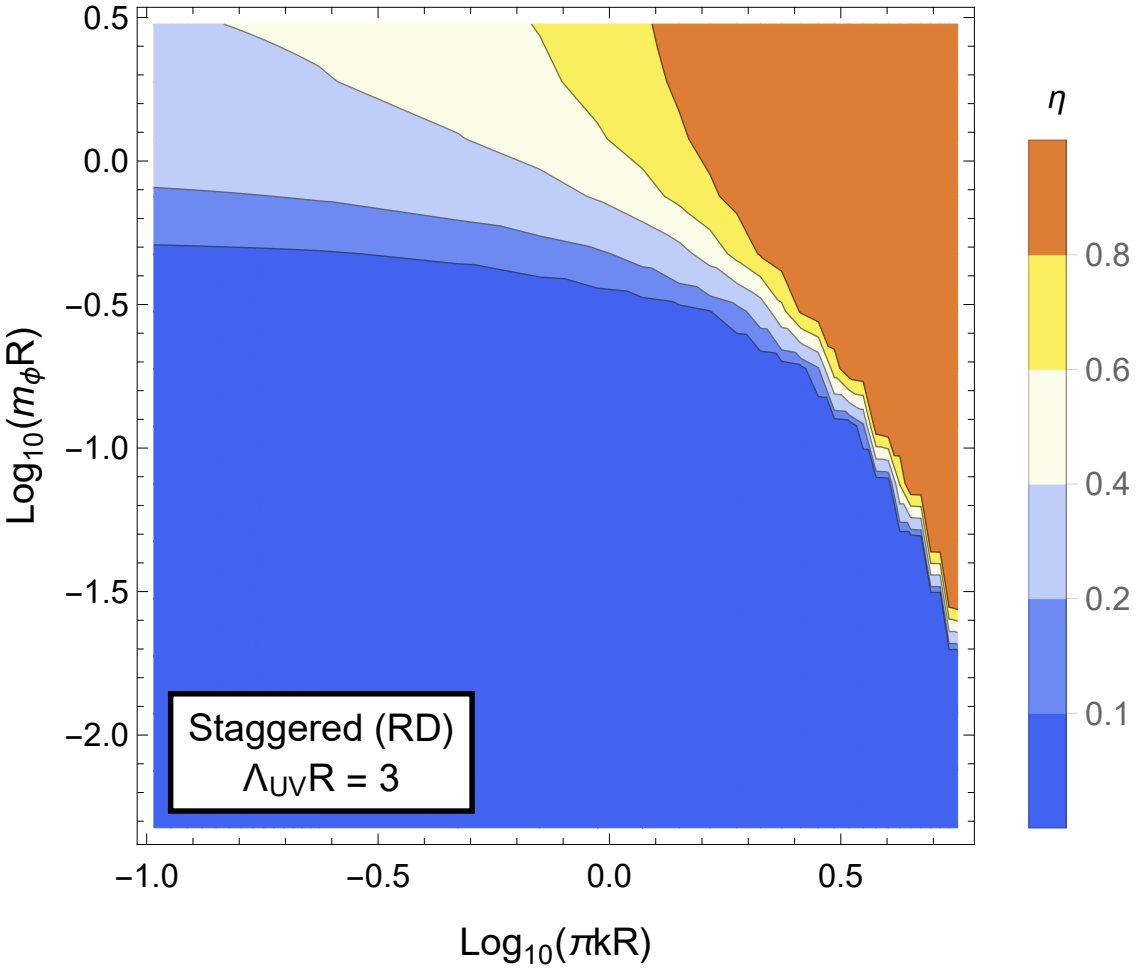

Figure 4.10: Contours of the initial value $\eta(t_0)$ of the DDM tower fraction, plotted within the same $(\pi kR, m_\phi R)$-plane shown in Figure 4.7. Once again, we take $\Lambda_{\rm UV}R = 3$.

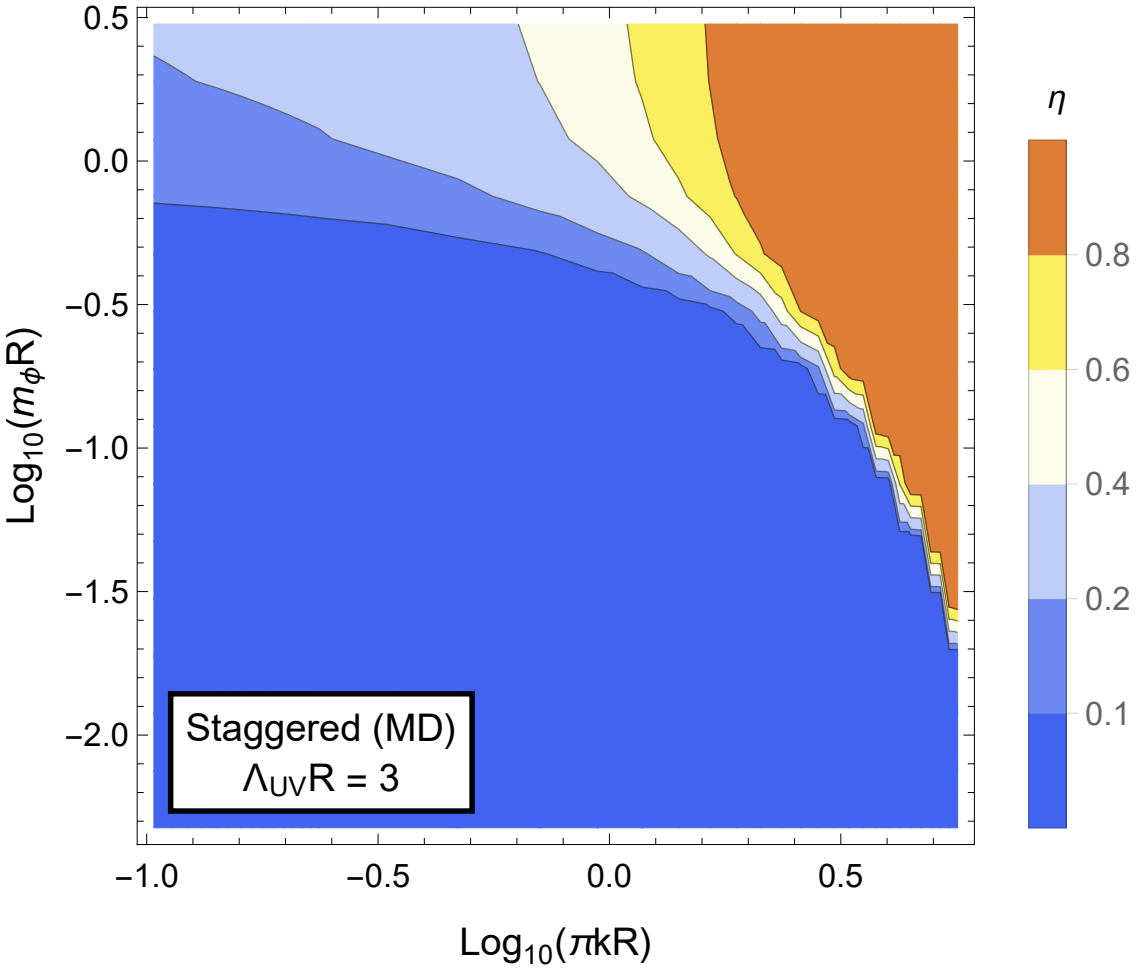

Figure 4.11: Contours of the initial value $\eta(t_0)$ of the DDM tower fraction, plotted within the same $(\pi kR, m_\phi R)$-plane shown in Figure 4.8. Once again, we take $\Lambda_{\rm UV}R = 3$.

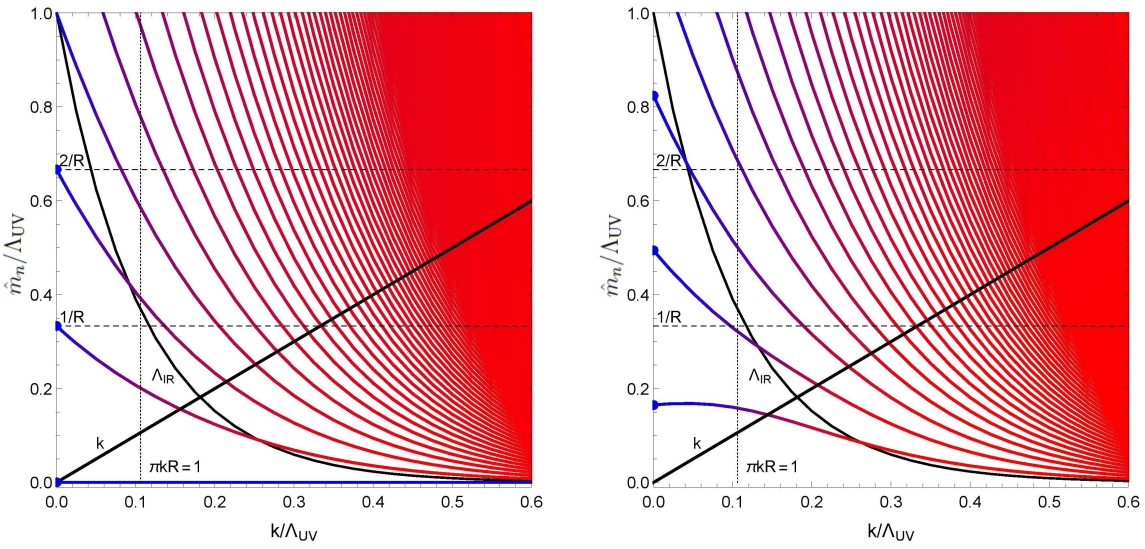

Figure 4.12: The mass spectrum of the 5D gravity dual of our partially composite DDM theory, plotted as a function of the AdS curvature scale k for two representative choices of m_ϕ. The results shown in the left panel correspond to the choice of $m_\phi = 10^{-4}\Lambda_{\rm UV}$, while the results shown in the right panel correspond to the choice of $m_\phi = \Lambda_{\rm UV}$. In both panels, we have taken $R = 3/\Lambda_{\rm UV}$. Each of the solid curves shown in each panel corresponds to a particular value of the index n and indicates the mass $\hat{m}_n$ of the corresponding ensemble constituent. Thus, the set of points obtained by taking a vertical "slice" through either panel collectively represent the mass spectrum of the theory for the corresponding value of k. The color at any given point along each curve provides information about the extent to which the corresponding state in the partially composite theory in 4D is primarily elementary or composite. In particular, the color indicates the absolute value of the projection coefficient A'_n at that point, normalized to the absolute value of the projection coefficient $A_n'^{(k=0)}$ obtained for the same choice of m_ϕ and R, but with $k = 0$. A value near $|A'_n/A_n'^{(k=0)}| = 0$ (red) suggests that the state is primarily composite, while a value near $|A'_n/A_n'^{(k=0)}| = 1$ (blue) suggests that the state is primarily elementary. Curves indicating the value of k (solid black line with unit slope), $1/R$ and $2/R$ (dashed black horizontal lines), and $\Lambda_{\rm IR}$ (dot-dashed black curve) are also provided for reference.

Chapter 5

Digging for light scalar particles

Based on our experience with QCD, we know that the composite states of a strongly-coupled gauge theory have masses around the confinement scale. Usually exceptions to this occur in the presence of an underlying symmetry as in the case of pions. Spontaneously broken global symmetries might be introduced to have light states when the symmetry is also broken explicitly. There have been previous studies that argued for the existence of a light scalar from a five-dimensional perspective [79, 80, 81]. In this chapter, we explore alternative ways of producing scalars lighter than the confinement scale of the theory in a simpler five-dimensional setup.

One can modify the theory in different ways such as coupling an elementary scalar to a composite operator or introducing effective interactions in the strong sector. These changes modify the mass spectrum of the theory, however, it is not straightforward to compute the effect due to the strong dynamics. Therefore, inspired by the AdS/CFT correspondence [1], we can construct the dual model in the extra dimensional space where the modifications of the mass spectrum are more tractable. In Section 5.1, we present the five-dimensional model dual to a composite operator of a strongly-coupled CFT. In Section 5.1.1, we review how the introduction of an elementary scalar modifies the mass spectrum. In Section 5.1.2, we introduce a multi-trace deformation in the strong sector and analyze the implications. In Section 5.2, an alternative way of introducing an elementary scalar is discussed.

5.1 Holographic basis with a massless mode

Consider the action for a real scalar field, $\phi(x^\mu, y)$, propagating on the AdS_5 background,

$$\mathcal{S} = \int d^5x\sqrt{-g}\left[-\frac{1}{2}\left(\partial_M\phi\right)^2 - \frac{1}{2}ak^2\phi^2\right], \tag{5.1}$$

where $a \geq -4$ parameterizes the bulk mass and y is the coordinate of the fifth dimension. The metric for this background is

$$ds^2 = e^{-2ky}\eta_{\mu\nu}dx^\mu dx^\nu + dy^2, \tag{5.2}$$

where k is the AdS_5 curvature scale. Using the AdS/CFT dictionary, we know that this five-dimensional field corresponds to an operator of dimension: $\dim[O] \equiv \Delta = 2 + \sqrt{4+a}$ in the four-dimensional theory [82]. The equation of motion derived from the variation of the action is

$$\Box\phi + e^{2ky}\partial_y\left(e^{-4ky}\partial_y\phi\right) - ak^2e^{-2ky}\phi = 0, \tag{5.3}$$

where $\Box = \eta^{\mu\nu}\partial_\mu\partial_\nu$. The solution for ϕ can be written in momentum space as

$$\phi(p,y) = C_1(p)e^{2ky}\left[J_\alpha\left(\frac{ip}{k_y}\right) + C_2(p)Y_\alpha\left(\frac{ip}{k_y}\right)\right], \tag{5.4}$$

where $k_y \equiv ke^{-ky}$ and $\alpha \equiv \sqrt{4+a}$. $C_1(p)$ and $C_2(p)$ are unknown functions that can be calculated once the boundary conditions are imposed. The solution is presented in this specific form just to be consistent with the solutions which will be presented later. It behaves near the AdS_5 boundary, $y \to -\infty$, as

$$\phi(p,y) \to -C_1(p)C_2(p)\frac{2^\alpha\Gamma(\alpha)}{\pi}\left(\frac{ip}{k}\right)^{-\alpha}e^{(2-\alpha)ky} + C_1(p)\frac{2^{-\alpha}}{\Gamma(1+\alpha)}\left(\frac{ip}{k}\right)^{\alpha}e^{(2+\alpha)ky}, \tag{5.5}$$

which is consistent with [82]. Now let us consider a slice of AdS_5 where the extra coordinate is compactified on an $S^1/\mathbb{Z}_2$ orbifold with UV and IR branes that exist at the orbifold fixed points, y_0 and y_1 respectively [26]. It is customary to define a variable for the UV boundary value of the bulk field as $\varphi(p) \equiv \phi(p, y_0)$. The solution then becomes

$$\phi(p,y) = \varphi(p)e^{2k(y-y_0)}\frac{J_\alpha(ip/k_y) + C_2(p)Y_\alpha(ip/k_y)}{J_\alpha(ip/k_{y_0}) + C_2(p)Y_\alpha(ip/k_{y_0})}. \tag{5.6}$$

Note that defining a variable for the UV boundary value does not specify the UV boundary condition yet. Minimizing the action on the branes as well determines the boundary conditions and the result depends on whether the boundary value is fixed, $\delta\varphi|_{y=y_0} = 0$, or not. Since we do not fix the IR boundary value of the bulk field, the IR boundary condition is determined using $\delta\phi|_{y=y_1} \neq 0$. Therefore, $C_2(p)$ can be computed using the IR boundary condition. The existence of an IR brane implies that the conformal symmetry is broken in the dual theory. While there was no mass scale in the CFT before introducing the UV and IR branes, now the particle bound states appear at the IR scale. The mass spectrum of the theory can be computed from the AdS/CFT correspondence. It is known that there is no massless mode for the broken CFT described by Eq.(5.1) [22]. The massless mode requires us to add brane masses in the following way,

$$\mathcal{S} = \int d^5x\sqrt{-g}\left[-\frac{1}{2}\left(\partial_M\phi\right)^2 - \frac{1}{2}ak^2\phi^2 - bk\phi^2\left[\delta(y-y_0) - \delta(y-y_1)\right]\right], \tag{5.7}$$

where $b \equiv 2 \pm \alpha$. The parameter range, $b < 2$ ($b > 2$), is called $-$ ($+$) branch respectively. Supersymmetry forces both brane masses to be related to each other in this form, so it can be generalized to different brane masses if the theory is not supersymmetric [40]. These terms on the branes are necessary to have a light mode but not sufficient as we will see later. The term on the IR brane simply modifies the IR boundary condition and hence $C_2(p)$. As mentioned earlier, since we do not fix the IR boundary value, the IR boundary condition becomes $\left(\partial_y - bk\right)\phi|_{y=y_1} = 0$. Plugging the solution, Eq.(5.6), back into the action, Eq.(5.7), the on-shell bulk action can be written as

$$I[\varphi] = -\frac{1}{2}\int d^4p\ \varphi(p)\Sigma(p)\varphi(-p)\,, \tag{5.8}$$

where $\Sigma(p) = e^{-3ky_0}p\frac{F(p,y_0)}{G(p,y_0)}$ and

$$\begin{aligned} G(p,y) &\equiv J_\alpha\left(\frac{ip}{k_y}\right)Y_{\alpha\pm1}\left(\frac{ip}{k_{y_1}}\right) - Y_\alpha\left(\frac{ip}{k_y}\right)J_{\alpha\pm1}\left(\frac{ip}{k_{y_1}}\right) \\ F(p,y) &\equiv J_{\alpha\pm1}\left(\frac{ip}{k_y}\right)Y_{\alpha\pm1}\left(\frac{ip}{k_{y_1}}\right) - Y_{\alpha\pm1}\left(\frac{ip}{k_y}\right)J_{\alpha\pm1}\left(\frac{ip}{k_{y_1}}\right). \end{aligned} \tag{5.9}$$

Another useful quantity that can be computed in the five-dimensional theory is the conjugate variable, $\breve{\varphi} = -\delta I[\varphi]/\delta\varphi$, which is dual to $\langle O\rangle$. The original AdS/CFT correspondence recipe lets us determine the n-point functions, $\langle O...O\rangle$, for the strongly-coupled CFT from

the five-dimensional theory [83]. However, for general deformations of the bulk action, $\int d^4p\ (W[\breve{\varphi}] + \phi_s\breve{\varphi}/g_5)$, where g_5 is an expansion parameter with $\dim[g_5] = -1/2$, $W[\breve{\varphi}]$ is an arbitrary function of $\breve{\varphi}$, and ϕ_s is the four-dimensional source, we follow [84] to compute the improved correspondence formula. The Legendre transform of $I[\varphi]$,

$$J[\breve{\varphi}] = I - \int d^4p\ \varphi\frac{\delta I}{\delta\varphi}, \tag{5.10}$$

can then be used to construct a generating functional, $\mathcal{S}_{\text{holo}}$, from which one can compute the mass spectrum. Let us construct the generating functional,

$$\mathcal{S}_{\text{holo}} = J[\breve{\varphi}] + \int d^4p\ \left(W[\breve{\varphi}] + \frac{1}{g_5}\phi_s\breve{\varphi}\right), \tag{5.11}$$

whose minimization, $\delta\mathcal{S}_{\text{holo}}/\delta\breve{\varphi} = 0$, determines the relationship between $\breve{\varphi}$ and the source, ϕ_s. Plugging the solution for $\breve{\varphi}$ back into Eq.(5.11) results in a functional, $\mathcal{S}_{\text{holo}}[\phi_s]$. The AdS/CFT correspondence can therefore be expressed as the following relation between the four- and five-dimensional theories,

$$e^{-\left(\mathcal{S}_{\text{holo}}[\phi_s]-\mathcal{S}_{\text{holo}}[\phi_s=0]\right)} = \left\langle e^{-\int d^4p\ \frac{1}{\Lambda_{\text{UV}}^{\Delta-3}}\phi_s O}\right\rangle_{W[O]}, \tag{5.12}$$

where $\Lambda_{\text{UV}} \equiv 2k_{y_0}$ is the cut-off scale. This definition can be considered as choosing an origin for the location of the UV brane in the fifth dimension. With this definition, following the literature and picking $y_0 = 0$, the curvature would obey the inequality, $k/\Lambda_{\text{UV}} \lesssim 2$, in order for the classical metric solution to be valid [50].

Let us start with no deformation of the CFT other than the addition of the source term, $W = 0$. For such linear deformations of the CFT, i.e. single-trace perturbations, the result of minimizing $\mathcal{S}_{\text{holo}}$, $\varphi = \phi_s/g_5$, is compatible with the original AdS/CFT recipe. This results in a trivial generating functional, $\mathcal{S}_{\text{holo}}[\phi_s] = I[\phi_s/g_5]$. Using the generating functional from the five-dimensional theory, and noting that $\mathcal{S}_{\text{holo}}\left[\phi_s = 0\right] = 0$ for $W = 0$, we can compute the two-point functions,

$$\begin{aligned}\Lambda_{\text{UV}}^{2\Delta-6}\frac{\delta^2\mathcal{S}_{\text{holo}}\left[\phi_s\right]}{\delta\phi_s(p)\delta\phi_s(-p)} &= \langle O(p)O(-p)\rangle \\ -\frac{\Lambda_{\text{UV}}^{2\Delta-6}}{2g_5^2}\Sigma(p) &\sim \begin{cases} p^{2\alpha} + \text{c. t.} & y_1 \to \infty \\ \sum_n \frac{a_n^2}{p^2+m_n^2} & \text{finite } y_1, \end{cases}\end{aligned} \tag{5.13}$$

where $a_n = \langle 0|O|\widetilde{\phi}_n\rangle$ is the matrix element for O to create the nth meson, $\widetilde{\phi}_n$, with mass $\widetilde{m}_n$ from the vacuum [41]. The dimension of the operator, O, can be read by considering the limit, $y_1 \to \infty$. The mass spectrum of the particle bound states after confinement can then be found by calculating the poles of $pF(p, y_0)/G(p, y_0)$ for a finite y_1, which are given by the solutions of the following equation,

$$J_\alpha\left(\frac{\widetilde{m}_n}{k_{y_0}}\right) Y_{\alpha\pm1}\left(\frac{\widetilde{m}_n}{k_{y_1}}\right) = J_{\alpha\pm1}\left(\frac{\widetilde{m}_n}{k_{y_1}}\right) Y_\alpha\left(\frac{\widetilde{m}_n}{k_{y_0}}\right). \tag{5.14}$$

This means that the bulk field can be decomposed as a tower of the particle bound states,

$$\phi(x^\mu, y) = \sum_{n=1}^{\infty} \widetilde{\phi}_n(x^\mu)\widetilde{\zeta}_n(y). \tag{5.15}$$

The profiles, $\widetilde{\zeta}_n(y)$, that satisfy the bulk equation of motion, Eq.(5.3), with $\Box\widetilde{\phi}_n = \widetilde{m}_n^2\widetilde{\phi}_n$ can be written as

$$\widetilde{\zeta}_n(y) = N_n e^{2ky}\left[J_\alpha\left(\frac{\widetilde{m}_n}{k_y}\right) + \kappa(\widetilde{m}_n) Y_\alpha\left(\frac{\widetilde{m}_n}{k_y}\right)\right], \tag{5.16}$$

where N_n is the normalization constant and $\kappa(\widetilde{m}_n)$ is determined by imposing the boundary conditions. Consider the lightest mode in the mass spectrum coming from Eq.(5.14),

$$\widetilde{m}_1 \sim \begin{cases} k_{y_1} & -\text{ branch} \\ k_{y_1} e^{\alpha k(y_0 - y_1)} & +\text{ branch.} \end{cases} \tag{5.17}$$

Note that only the + branch has a mode whose mass is lighter than the confinement scale, $\Lambda_{\rm IR} \equiv k_{y_1}$. To compute the mass spectrum for the pure bound states, one needs to remove the UV brane, $y_0 \to -\infty$. This tells us that the + branch has a massless mode but it is modified by the finite UV cut-off effects. On the other hand, the − branch never has a mode lighter than the confinement scale. Eq.(5.14) implies the following boundary conditions for the profiles of the composite states,

$$\widetilde{\zeta}_n(y_0) = 0 \quad \text{and} \quad \left(\partial_y - bk\right)\widetilde{\zeta}_n\big|_{y=y_1} = 0\,. \tag{5.18}$$

Note that this implies a fixed UV boundary value of the bulk field, $\delta\phi\big|_{y=y_0} = 0$, even though the bound states are dynamical fields with $\delta\widetilde{\phi}_n \neq 0$. Since ϕ_s is not a dynamical field, one can set it to zero at the end of the calculations. Therefore, we need to deform the action to have a massless or a light mode in the theory especially for the − branch. Now we consider

different ways of deforming the theory for that purpose.

5.1.1 A linear mixing with an elementary scalar

We introduce an elementary scalar field, $\phi_{(0)}$, that linearly mixes with the operator, O. This is also known as the single - trace deformation of the CFT, $\int d^4p\, \phi_{(0)} O/\Lambda_{\rm UV}^{\Delta-3}$, which means $W[O] = 0$. Then the five-dimensional theory is perturbed by $\int d^4p\, \phi_{(0)}\check{\varphi}/g_5$, and we observe that this is very similar to the term that we added to compute the two-point functions. The difference is that now $\phi_{(0)}$ is a dynamical field with $\delta\phi_{(0)} \neq 0$ unlike the fixed source, ϕ_s. $\phi_{(0)}$ mixes with the composite states and the mass spectrum of the theory is modified. The modified mass spectrum can be computed by minimizing the effective action, $\mathcal{S}_{\rm holo}[\phi_{(0)}]$. Minimizing the effective action,

$$\delta\mathcal{S}_{\rm holo}[\phi_{(0)}] = \frac{\delta\mathcal{S}_{\rm holo}[\phi_{(0)}]}{\delta\phi_{(0)}(p)}\delta\phi_{(0)} = 0\,, \tag{5.19}$$

requires $\Sigma(p)$ to be zero since $\phi_{(0)}(-p) \neq 0$, which is satisfied only for certain momentum values. Therefore, the modified mass spectrum, m_n, is given by the zeros of $pF(p, y_0)/G(p, y_0)$ instead of its poles. The zeros are given by

$$J_{\alpha\pm1}\left(\frac{m_n}{k_{y_0}}\right) Y_{\alpha\pm1}\left(\frac{m_n}{k_{y_1}}\right) = J_{\alpha\pm1}\left(\frac{m_n}{k_{y_1}}\right) Y_{\alpha\pm1}\left(\frac{m_n}{k_{y_0}}\right). \tag{5.20}$$

In this case, there is a massless mode, $m_0 = 0$. We conclude that these modified modes are admixtures of $\phi_{(0)}$ and $\widetilde{\phi}_n$. Then the decomposition of the bulk field should be supplemented by a new four-dimensional field, $\phi_{(0)}(x^\mu)$, with a profile, $\zeta_{(0)}(y)$, that has a nonzero value on the UV brane,

$$\phi(x^\mu, y) = \phi_{(0)}(x^\mu)\zeta_{(0)}(y) + \sum_{n=1}^{\infty} \widetilde{\phi}_n(x^\mu)\widetilde{\zeta}_n(y), \tag{5.21}$$

where $\zeta_{(0)}(y)$ also satisfies the bulk equation of motion, Eq.(5.3), with $\Box\phi_{(0)} = m_{(0)}^2\phi_{(0)}$ and it is normalized so that the kinetic terms in the resulting four-dimensional theory are canonical. This is called the holographic basis. The new profile, $\zeta_{(0)}(y)$, can also be written as

$$\zeta_{(0)}(y) = N_{(0)}e^{2ky}\left[J_\alpha\left(\frac{m_{(0)}}{k_y}\right) + \kappa(m_{(0)})Y_\alpha\left(\frac{m_{(0)}}{k_y}\right)\right], \tag{5.22}$$

where $N_{(0)}$ is the normalization constant and $m_{(0)}$ is the mass term for $\phi_{(0)}$. The constant, $\kappa(m_{(0)})$, is determined by imposing the boundary conditions. Since $\phi_{(0)}$ is proportional to $\phi(p, y_0)$, we expect its profile to satisfy the boundary condition,

$$\left[\partial_y - (2-\alpha)k\right] \zeta_{(0)}(y)\big|_{y=y_0} = 0\,, \tag{5.23}$$

from Eq.(5.5). This boundary condition makes sure that the profile, $\zeta_{(0)}(y)$, looks like the dominant term in Eq.(5.5) near the UV boundary. On the other hand, different boundary conditions for $\zeta_{(0)}(y)$ on the IR brane can be imposed, which in turn determines the nature of the mixing between the elementary and composite scalars. For example, [42] implicitly picks

$$\left[\partial_y - (2-\alpha)k\right] \zeta_{(0)}(y)\big|_{y=y_1} = 0\,, \tag{5.24}$$

which brings the following equation for the $-$ branch, $b < 2$,

$$J_{\alpha-1}\left(\frac{m_{(0)}}{k_{y_0}}\right) Y_{\alpha-1}\left(\frac{m_{(0)}}{k_{y_1}}\right) = J_{\alpha-1}\left(\frac{m_{(0)}}{k_{y_1}}\right) Y_{\alpha-1}\left(\frac{m_{(0)}}{k_{y_0}}\right)\,, \tag{5.25}$$

which is the same with Eq.(5.20). Therefore, one of the solutions to this equation is $m_{(0)} = 0$. In this case there is only a kinetic mixing between $\phi_{(0)}$ and $\widetilde{\phi}_n$ in the resulting four-dimensional theory. However, for the + branch, $b > 2$, [42] finds both kinetic and mass mixing. The main conclusion for this way of achieving a massless mode is that the massless scalar is an admixture of elementary and composite scalars.

5.1.2 A multi - trace deformation

We introduce a new interaction,

$$W[\mathcal{O}] = -\frac{\xi}{\Lambda_{\rm UV}^{2\Delta-4}}\mathcal{O}^2\,, \tag{5.26}$$

into the theory, where ξ is a dimensionless constant. This is also known as the multi - trace deformation of the CFT. Since we did not introduce a dynamical field like $\phi_{(0)}$ in this case, we need to add an additional deformation, $\phi_s\mathcal{O}/\Lambda_{\rm UV}^{\Delta-3}$, where $\delta\phi_s = 0$ as before to be able to probe the theory and calculate the mass spectrum. To determine the five-dimensional counterpart of this deformation, we need to know the relationship between $\breve{\varphi}$ and $\langle\mathcal{O}\rangle$. This

can be achieved by comparing the linear deformations with ϕ_s from both sides,

$$\frac{\check{\varphi}}{g_5} \leftrightarrow \frac{\langle O \rangle}{\Lambda_{\rm UV}^{\Delta-3}}. \tag{5.27}$$

Then the five-dimensional theory is deformed by $\int d^4p \left(-\xi\check{\varphi}^2/(g_5^2\Lambda_{\rm UV}^2) + \phi_s\check{\varphi}/g_5\right)$. For such multi-trace deformations of the CFT, minimizing $\mathcal{S}_{\rm holo}$ results in a more complicated generating functional,

$$\mathcal{S}_{\rm holo}\left[\phi_s\right] = -\frac{1}{2}\int d^4p\ \phi_s(p)\frac{\Sigma(p)/g_5^2}{1-\xi\Sigma(p)/(g_5^2\Lambda_{\rm UV}^2)}\phi_s(-p). \tag{5.28}$$

Using the generating functional from the five-dimensional theory and noting that $\mathcal{S}_{\rm holo}\left[\phi_s = 0\right] = 0$, we can compute the two-point functions,

$$\begin{aligned} \Lambda_{\rm UV}^{2\Delta-6}\frac{\delta^2\mathcal{S}_{\rm holo}\left[\phi_s\right]}{\delta\phi_s(p)\delta\phi_s(-p)} &= \langle O(p)O(-p)\rangle \\ -\frac{\Lambda_{\rm UV}^{2\Delta-4}}{2}\frac{\Sigma(p)}{g_5^2\Lambda_{\rm UV}^2-\xi\Sigma(p)} &\sim \sum_n \frac{a_n^2}{p^2+\hat{m}_n^2} \qquad \text{for finite } y_1. \end{aligned} \tag{5.29}$$

Note that the expression for $y_1 \to \infty$ would not be as trivial as the one in Eq.(5.13). This means that the dimension of the operator is not trivially related to the bulk mass parameter anymore. The mass spectrum of the particle bound states after confinement are then given by the solutions of the following equation,

$$\frac{1}{\xi} = \frac{\Sigma(p)}{g_5^2\Lambda_{\rm UV}^2}. \tag{5.30}$$

Note that the mass spectrum of the original broken CFT, $\xi = 0$, was given by the poles of $\Sigma(p)$. If we consider the limit, $\xi \to \infty$, the solutions, $\hat{m}_n$, are given by the zeros of $\Sigma(p)$. The mass spectrum of the maximally deformed CFT, $\xi \to \infty$, is then computed by using the equation, Eq.(5.20). Therefore, this particular type of maximal CFT deformation modifies the mass spectrum such that $\hat{m}_n = m_n$ and there is a massless scalar without introducing a new elementary field like $\phi_{(0)}$. How the mass eigenvalues change from the poles of $\Sigma(p)$ to the zeros of $\Sigma(p)$ can be seen in Figure 5.1. This phenomenon is also observed in a string theory setup, [85], where a light composite fermion is achieved in a similar limit. The bulk

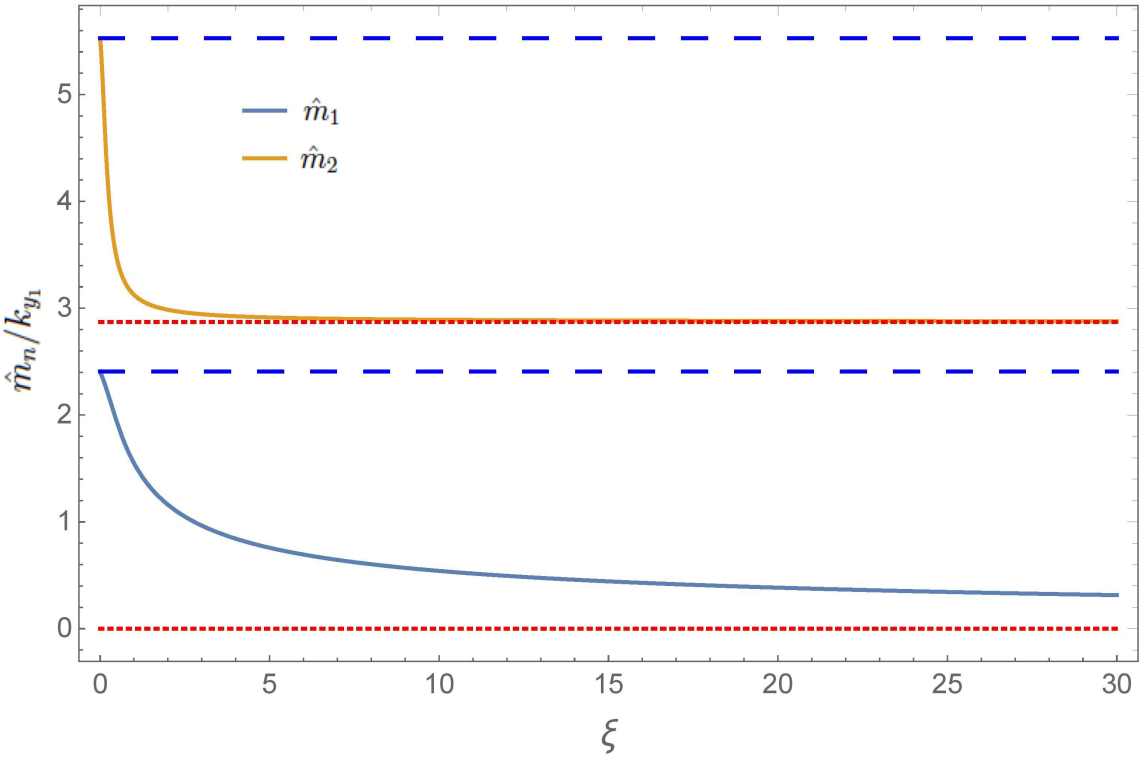

Figure 5.1: The lightest and the second lightest masses of the spectrum as a function of the deformation, ξ, for $e^{ky_0} = 0.1$, $g_5^2\Lambda_{\rm UV} = 1$, $\alpha = 1$, and $\pi k(y_1 - y_0) = 4$. Horizontal dashed lines show the poles of $\Sigma(p)$ while the horizontal dotted lines show the zeros of $\Sigma(p)$ [86].

field can then be decomposed as a tower of the particle bound states,

$$\phi(x, y) = \sum_{n=0}^{\infty} \phi_n(x)\zeta_n(y), \tag{5.31}$$

where $\zeta_n(y)$ are the new profiles. These profiles, $\zeta_n(y)$, that satisfy the bulk equation of motion, Eq.(5.3), with $\Box\phi_n = m_n^2\phi_n$ can be written as

$$\zeta_n(y) = N_n e^{2ky}\left[J_\alpha\left(\frac{m_n}{k_y}\right) + \kappa(m_n)Y_\alpha\left(\frac{m_n}{k_y}\right)\right], \tag{5.32}$$

where N_n is the normalization constant and $\kappa(m_n)$ is determined by imposing the boundary conditions,

$$\left(\partial_y - bk\right)\zeta_n|_{y=y_0} = 0 \quad \text{and} \quad \left(\partial_y - bk\right)\zeta_n|_{y=y_1} = 0\,. \tag{5.33}$$

This process describes only how the on-shell five-dimensional action needs to be modified for such deformations, $W[\mathcal{O}]$. How ξ can take large values is not obvious but we can understand

its physical implications. Expanding Eq.(5.29) in this limit,

$$\lim_{\xi\to\infty} \frac{\Lambda_{\rm UV}^{2\Delta-4}}{2} \frac{-\Sigma(p)}{g_5^2\Lambda_{\rm UV}^2 + \xi\Sigma(p)} \sim -\frac{\Lambda_{UV}^{2\Delta-4}}{2\xi} + \frac{g_5^2\Lambda_{UV}^{2\Delta-2}}{2\xi^2}\frac{1}{\Sigma(p)}, \tag{5.34}$$

and looking at the leading non-analytic term with p for $y_1 \to \infty$ we can compute the dimension, Δ', of the modified operator, O'. Note that this result, $\Delta' = 2 - \alpha$, is very similar to the one in [87], where the Legendre transform of the on-shell bulk action inverts the expression for the two-point function, $\langle O(p)O(-p)\rangle$. Of course, this interpretation should be restricted to the following parameter values, $0 \le \alpha \le 1$, so that $\Delta' \ge 1$. Considering the AdS/CFT formula, Eq.(5.12), this result can be summarized as

$$\lim_{\xi\to\infty} \langle e^{-\int d^4p\ \frac{1}{\Lambda_{\rm UV}^{\Delta-3}}\phi_s O} \rangle_{-\frac{\xi O^2}{\Lambda_{\rm UV}^{2\Delta-4}}} \to \langle e^{-\int d^4p\ \frac{1}{\Lambda_{\rm UV}^{\Delta'-3}}\phi_s O'} \rangle_0. \tag{5.35}$$

The modified generating functional for the same limit in the five-dimensional theory should thus be constructed differently,

$$\mathcal{S}'_{\rm holo} = I[\varphi] + \int d^4p\ \frac{\Lambda_{\rm UV}}{g_5}\phi_s\varphi, \tag{5.36}$$

whose minimization, $\delta\mathcal{S}'_{\rm holo}/\delta\varphi = 0$, determines the relationship between φ and the source, ϕ_s. This is consistent with the interpretation of [87] that says that the roles of two solutions near the AdS boundary, φ and $\check{\varphi}$, are interchanged. Plugging the solution for φ back into Eq.(5.36) results in a functional,

$$\mathcal{S}'_{\rm holo}[\phi_s] = -\int d^4p\ \frac{\Lambda_{\rm UV}^2}{2g_5^2}\phi_s(p)\frac{1}{\Sigma(p)}\phi_s(-p), \tag{5.37}$$

which is equivalent to Eq.(5.34) in terms of the dimension of the composite operator that it describes and the mass spectrum when there is confinement.

5.2 An alternative holographic basis with a massless mode

In Section 5.1.1, we stated that different boundary conditions for the profile, $\zeta_{(0)}(y)$, can be imposed on the IR brane. Let us pick $\zeta_{(0)}(y_1) = 0$ instead of the modified Neumann condition that we used before. These boundary conditions lead to the following equation for

$b < 2$,

$$J_{\alpha-1}\left(\frac{m_{(0)}}{k_{y_0}}\right) Y_\alpha\left(\frac{m_{(0)}}{k_{y_1}}\right) = J_\alpha\left(\frac{m_{(0)}}{k_{y_1}}\right) Y_{\alpha-1}\left(\frac{m_{(0)}}{k_{y_0}}\right), \tag{5.38}$$

that can be solved for new nonzero $m_{(0)}$ values. The smallest solution is given by

$$m_{(0)} \sim \begin{cases} k_{y_1} e^{(\alpha-1)k(y_0-y_1)} & \alpha > 1 \\ k_{y_1} & 0 \leq \alpha < 1. \end{cases} \tag{5.39}$$

We showed that there is no $m_{(0)} = 0$ for $b < 2$ unlike the case in Section 5.1.1 but we need to check whether this new solution also allows the system to have a massless mode. Inserting the holographic basis into the action, we find

$$\mathcal{S}_{\text{mix}} = \int d^4x \sum_{n=1}^{\infty} \left[-\frac{1}{2} z_n \partial_\mu \phi_{(0)} \partial^\mu \widetilde{\phi}_n - \frac{1}{2} \mu_n^2 \phi_{(0)} \widetilde{\phi}_n \right], \tag{5.40}$$

where $\mathcal{S}_{\text{mix}}$ includes the kinetic, z_n, and mass mixings, μ_n^2. If we can show that the determinant of the mass matrix is zero, we are done with proving that there is a massless mode. For this purpose, we need to know what the mass mixing terms, μ_n^2, are. Using the profiles and integrating by parts in two different ways, they are given by

$$\begin{aligned} \mu_n^{2A} &\equiv \int_{y_0}^{y_1} dy\, m_{(0)}^2 \zeta_{(0)} \left[e^{-2ky} \widetilde{\zeta}_n(y) - \widetilde{\zeta}_n(y_1) e^{-bky_1} e^{(b-2)ky} \right] \\ \mu_n^{2B} &\equiv \int_{y_0}^{y_1} dy\, \widetilde{m}_n^2 \widetilde{\zeta}_n \left[e^{-2ky} \zeta_{(0)}(y) - \zeta_{(0)}(y_0) e^{-bky_0} e^{(b-2)ky} \right], \end{aligned} \tag{5.41}$$

where $\mu_n^2 = \mu_n^{2A} = \mu_n^{2B}$. The mass matrix has a massless mode if

$$\sum_{n=1}^{\infty} \frac{\mu_n^4}{\widetilde{m}_n^2} = m_{(0)}^2 \,. \tag{5.42}$$

This equation can be proven by computing $\sum_{n=1}^{\infty} \frac{\mu_n^{2A} \mu_n^{2B}}{\widetilde{m}_n^2}$ with the help of the completeness relation,

$$\sum_{n=1}^{\infty} \widetilde{\zeta}_n(y) \widetilde{\zeta}_n(y') = e^{2ky} \delta(y - y') \,. \tag{5.43}$$

Therefore, there is a massless mode in this holographic basis as well. The difference from the holographic basis in Section 5.1.1 is that there are both kinetic and mass mixings in this basis for $b < 2$. A truncated version of this type of mass mixing is observed in a supersymmetric

model [65]. Note that the results of [65] comes from a purely four-dimensional consideration.

Je suis venu du pays de Babel pour faire retentir un cri à travers le monde.

Mani

Chapter 6

Conclusion

We believe that the holographic principle is a very powerful tool that can be applied to a variety of particle physics concepts. In particular, the AdS/CFT correspondence (the famous example of such a holographic duality) gives valuable insights on the mass spectrum of MSSM, distinct properties of the dark matter sector and the origin of light scalar particles. In this thesis, we presented applications of holography on these topics in great detail. The main ingredient in all of these applications is the idea of partial compositeness. Relaxing the widely used assumption of a point-like nature of the fundamental particles and introducing compositeness of varying degrees was shown to have very interesting consequences. Holography helped us map our four-dimensional theories with partial compositeness into their five-dimensional dual theories, and vice versa.

In Chapter 3, we presented a minimal supersymmetric model that uses partial compositeness to relate the SM fermion mass hierarchy to the sfermion mass hierarchy. This occurs by assuming that the SM gauge fields, Higgs sector, and the third-generation matter are (mostly) elementary, while the first two generations of matter are composite due to some unknown strong dynamics that confines at a scale $\Lambda_{\rm IR}$. Hierarchies are then generated when elementary superfields linearly mix with supersymmetric operators that have large anomalous dimensions. Since Higgs fields are elementary, the more composite the fermion, the lighter the corresponding fermion mass. The strong dynamics is also assumed to dynamically break supersymmetry, such that the composite sparticle states directly feel the supersymmetry breaking. The predominantly elementary states, such as the third-generation sfermions, Higgsinos, and gauginos, are therefore split from the much heavier first- and second-generation composite sfermions. Thus, the partially composite supersymmetric model generically predicts that light (heavy) SM fermions have heavy (light) sfermion

superpartners. Moreover, since the gravity multiplet mixes with the stress-energy tensor (via an irrelevant term), the gravitino is much lighter than gauginos. It therefore becomes the LSP that can play the role of dark matter.

To obtain quantitative predictions and to model the unknown strong dynamics responsible for the composite states and large anomalous dimensions, we use the AdS/CFT correspondence to study a 5D version of our 4D model (where the strong dynamics is specifically due to a large-N gauge theory (CFT)). In a slice of AdS_5, the Higgs sector is confined to the UV brane, while the remaining MSSM superfields are located in the bulk. Supersymmetry breaking occurs on the IR brane. The MSSM fields are identified with the zero modes of the corresponding 5D fields. The zero-mode profile depends on a bulk mass (dimensionless) parameter c that can be arbitrarily varied to localize the zero-mode superfield anywhere in the bulk. The fermion and sfermion mass hierarchy is now dictated by the 5D fermion geography. Since the Higgs fields are confined to the UV brane, the third-generation SM fermions are UV-localized, while the first- and second-generation SM fermions are IR-localized. This naturally leads to an *inverted* sfermion mass hierarchy, where the first- and second-generation sfermions are heavy, while those of the third generation are light.

At tree level, the sfermion hierarchy may be exponentially large due to the suppressed coupling between the UV-localized fields and the supersymmetry-breaking sector. The mass scale of the third-generation sfermions is therefore set by radiative corrections from the heavy states, which transmit the breaking of supersymmetry at loop order and become the dominant soft mass contribution. At one loop in 5D, these corrections arise from bulk gauginos and scalars. Since the Higgs fields are localized on the UV brane, both the Higgs-sector soft masses and the soft trilinear scalar couplings (a-terms) are zero at tree level, but they, too, receive radiative corrections from the bulk.

The overall scales in the 5D model can be fixed by imposing a number of phenomenological constraints: (i) the LSP gravitino is assumed to be the dark matter with a mass $\gtrsim 1$ keV; (ii) electroweak symmetry is broken, consistent with a 125 GeV Higgs boson; (iii) the first- and second-generation sfermions are at least as heavy as 100 TeV to ameliorate the supersymmetric flavor problem; (iv) the gaugino and Higgsino masses are constrained, so as to preserve gauge coupling unification as in the usual MSSM (assuming any underlying dynamics preserves SU(5)); and (v) only the MSSM fields are present in the theory below the scale of compactification. The SM fermion mass spectrum is used to constrain the bulk fermion mass parameters c_i. The 5D model then predicts the sfermion masses at the IR-brane scale, Λ_{IR}, which are run down to lower energies using renormalization group

equations. Since the boundary conditions for the sfermion masses are nonuniversal and flavor-dependent, tachyonic constraints that avoid charge- and color-breaking minima must be imposed to further restrict the parameter space.

Our model provides a predictive split supersymmetry scenario where the SM fermion mass hierarchy is explicitly related to the inverted sfermion mass hierarchy. It clearly demonstrates the implications of the recent Higgs boson discovery on the sfermion mass spectrum. A set of ranges for the masses of superpartners are predicted and they are compatible with the measured mass of the Higgs boson. Whatever the NLSP is could eventually be probed at a future 100 TeV collider. Moreover, the heavy first- and second-generation sfermions could be indirectly probed via rare-decay experiments, such as the flavor-violating Mu2e experiment [66], or experiments attempting to measure the electric dipole moment of the electron [67]. Now the ultimate judge, nature, will be the final arbiter in the accuracy of our predictions.

In Chapter 4, we investigated a novel realization of the DDM framework within the context of a strongly-coupled CFT. In this scenario, the constituent particles of the DDM ensemble are the composite states which emerge in the spectrum of the theory below the scale at which conformal invariance is spontaneously broken. Abundances and decay widths for these ensemble constituents can be generated through mixing between these composite states and an additional elementary scalar, ϕ_0, yielding a spectrum of partially composite mass eigenstates whose degree of compositeness varies across the ensemble. Informed by the AdS/CFT correspondence, we have derived the masses, decay widths, and cosmological abundances for these partially composite states within the context of the gravity dual of this scenario — a theory involving a scalar field propagating in the bulk of a slice of AdS_5. We have investigated the extent to which model-independent bounds on the total abundance and the equation of state for the ensemble constrain the parameter space of this scenario, and we have shown that indeed a balancing between decay widths and abundances appropriate for a DDM ensemble arises within large regions of that parameter space, even within the regime wherein the degree of warping in the dual theory is significant — a regime in which there exists a significant hierarchy of scales $\Lambda_{\rm IR} \ll \Lambda_{\rm UV}$ in the partially composite theory. However, we have also shown that constraints on the ensemble become increasingly stringent as the degree of warping increases. Moreover, we have shown that interesting qualitative features, such as non-monotonicities in the spectrum of decay widths, can develop in the highly-warped regime of the dual theory which do not arise in the flat-space limit.

A few comments are in order. First of all, we have regarded the 5D gravity dual of this

theory primarily as a calculational tool for obtaining information about the properties of the ensemble in the 4D theory. However, the fact that a viable DDM ensemble can emerge in the context of a scenario involving a warped extra dimension is interesting in its own right. Indeed from this perspective, we may regard the results in Section 4.2 and Section 4.3 as generalizations of the flat-space results derived in [13, 14] to warped space.

On a final note, in constraining the parameter space of our scenario, we have focused on considerations such as limits on $w_{\rm eff}$ and $\Omega_{\rm tot}$ in bounding the parameter space of our scenario — considerations which do not depend sensitively on the identities of the final-state particles into which the ensemble constituents decay. If the $\hat{\phi}_n$ decay solely into other, lighter dark-sector particles which reside within the dark sector but are external to the ensemble (e.g., particles which behave as dark radiation), these constraints are typically the leading ones. By contrast, if the $\hat{\phi}_n$ decay into final states involving visible-sector particles, additional constraints apply. It would be interesting to consider how such constraints further restrict the parameter space of our ensemble for certain well-motivated decay scenarios in which decays to SM particles dominate the width of each $\hat{\phi}_n$.

In Chapter 5, we showed how an effective interaction term in the strong sector can produce a composite scalar lighter than the confinement scale. How much lighter this state is depends on the interaction strength. The physical origin of this interaction strength and how it can take large values are subjects that need further investigation. However, when one does not need a big suppression from the confinement scale, a reasonable interaction strength is useful enough. A light composite scalar as we discussed in this chapter might be used for dark matter models with light scalar mediators. Moreover, the strong dynamics that produce a composite Higgs boson could also give rise to such light composite scalars, which would affect the Higgs decay channels. Or more drastically, the Higgs boson itself could be imagined as the light composite state of a strongly-coupled gauge theory with a confinement scale around TeV. These kind of models would allow for heavier composite scalars to be above the several TeV range that is consistent with LHC results.

This thesis is by no means a complete coverage of what one can do with holography. There is a vast landscape to discover beyond the Standard Model of particle physics. The holographic principle can teach us a lot more and it can guide us in these uncharted areas. Moreover, we have a lot to think about even in the fields that we think we have already mastered, i.e. foundations of quantum mechanics. Who knows, holography may one day tell us more about the fundamental relation between classical physics and the quantum world.

Contemplez-moi, rassasiez-vous de mon image,
car sous cette apparence vous ne me reverez plus.

Mani

Bibliography

[1] J. M. Maldacena, Int. J. Theor. Phys. **38** (1999) arXiv:9711200 [hep-th]

[2] Chatrchyan, Serguei *et al*. (CMS), Phys. Lett. B **716**, 30 (2012) [arXiv:1207.7235 [hep-ex]].

[3] Aad, Georges *et al*. (ATLAS), Phys. Lett. B **716**, 1 (2012) [arXiv:1207.7214 [hep-ex]].

[4] Aad, Georges *et al*. (ATLAS, CMS), Phys. Rev. Lett. **114**, 191803 (2015) [arXiv:1503.07589 [hep-ex]].

[5] Wells, James D., Phys. Rev. D **71**, 015013 (2005) [hep-ph/0411041].

[6] Arkani-Hamed, Nima and Dimopoulos, Savas, JHEP **06**, 073 (2005) [hep-th/0405159].

[7] Arvanitaki, Asimina and Craig, Nathaniel and Dimopoulos, Savas and Villadoro, Giovanni, JHEP **02**, 126 (2013) [arXiv:1210.0555 [hep-ph]].

[8] Arkani-Hamed, Nima and Gupta, Arpit and Kaplan, David E. and Weiner, Neal and Zorawski, Tom, (2012) [arXiv:1212.6971 [hep-ph]].

[9] Batell, Brian and Giudice, Gian F. and McCullough, Matthew, JHEP **12**, 162 (2015) [arXiv:1509.00834 [hep-ph]].

[10] Evans, Jason L. and Gherghetta, Tony and Nagata, Natsumi and Thomas, Zachary, JHEP **09**, 150 (2016) [arXiv:1602.04812 [hep-ph]].

[11] Kaplan, David B., Nucl. Phys. B **365**, 259 (1991)

[12] Altmannshofer, Wolfgang and Frugiuele, Claudia and Harnik, Roni, JHEP **12**, 180 (2014) [arXiv:1409.2522 [hep-ph]].

[13] K. R. Dienes and B. Thomas, Phys. Rev. D **85**, 083523 (2012) [arXiv:1106.4546 [hep-ph]].

[14] K. R. Dienes and B. Thomas, Phys. Rev. D **85**, 083524 (2012) [arXiv:1107.0721 [hep-ph]].

[15] K. R. Dienes, E. Dudas and T. Gherghetta, Phys. Rev. D **62**, 105023 (2000) [hep-ph/9912455].

[16] K. R. Dienes and B. Thomas, Phys. Rev. D **86**, 055013 (2012) [arXiv:1203.1923 [hep-ph]].

[17] K. R. Dienes, J. Fennick, J. Kumar and B. Thomas, Phys. Rev. D **93**, no. 8, 083506 (2016) [arXiv:1601.05094 [hep-ph]].

[18] K. R. Dienes, F. Huang, S. Su and B. Thomas, Phys. Rev. D **95**, no. 4, 043526 (2017) [arXiv:1610.04112 [hep-ph]].

[19] K. R. Dienes, F. Huang, S. Su and B. Thomas, PoS Confinement **2018**, 008 (2018).

[20] Xing, Zhi-zhong and Zhang, He and Zhou, Shun, Phys. Rev. D **86**, 013013 (2012) [arXiv:1112.3112[hep-ph]].

[21] Martin, Stephen P., (2010) [hep-ph/9709356].

[22] Gherghetta, Tony, (2011) [arXiv:1008.2570 [hep-ph]].

[23] Goldberger, Walter D. and Wise, Mark B., Phys. Rev. Lett. **83**, 4922 (1999) [hep-ph/9907447].

[24] Goh, Hock-Seng and Luty, Markus A. and Ng, Siew-Phang, JHEP **01**, 040 (2005) [hep-th/0309103].

[25] Gherghetta, Tony and von Harling, Benedict and Setzer, Nicholas, JHEP **07**, 011 (2011) [arXiv:1104.3171 [hep-ph]].

[26] Randall, Lisa and Sundrum, Raman, Phys. Rev. Lett. **83**, 3370 (1999) [hep-ph/9905221].

[27] Aad, Georges *et al*. (ATLAS), (2019) [arXiv:2004.14060[hep-ex]].

[28] Aaboud, Morad *et al.* (ATLAS), Phys. Rev. D **99**, 092007 (2019) [arXiv:1902.01636[hep-ex]].

[29] Contino, Roberto and Pomarol, Alex, JHEP **11**, 058 (2004) [hep-th/0406257].

[30] Cacciapaglia, Giacomo and Marandella, Guido and Terning, John, JHEP **06**, 027 (2009) [arXiv:0802.2946 [hep-th]].

[31] Arkani-Hamed, Nima and Luty, Markus A. and Terning, John, Phys. Rev. D **58**, 015004 (1998) [hep-ph/9712389].

[32] Luty, Markus A. and Terning, John, Phys. Rev. D **62**, 075006 (2000) [hep-ph/9812290].

[33] Gherghetta, Tony and Pomarol, Alex, Nucl. Phys. B **602**, 3 (2001) [hep-ph/0012378].

[34] Gabella, Maxime and Gherghetta, Tony and Giedt, Joel, Phys. Rev. D **76**, 055001 (2007) [arXiv:0704.3571[hep-ph]].

[35] Franco, Sebastian and Kachru, Shamit, Phys. Rev. D **81**, 095020 (2010) [arXiv:0907.2689[hep-ph]].

[36] Craig, Nathaniel and Essig, Rouven and Franco, Sebastian and Kachru, Shamit and Torroba, Gonzalo, Phys. Rev. D **81**, 075015 (2010) [arXiv:0911.2467[hep-ph]].

[37] Aharony, Ofer and Berdichevsky, Leon and Berkooz, Micha and Hochberg, Yonit and Robles-Llana, Daniel, Phys. Rev. D **81**, 085006 (2010) [arXiv:1001.0637[hep-ph]].

[38] Buyukdag, Yusuf and Gherghetta, Tony and Miller, Andrew S., Phys. Rev. D **99**, 055018 (2019) [arXiv:1811.08034[hep-ph]].

[39] Grossman, Yuval and Neubert, Matthias, Phys. Lett. B **474**, 361 (2000) [hep-ph/9912408].

[40] T. Gherghetta and A. Pomarol, Nucl. Phys. B **586**, 141 (2000) [hep-ph/0003129].

[41] Witten, Edward, Nucl. Phys. B **160**, 57 (1979)

[42] Batell, Brian and Gherghetta, Tony, Phys. Rev. D **76**, 045017 (2007) [arXiv:0706.0890[hep-ph]].

[43] Agashe, K. and Delgado, A., Phys. Rev. D **67**, 046003 (2003) [hep-th/0209212].

[44] Weinberg, Steven, The quantum theory of fields. Vol. 3: Supersymmetry, Cambridge University Press (2003).

[45] O'Connell, Heath Bland and Pearce, B. C. and Thomas, Anthony William and Williams, Anthony Gordon, Prog. Part. Nucl. Phys. **39**, 201 (1997) [hep-ph/9501251].

[46] Ferrara, S. and Zumino, B., Nucl. Phys. B **134**, 301 (1978)

[47] Gherghetta, Tony and Pomarol, Alex, JHEP **12**, 069 (2011) [arXiv:1107.4697 [hep-ph]].

[48] Giudice, G. F. and Masiero, A., Phys. Lett. B **206**, 480 (1988)

[49] Kim, Jihn E. and Nilles, Hans Peter, Phys. Lett. B **138B**, 150 (1984)

[50] Agashe, Kaustubh and Davoudiasl, Hooman and Perez, Gilad and Soni, Amarjit, Phys. Rev. D **76**, 036006 (2007) [hep-ph/0701186].

[51] Casagrande, S. and Goertz, F. and Haisch, U. and Neubert, M. and Pfoh, T., JHEP **10**, 094 (2008) [arXiv:0807.4937 [hep-ph]].

[52] Huber, Stephan J. and Shafi, Qaisar, Phys. Lett. B **498**, 256 (2001) [hep-ph/0010195].

[53] Bauer, M. and Casagrande, S. and Haisch, U. and Neubert, M., JHEP **09**, 017 (2010) [arXiv:0912.1625 [hep-ph]].

[54] Goldberger, Walter D. and Nomura, Yasunori and Tucker-Smith, David, Phys. Rev. D **67**, 075021 (2003) [hep-ph/0209158].

[55] Huber, Stephan J. and Shafi, Qaisar, Phys. Lett. B **583**, 293 (2004) [hep-ph/0309252].

[56] Gherghetta, Tony, Phys. Rev. Lett. **92**, 161601 (2004) [hep-ph/0312392].

[57] Agashe, Kaustubh and Hong, Sungwoo and Vecchi, Luca, Phys. Rev. D **94**, 013001 (2016) [arXiv:1512.06742 [hep-ph]].

[58] Randall, Lisa and Sundrum, Raman, Nucl. Phys. B **557**, 79 (1999) [hep-th/9810155].

[59] Luty, Markus A. and Sundrum, Raman, Phys. Rev. D **64**, 065012 (2001) [hep-th/0012158].

[60] Luty, Markus A., Phys. Rev. Lett. **89**, 141801 (2002) [hep-th/0205077].

[61] Gherghetta, Tony and Pomarol, Alex, Phys. Lett. B **536**, 277 (2002) [hep-th/0203120].

[62] Chacko, Z. and Ponton, Eduardo, JHEP **11**, 024 (2003) [hep-ph/0301171].

[63] Itoh, Hideo and Okada, Nobuchika and Yamashita, Toshifumi, Phys. Rev. D **74**, 055005 (2006) [hep-ph/0606156].

[64] Heidenreich, Ben and Nakai, Yuichiro, JHEP **10**, 182 (2014) [arXiv:1407.5095 [hep-ph]].

[65] Buyukdag, Yusuf and Gherghetta, Tony and Miller, Andrew S., Phys. Rev. D **99**, 035046 (2019) [arXiv:1811.12388[hep-ph]].

[66] Bartoszek, L. *et al*., Mu2e Technical Design Report (2014) arXiv: 1501.05241

[67] Andreev, V. *et al*., Improved limit on the electric dipole moment of the electron Nature **562** 355 (2018)

[68] J. M. Maldacena, Int. J. Theor. Phys. **38**, 1113 (1999) [Adv. Theor. Math. Phys. **2**, 231 (1998)] [hep-th/9711200].

[69] S. S. Gubser, I. R. Klebanov and A. M. Polyakov, Phys. Lett. B **428**, 105 (1998) [hep-th/9802109].

[70] E. Witten, Adv. Theor. Math. Phys. **2**, 253 (1998) [hep-th/9802150].

[71] J. E. Kim, Phys. Rev. D **31**, 1733 (1985).

[72] R. Contino and A. Pomarol, JHEP **0411**, 058 (2004) [hep-th/0406257].

[73] E. Witten, Nucl. Phys. B **160**, 57 (1979).

[74] I. R. Klebanov and E. Witten, Nucl. Phys. B **556**, 89 (1999) [hep-th/9905104].

[75] T. Gherghetta and A. Pomarol, Nucl. Phys. B **586**, 141 (2000) [hep-ph/0003129].

[76] B. Batell and T. Gherghetta, Phys. Rev. D **76**, 045017 (2007) [arXiv:0706.0890 [hep-th]].

[77] K. R. Dienes, J. Fennick, J. Kumar and B. Thomas, Phys. Rev. D **97**, no. 6, 063522 (2018) [arXiv:1712.09919 [hep-ph]].

[78] Buyukdag, Yusuf and Dienes, Keith R. and Gherghetta, Tony and Thomas, Brooks, Phys. Rev. D **101**, 075054 (2020) [arXiv:1912.10588 [hep-ph]].

[79] K. Bitaghsir Fadafan, W. Clemens, and N. Evans, Phys. Rev. D **98**, 066015 (2018) arXiv:1807.04548 [hep-ph]

[80] A. Pomarol, O. Pujolas, and L. Salas, JHEP **10**, 202 (2019) arXiv:1905.02653 [hep-th]

[81] D. Elander and M. Piai, JHEP **01**, 026 (2011) arXiv:1010.1964 [hep-th]

[82] E. Witten, Adv. Theor. Math. Phys. **2** 253 (1998) arXiv: 9802150 [hep-th]

[83] E. Witten, (2001) arXiv: 0112258 [hep-th]

[84] W. Mueck, Phys. Lett. B **531**, (2002) arXiv: 0201100 [hep-th]

[85] R. Abt, J. Erdmenger, N. Evans and K. S. Rigatos, JHEP **11**, 160 (2019) arXiv: 1907.09489 [hep-th]

[86] Buyukdag, Yusuf, (2019) arXiv: 1911.12328 [hep-th]

[87] I.R. Klebanov and E. Witten, Nucl. Phys. B **89** 556 (1999) arXiv: 9905104v2 [hep-th]